UNIVERSITY OF GHANA

COLLEGE OF BASIC AND APPLIED SCIENCES

HIGH-PRESSURE GRANULITES AND ECLOGITES OF THE DAHOMEYIDE SUTURE ZONE (ADAKLU, SOUTHEASTERN GHANA): PETROGENETIC EVOLUTION AND TECTONIC IMPLICATIONS

PRESENTED

BY

AMPONSAH ISAAC

(10275106)

THIS THESIS IS SUBMITTED TO THE UNIVERSITY OF GHANA, LEGON IN PARTIAL FULFILMENT OF THE REQUIREMENT FOR THE AWARD OF MPHIL GEOLOGY DEGREE.

July, 2015.

DECLARATION

This is to certify that this thesis is the result of research undertaken by Amponsah Isaac towards the award of Master of Philosophy degree in Geology in the Department of Earth Science, University of Ghana.

…….. Date……

AMPONSAH ISAAC

(MPhil. Candidate)

…….... Date…….

PROF. PROSPER M. NUDE

(Principal Supervisor)

…… Date…….

PROF. SAMUEL B. DAMPARE

(Co-Supervisor)

ABSTRACT

The Dahomeyide suture zone marks continental amalgamation between the Paleoproterozoic West African Craton (WAC) and the Sahara Metacraton (SMC). This suture zone of the Pan-African orogenic belt is encrusted by UHP/HP metamorphic rock bodies and associated ultramafic igneous plutonic rocks in SE Ghana through to Togo and Benin. The main identified rock types consist of mafic granulites (hornblende-garnet-pyroxene gneiss and pyroxene-garnet-hornblende gneiss), felsic gneiss, eclogite and pyroxenite. The petrography, structures and geochemistry of these rocks have been studied with the objective of inferring their petrogenesis and tectonic setting. Forty (40) thin sections were prepared and twenty-six samples were analyzed for major and trace elements using the Inductively Coupled Plasma Atomic Emission Spectrometry (ICP-AES) and Inductively Coupled Plasma Mass Spectrometry (ICP-MS). Some garnet porphyroblasts observed in the mafic granulite of the suture zone have preserved an indicative microstructure of UHP and prograde-retrograde metamorphism. These were respectively attributed to the exsolved rutile rods in garnet and also disequilibrium textures (corona textures) of incomplete reactions observed within the granulites and eclogites. The area has been affected by three deformational events: D_1, D_2 and D_3. The D_1 event (characterized by dextral sense of deformation) was a transpressional event which produced the penetrative S_1 foliations which are sub-parallel to the axial plane and axis of fold F_1. D_2 is marked by a dominant extensional event which resulted in the normal faults (Ft_1 and Ft_2) of the area and the stretched and rotated boudins in the pyroxene-garnet-hornblende gneiss. D_2 is marked by sinistral sense of deformation and a subordinate compressional event which is evident by the thrusting of the boudins. D_3 which is the last of the main phases of deformation (dextral sense) was a compressional event which is evident in

the garnet-hornblende gneiss at Torkor. D_3 resulted in the formation of the recumbent folds F_2 which have over-printed F_1. These three deformation events confirm with a typical convergent boundary deformation which starts with collision, extension and a final collision which are all represented by the D_1, D_2 and D_3 respectively. The suture zone rocks at Adaklu consist largely of rocks with IAT affinities and also include suites of rocks with N-MORB (oceanic crust) and subordinate calc-alkaline geochemical signatures. These signatures are typical characteristics of an arc environment setting. There is also some crust contamination in the mafic rocks and hence the crust (lower crust) played an active role during the evolution of these rocks. In contrast the mafic/ultramafic rocks show very little crustal contamination as these rocks show negative Th, moderate U and almost flat Zr-Hf anomalies. Low Th/Yb and high Nb/Th ratios in the mafic/ultrmafic rocks are inconsistent with crustal contamination. However, comparably, the felsic gneiss has higher Th and Pb contents, higher Th/Yb and low Nb/Th ratios. Based on the geochemical data represented on the pyroxenites (high Ba/Nb, ~36-262; Ba/Zr, ~1.44-4.03; Ba/Th, ~144-524; and U/Th, ~0.5-1 relative to the primitive mantle and Mg# and Ni content), it is proposed that the primary melts of these ultramafic plutonic rocks in the area were derived from the normal lithospheric mantle wedge which had not been depleted by previous melt extractions and strongly modified by hydrous fluids.

DEDICATION

This research work is dedicated to the Almighty God, my supportive Parents Mr. and Mrs. Amponsah, my siblings and to all my dear friends at the Department of Earth Science, University of Ghana.

ACKNOWLEDGEMENT

"Trust in God with all your heart, and lean not upon your own understanding: In all your ways acknowledge Him, and He will direct your paths." Proverbs 3:5-6.

My first gratitude goes to God for making me a curious being who loves to explore His creation and for giving me the opportunity, strength, wisdom and understanding to write this thesis. I thank God who protected me both spiritually and physically throughout my stay in a foreign environment to work on this important project. Without Him, I can do nothing.

My profound gratitude goes to my supervisors, Prof. Prosper M. Nude and Prof. Samuel B. Dampare for their excellent guidance, support and encouragement. I would also like to express my heartfelt gratitude to my family for their prayers, love and care.

My sincere gratitude also goes to Prof. J. Manu who willingly helped and inculcated into my mind the thought of starting my master's degree right after my national service at the Department of Earth Science.

I acknowledge the financial support provided by the Department of Earth Science Capacity Building Project, University of Ghana, Legon.

I acknowledge the chief, elders, committee members, Mr. Gabriel, Mr Anani and all the people of Adaklu Community in the Volta Region, Ghana for their hospitality and generosity to me during my field work.

Finally, to my friends and colleagues I say thank you for your love, encouragement and assistance.

Amponsah Isaac, 2015

TABLE OF CONTENTS

LIST OF FIGURES

LIST OF TABLES

LIST OF ABBREVIATIONS

AFM	A triangular variation diagram showing Alkalis ($Na_2O + K_2O$); FeO and MgO
BSU	Buem Structural Unit
CIPW	Cross-Iddings-Pirsson-Washington Norm
CAB	Calc-alkaline basalt
GPS	Global Positioning System
HP	High-pressure metamorphism
HFSE	High Field Strength Elements
HIPGE	High-pressure granulites and eclogites
HPE	Heat-producing elements
IAT	Island-arc tholeiite
ICP-AES	Inductively Coupled Plasma-Atomic Emission Spectrometry
ICP-MS	Inductively Coupled Plasma-Mass Spectrometry
kbar	Pressure expressed in kilobars; 1kbar = 0.1GPa
LC	Lower crust compositional range
LILE	Large Ion Lithophile Elements
LOI	Loss on ignition
MORB	Mid-ocean ridge basalt
OIT	Oceanic island basalt
ppm	Parts per million (1 in 10^6)
REE	Rare Earth Elements
SMC	Sahara Metacraton
SSZ	Supra-subduction zone
TAS	Total Alkaline-Silica diagram – a means of classifying volcanic rocks on the basis of their ($Na_2O + K_2O$) and SiO_2 content
UHP	Ultrahigh-pressure metamorphism
WAC	West Africa Craton
WGS	World Geodetic System
WPB	Within-plate basalt

CHAPTER ONE

INTRODUCTION

This thesis comprises textural, structural, mineralogical, as well as major and trace elements compositional study of rocks and geological field report of geological mapping project carried out within the Dahomeyide suture zone in Volta Region, southeastern Ghana.

The thesis encompasses a study of the different type of rocks in the study area based on mineralogical, textures, structures, new petrological and geochemical data from the rocks, and field relations of the rocks for better understanding of petrogenesis and tectonic implications of these high pressure rocks of the suture zone.

1.1 BACKGROUND

The Pan-African (Neoproterozoic) orogens resulted from the assembly of northwest Gondwana from various fragments including the West African Craton [WAC] (Hoffman, 1991; Trompette, 1994; Attoh and Morgan, 2004 and references therein). Attoh et al. (1997) indicated that nappe complexes comprising passive margin sediments and accreted exotic magmatic rocks in Ghana and Togo were produced by orogenic contraction which resulted from the collision between the WAC and the Benino-Nigerian Shield. The principal tectonic elements of the Dahomeyide orogen proposed by Attoh et al., (1997); and Attoh and Nude (2008) are: (a) the external unit which consists of the deformed edge of the West African Craton (WAC) with its cover rocks of the Akwapimian/Atacora and Buem Structural Units as the cover sequence; (b) the suture zone representing the eastern boundary between the WAC and the exotic rocks of the Dahomeyan lithotectonic units; and (c) the eastern internal unit

which consists of exotic rocks that form the granitoid-migmatite gneiss complexes east of the suture zone (known as the Benino-Nigerian Precambrian basement). Distinctive orogenic mafic and ultramafic rocks can be traced for about 2000 km from the Sahara to the Gulf of Guinea within the suture zone which marks the collisional zone between the WAC and the Benino-Nigerain Shield (Trompette, 1994). These rocks are the high-pressure (HP) granulite gneisses referred to as the Shai Hills Gneiss (Attoh and Morgan, 2004) and they also include the ultrahigh-pressure (UHP) gneisses of the Adaklu Inselberg both in southeastern Ghana.

The mafic and ultramafic suture zone rocks in Adaklu are the northeastern extension of the Shai Hill rocks in Ghana which extends to Togo and Benin in West Africa (Fig. 1.1). The study area is sandwiched between the Shai Hills in south-eastern Ghana and the Lato Hills in southern Togo, all part of the Dahomeyide suture zone in West Africa. Samples for this research were taken mainly from the Adaklu district including the Adaklu Inselberg and the Gbeto Hill, within the Dahomeyan suture zone.

According to Attoh and Nude (2008), the association of these ultrahigh-pressure (UHP) metamorphism and high-pressure granulites and eclogites (HIPGE) rock types is linked to the subduction of the Dahomeyide suture zone rocks to mantle depths during the Pan-African orogeny.

There are some petrological and geochemical studies of HP granulites and eclogites and the associated alkaline intrusive rocks in the Dahomeyan suture zone of southeastern Ghana and southern Togo. However many questions remain unanswered regarding their geochronology, petrogenesis, structures as well as their tectonic evolution. Not much work has been done on the suture zone rock assemblages of the study area which is sandwiched between Shai Hills

and Lato Hills. Also there has been a considerable debate on the possible protoliths of these ultramafic suture zone rocks. Analytical data by Knorring and Kennedy (1958) and BGR/Hannover/FRG suggest a basaltic composition for the protoliths of the Shai Hill gneisses. However Hirdes and Davis (2002) suggested that the protoliths of the Shai Hill gneisses were immature wackes or fairly mafic volcaniclastic sediments or a mixture of both (Al_2O_3 values of >19% and Na_2O concentrations around 4.5% are high for normal igneous mafic rocks).

There is therefore the need to develop a vivid understanding of the geodynamic evolution of the high-pressure granulitic and eclogitic (HIPGE) rocks of the Adaklu segment of the Pan-African Dahomeyan suture zone in Ghana for better understanding of petrogenesis and tectonic implications of these rocks. This research is to communicate the textures, structures, petrological and new geochemical data for the HIPGE rocks of the Pan-African Dahomeyan orogenic belt in Ghana (precisely Adaklu inselberg and surrounding) and also interpret their significance for metamorphism in the region.

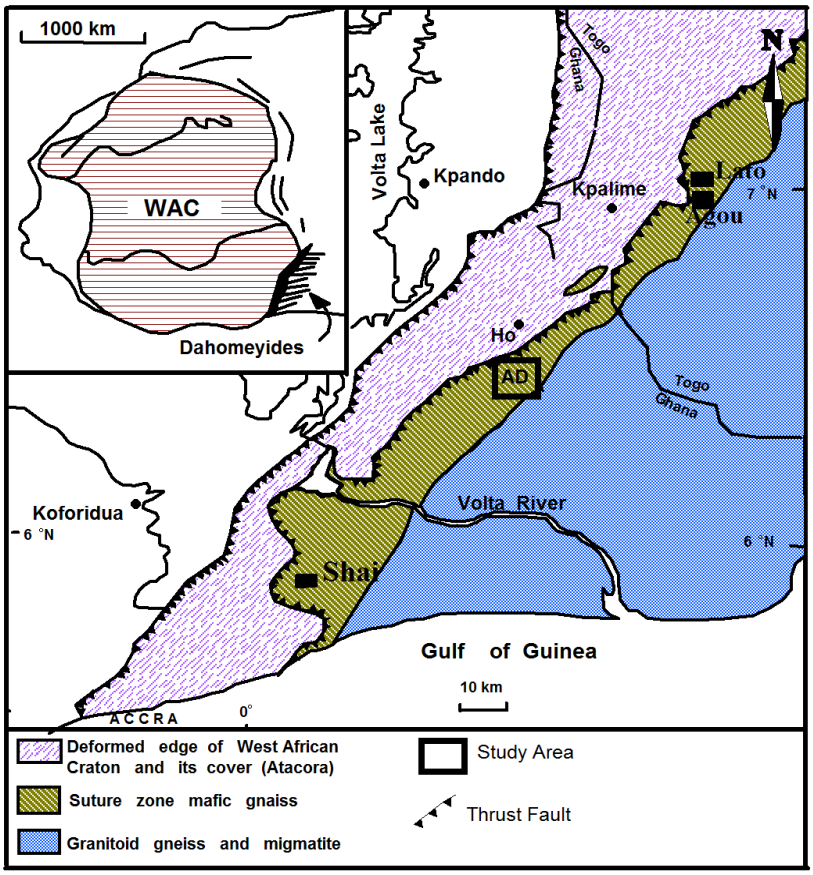

Fig. 1.1. Pan-African Dahomeyide Orogen showing the principal tectonic elements of the study area (after Attoh and Morgan, 2004)

1.2 OBJECTIVE

The main research objective is to deduce the petrogenesis and tectonic evolution of suture zone rocks in the study area. This will be carried out by the following means:

- To carry out an integrated study of petrography, structures, textures and composition of the rocks in the study area
- To determine major and trace elements compositions of the rocks
- Use the new petrological and geochemical data to infer the petrogenesis and tectonic evolution of the rocks.

1.3 STUDY AREA

1.3.1 LOCATION AND SIZE

The study area (Fig. 1.2) is the Adaklu inselberg and surrounding area which lies within the Dahomeyan suture zone of the Dahomeyides in southeastern Ghana. The study area is about 97.4 km^2 and is located in the Adaklu District in the Volta Region of Ghana.

Adaklu inselberg which is about 600 m above sea level is located 12 km from Ho in the Volta Region in southeastern Ghana. The study area is bordered by the coordinates latitudes 6°27′ and 6°32′ N of the Equator and longitudes 0°27′ and 0°33′ E of the Greenwich Meridian. The area is located on the Ghana national grid, on sheet numbers 0600A4, 0600B3 (northwest and northeast respectively), 0600C2 and 0600D1 (southwest and southeast respectively).

1.3.2 ACCESSIBILITY

The second class road of the study which runs through the study area is part of the Ho-Adidome-Sogakope road, running north-southeast through the whole length. The third class roads links Abuadi to Torkor and to Kodiagbe. Another third class road links Dwafanu through Abuadi to Waya and beyond (from north to southeast of the study area). Aside these, there is a number of footpaths and hunters' trails found in the vicinity. On the whole, the area is fairly accessible.

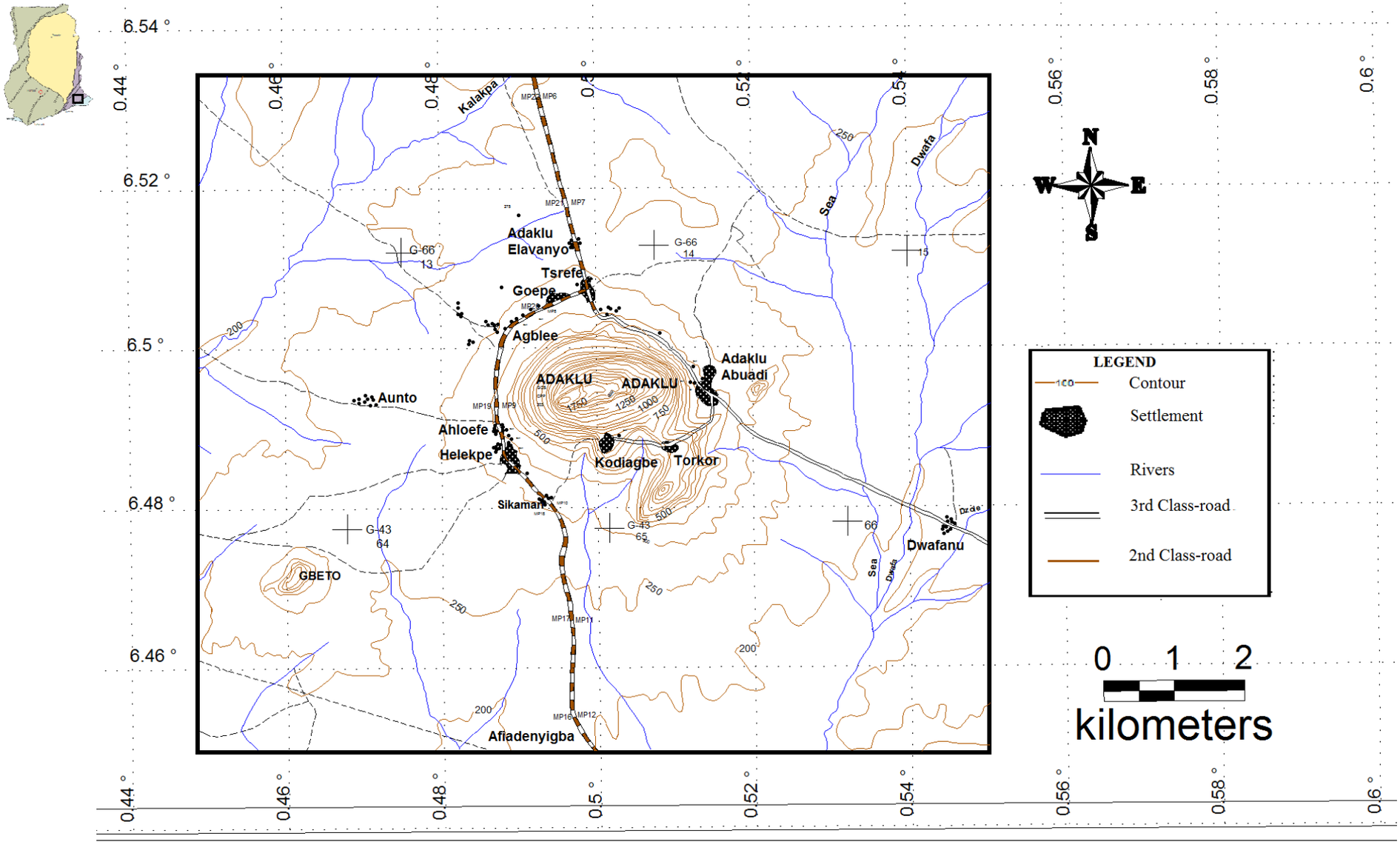

Fig 1.2. Topographical map of the study area showing the elevations, drainage and various towns in the area

1.3.3 TOPOGRAPHY AND DRAINAGE

The vast majority of the area are relatively low lying, with contour values as low as 60.96 m.

The low land stretch is occasionally spiced with isolated, conspicuous, individual highlands of elevations much higher and abruptly so than the surrounding. Most pronounced of these is the Adaklu inselberg. It is sandwiched between Abuadi (to the east) and Ahloepe (to the west) villages and towers steeply to 600 m at its peak. This is easily the highest elevation in the vicinity and nearby areas. The Adaklu inselberg occupies the central portion of the study area. There also is another small mount Gbeto, located in the in the southwest of the area, which is about 500 m high. These hills are made up of fairly resistant rocks which now tower as a result of erosion of their immediate surroundings. The relief of the area notably decreases from north to south generally.

The drainage pattern in the Adaklu area, is largely dendritic in nature. Three major water bodies (Kalakpa, Dwafa and Sea) with tributaries flow through the area from north to south. At the east, two streams flow through the game reserve and the stream sourcing around Kodiagbe flow through the middle and then southeast. Most of these stream channels in the north and west are of intermittent and were dry throughout the study time.

1.3.4 CLIMATE

The study area is a typical example of a tropical rain forest whose climate features distinct wet and dry seasons. The area experiences two rainy seasons: one from April to July, and then after intermittent rains in August and the other from September to November. The harmattan season is most intense in December and January. The average daily temperatures range from about

20°C to 25°C in January and from 15°C to 20°C in July. The mean annual rainfall ranges from about 1000 to 1800 mm (Dickson and Benneh, 1998).

1.3.5 SOIL AND VEGETATION

The two main types of soil in the study area are the Akuse black clays and lateritic sandy soil (Henry, 2000). The former develops over basic gneisses and being alkaline is rich in supplies of calcium, calcium oxide and magnesium. It is characteristically heavy, plastic and sticky during the rainy season but easily becomes compact and develops wide cracks during the dry season. Its colour ranges from black to brown. The area is vastly covered by the Akuse black clays or soil.

The lateritic sandy soil on the other hand develops over felsic rocks. It is hence acidic and highly deficient in organic matter and most often waterlogged. It is sandy and rather pale. This type of soil dominates southeastern portion of the study area in villages like Dwafanu.

A rare third type, known as stony or gravelly, is found pockets scattered around the area, especially east of Helekpe towards Gbeto.

1.4 GEOLOGICAL SETTING OF THE STUDY AREA

According to Affaton et al. (1980), the three main structural units in West Africa include a Precambrian basement referred to as the West African Craton (WAC), Pan-African (600 Ma) and Hercynian (350-300 Ma) orogenic fold belts and the Mesozoic to Cenozoic sedimentary basins (Fig. 1.3).

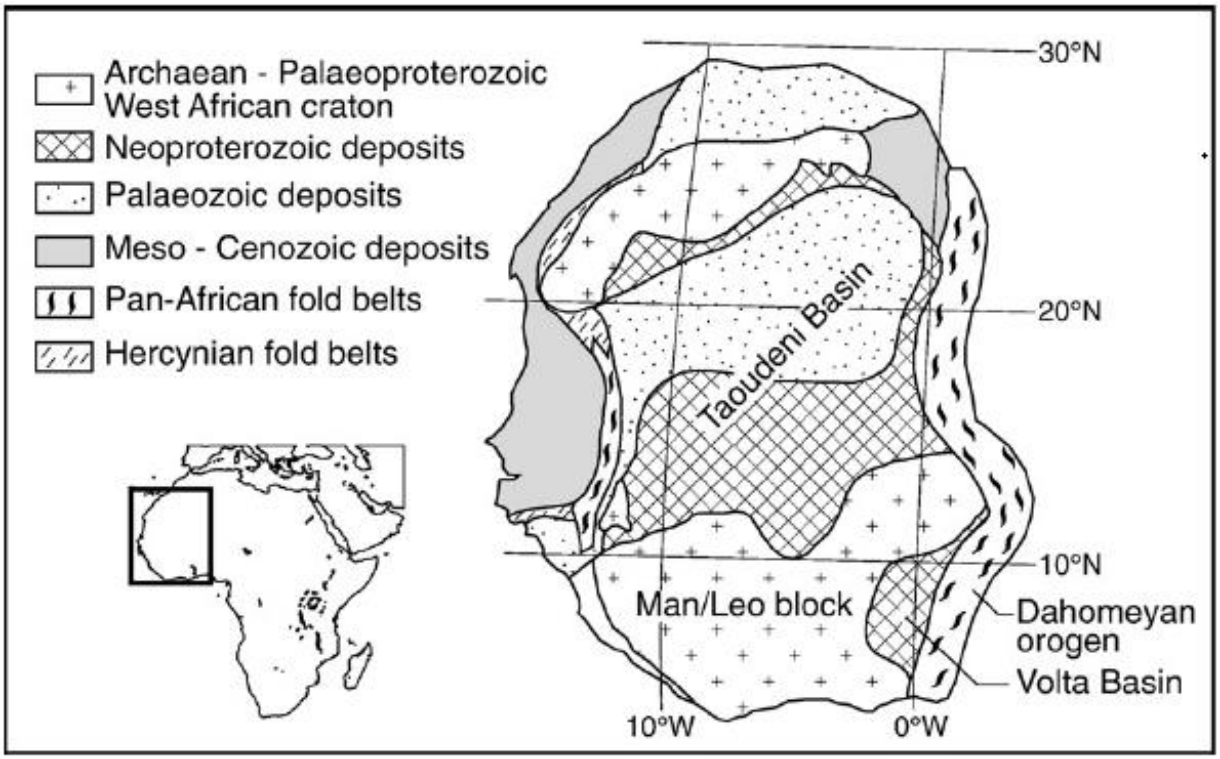

Fig. 1.3. Geological sketch map of West Africa sowing the various structural units (after Trompette, 1994).

Ghana can be divided into five main geological domains (Fig. 1.4) on the basis of age data, tectonics and lithology (Kesse, 1985). These five geological domains are: (1) the western units, found at the eastern margin of the WAC (known as the Birimian and Tarkwaian in Ghana); (2) the mobile belt units found at the southeastern part of the country (the Dahomeyide); (3) the Voltaian sediments at the central which occupies about two-thirds of the country (Voltaian Basin); (4) the coastal sedimentary basins; (5) the Tertiary to Recent deposits.

The Paleoproterozoic Birimian Supergroup, has yielded an Sm:Nd whole-rock isochron age of tholeiitic basalts of 2166 ± 66 Ma (Taylor et al., 1988, quoted in Hirdes et al., 1992) and a U/Pb zircon dating age on belt granitoid plutons of about 2175 Ma (Hirdes et al., 1992). The

Birimian Supergroup consists of metasedimentary rocks which were deposited in basinal areas separated by volcanic belts, that trend northeast– southwest in which mainly tholeiitic basalts occur. The rocks of the Tarkwaian Group represent the erosional products of the Birimian, and are dominated by coarse-clastic sediments. They are located mostly within the volcanic belts. The whole complex of basins and volcanic belts have been extensively intruded by granitoids (Eisenlohr, 1992). At the southeastern margin of the WAC the Dahomeyide in Ghana is bounded to the west by the Voltaian Basin and the Paleoproterozoic Birimian Supergroup at the south (Fig. 1.4).

In southeastern Ghana, the geology of the Dahomeyide belt has been described by various workers (Kesse, 1985 and references therein; Attoh et al., 2007) and is outlined in Fig. 1.1. According to Attoh et al. (2007), the principal tectonic units of the Dahomeyide are: (i) deformed eastern edge of the 2.1 Ga WAC which are mainly granitic augen gneisses (or Ho gneisses) with the Atacora and Buem structural units as cover rocks; (ii) the suture zone assemblage of distinct mafic and ultramafic rocks (within which the study area lies); and (iii) granitoid gneiss and migmatite assemblages east of the suture zone. The rocks of the deformed edge of the WAC are overthrust by rocks of the suture zone consisting of high-pressure (HP) mafic granulites and eclogites (Attoh et al., 2007).

The study area (Adaklu) is located within the suture zone of the Dahomeyide. The suture zone nappes are composed of garnet-bearing mafic-ultramafic rocks which can be traced continuously for c. 1000 km (Attoh and Morgan, 2004). These mafic gneisses were affected by extensive shearing where they were thrust over the external nappes along a crustal-scale ductile shear zone (Attoh et al., 1997). According to Attoh et al., (1997) the suture zone gneiss represents the boundary between the autochthonous WAC and inferred allochthonous rocks,

exposed to the east in the Accra Plains allochthon. The study area is characterized by different varieties of metamorphic rocks and an ultramafic igneous plutonic rock. The southeastern corner of the study area is occupied by rocks of the internal nappes but no samples were taken from this portion because they are not of prime interest to this research.

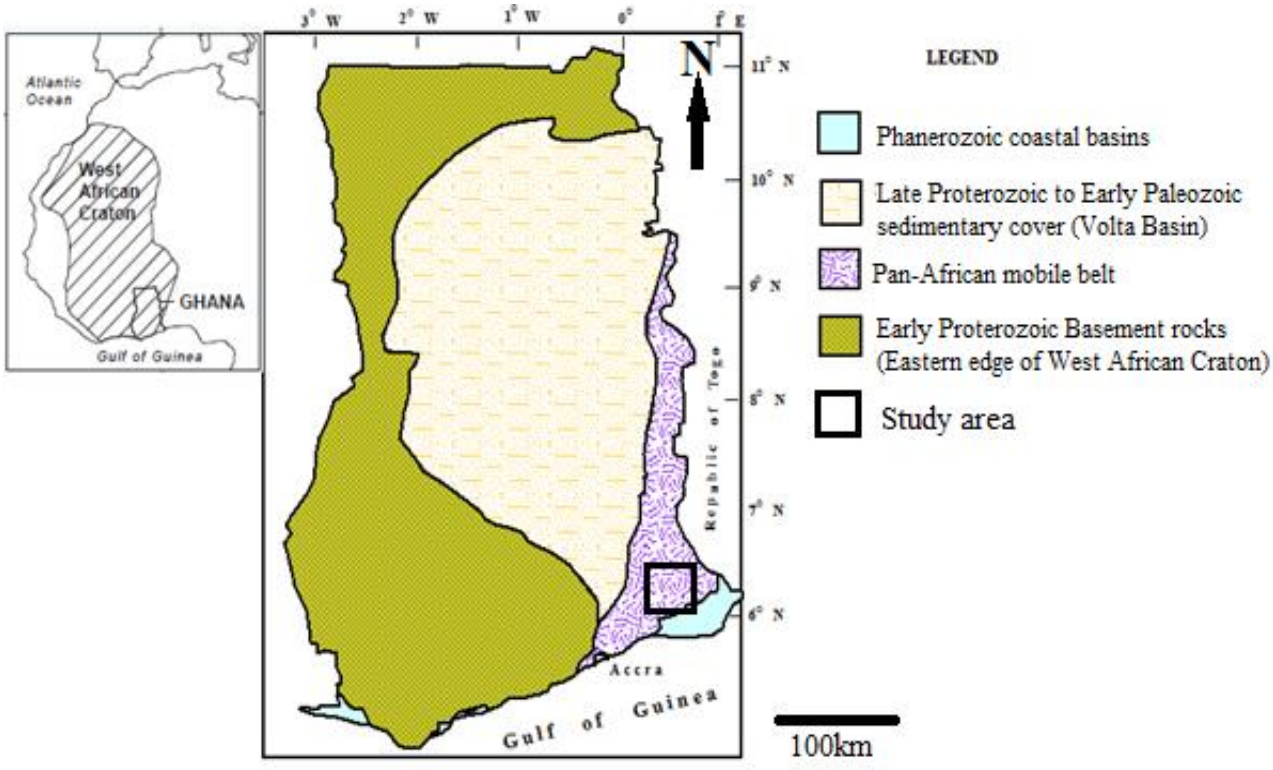

Fig. 1.4. Geological sketch map of Ghana showing the major geological domains and study area (after Osae et al., 2006).

CHAPTER TWO

LITERATURE REVIEW

2.1 WEST AFRICAN CRATON

West Africa is characterized by a wide variety of geological terranes with a complicated geological history. According to Griffis et al. (2002), the West African region features a West African Craton (WAC) of older Precambrian rocks surrounded by younger Precambrian and Phanerozoic units (Fig. 2.1).

The oldest Precambrian rocks of the WAC are Archean in age (>2500 Ma) which are limited to a core zone along the coastal region extending from western Cote d'Ivoire through Liberia, Sierra Leone and into southern Guinea (Griffis et al., 2002). According to the authors, the Archean units are mainly bounded on the east in Cote d'Ivoire by the very prominent Sassandran fault. Most of the regions feature highly metamorphosed mafic to felsic gneisses and migmatites representing old basement. Griffis et al. (2002) inferred that narrow greenstone belts of less metamorphosed supracrustal rocks are wedged into the basement. The Sassandran fault is a large N-S regional feature which generally separates the Archean units from younger Paleoproterozoic metasedimentary and metavolcanic units (Griffis et al., 2002).

The most extensive unit of the southern part of the WAC (called the Leo or the Man Shield) are the Paleoproterozoic metasedimentary rocks, metavolcanics and associated intrusive complexes that cover much of Ghana, Cote d'Ivoire, Burkina Faso and into southern Mali, northern Guinea and the southwest corner of Niger (Potrel et al., 1996; Griffis et al., 2002). The Volta Basin in central and northeastern Ghana is virtually underlain by these

Paleoproterozoic units of the WAC. From available age and isotopic data the building and amalgamation of the WAC basement took place through four major orogenic cycles: (1) Leonian cycle (3.5–3.0 Ga; Potrel et al., 1996; Kroner et al., 2001; Thieblemont et al., 2004), (2) the Liberian cycle (2.95–2.75 Ga; Auvray et al., 1992; Potrel et al., 1998; Key et al., 2008), (3) the Eburnian–Birimian cycle (2.2–1.75 Ga; Abouchami et al., 1990; Liegeois et al., 1991; Hirdes et al., 1992; Schofield et al., 2006) and (4) the Pan-African remobilization (760–660 Ma; Saquaque et al., 1989; Hefferan et al., 2000; Thomas et al., 2002; Samson et al., 2004). One of the main characteristics of the WAC is that no Mesoproterozoic events or rocks are known, suggesting a quiescent period between 1.7 and 1.0 Ga (e.g. Abati et al., 2012 and references therein).

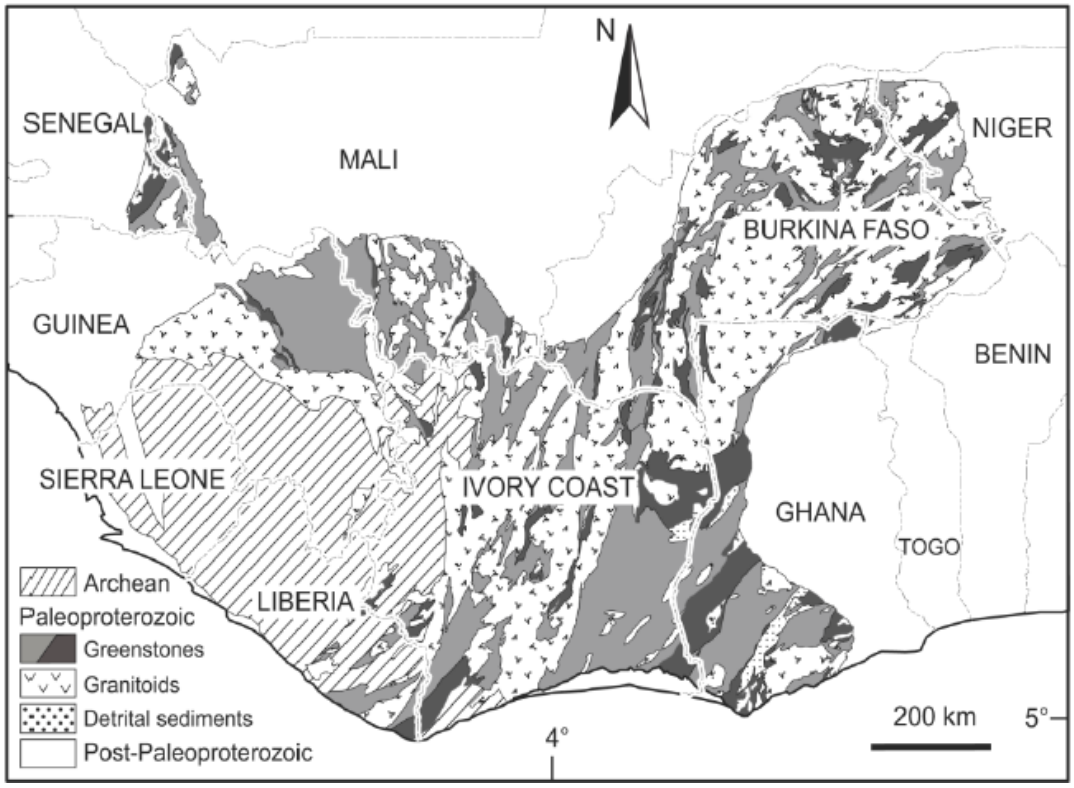

Fig. 2.1. Regional geological map of the West African Craton showing various geological domains (Milési et al., 1989 and Vidal et al., 1996).

2.2 THE PAN-AFRICAN OROGENY

The Pan-African event was defined by Kennedy in 1964 as a major continental-wide (wide-spread) tectono-thermal event that affected and structurally deformed, consolidated and differentiated the African continental crust into cratons and orogenic zones at about 500±100 Ma (Neoproterozoic age). This event affected all parts of Africa and other parts of the world; hence the term Pan-African. The term 'Pan-African' was defined both for the orogenic event and the geologic time occurrence. The concept was then extended to the Gondwana continents (Fig. 2.2) although regional names such as Brasiliano for South America, Adelaidean for Australia, and Beardmore for Antarctica were proposed (Kroner and Stern, 2005).

New knowledge from other researches have indicated that the Pan-African orogenic event as defined by Kennedy (1964) only referred to the final thermal stages of an entire orogenic cycle (event) which lasted from at least 900 Ma to about 450 Ma (Kroner, 1984). This tectono-thermal event produced several orogenies in African: (1) Trans-Saharan mobile belts (including the Pharusides and Dahomeyides); (2) Rockelides, the Bassarides, the Mauritanides, all in West Africa; (3) Damarides and Lufilides between the Zaire-Tanzanian and Kalahari cratons; (4) Katangan belt between the Zaire and Tanzanian cratons and (5) Mozambique belt in eastern Africa.

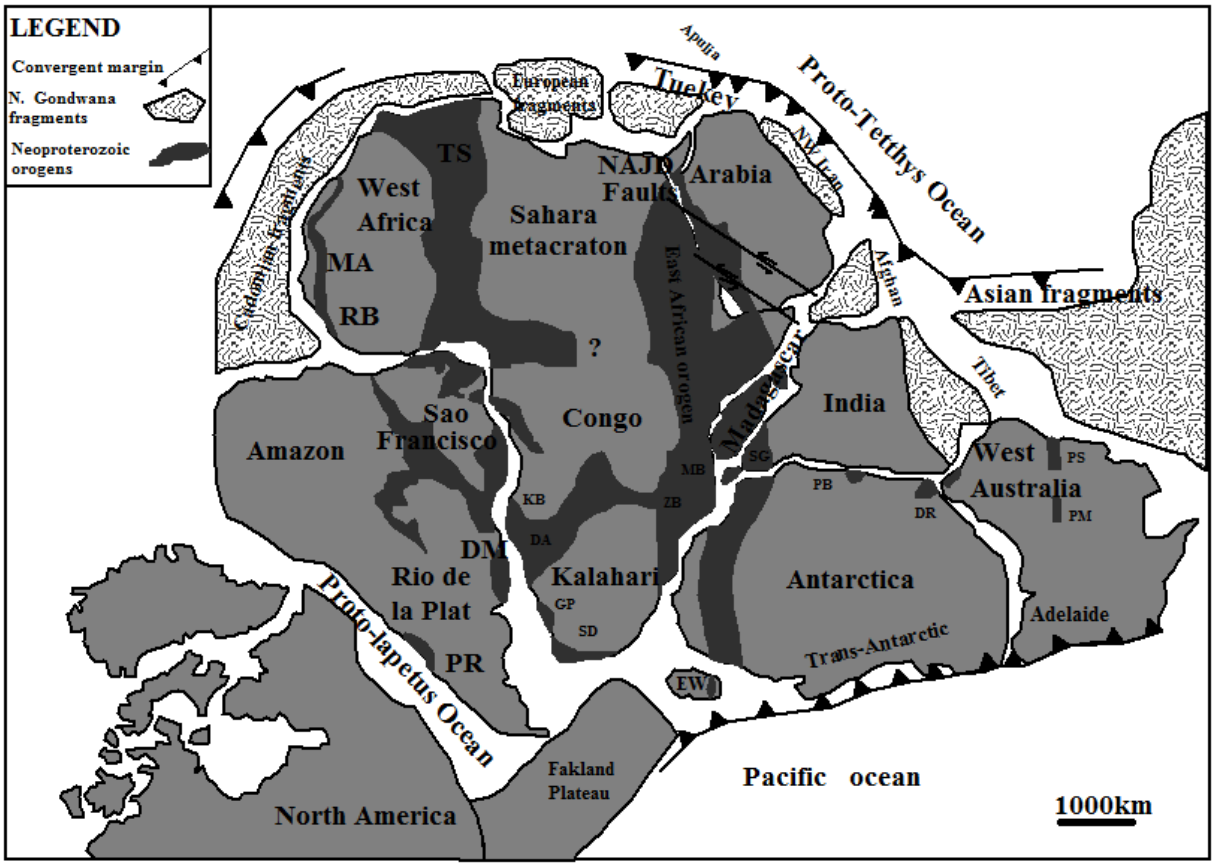

Fig. 2.2. Map of Gondwana at the end of Neoproterozoic time (~540 Ma) showing the general arrangement of Pan African belts. AS, Arabian Shield; BR, Brasiliano; DA, Damara; DM, Dom Feliciano; DR, Denman Darling; EW, Ellsworth Whitmore Mountains; GP, Gariep; KB, K;Kaoko; MA, Mauretanides; MB, Mozambique Belt; NS, Nubian Shield; PM, Peterman Ranges; PB, Pryolz Bay; PR, Pampean Ranges; PS, Paterson; QM, Queen Maud Land; RB, Rokelides; SD, Saldania; SG, Southern Granulite Terrane; TS, Trans Sahara Belt; WB, West Congo; ZB, Zambezi. (Extracted from Kroner and Skern, 2005).

2.3 THE PAN-AFRICAN OROGENY IN GHANA

The Pan-African orogen in West Africa is the southern extension of the 2000 km long Trans-Saharan belt which formed on the eastern margin of the West African Craton (Attoh et al., 2007 and references therein). The Pan-African Dahomeyide orogen of Western Africa

represents a model of collision belt between the passive continental margin of the WAC and the Benino-Nigerian and Touareg shields (Agbossoumondé et al., 2004 and references therein). According to recent concepts of supercontinent fragmentation and construction (Hoffman, 1991; Dalziel et al., 2000), this belt represents the final and striking structure related to the amalgamation of the WAC to Central Gondwana (Trompette, 2000).

The Dahomeyide orogen in southeastern Ghana is a result of the Neoproterozoic Pan-African event about 600 Ma ago. The southeastern segment of the Trans-Saharan belt exposed in southeastern Ghana and adjoining parts of Togo and Benin comprises the Dahomeyide orogen (Affaton et al., 1991; Castaing et al., 1993; Attoh et al., 1997).

According to Attoh et al. (1997) and Attoh and Nude (2008), the principal tectonic elements of the Dahomeyide orogeny (Fig. 1.1) from the west to the east are: (1) the deformed edge of the WAC; (2) the suture zone; (3) exotic rocks. The Togo and the Buem structural units are the cover sequence (rocks) of the deformed edge of the WAC known as the Ho gneisses in Ghana.

The Dahomeyide belt consists, from west to east, three structural divisions (Affaton et al., 1980): the Buem Structural Unit, the Togo Structural Unit (known as the Akwapimian or Atacora Unit) and, the Dahomeyan Structural Unit. These three units are bounded by thrust faults at their boundaries.

2.3.1 BUEM STRUCTURAL UNIT (BSU)

The Buem Structural Unit (BSU) is believed to be the youngest of the Dahomeyide and is composed predominantly of intercalations of volcanics and sediments, and the sedimentary unit has been dated 624 Ma (K/Ar on glauconite by Bozhko et al., 1971).

About four major lithologic facies can be distinguished in the BSU in the study area (Junner, 1940; Jones, 1990; Osae et al., 2006): (a) clastic sediments, (b) limestone and jasperoids, (c) volcanic rocks, and (d) serpentinites. The uppermost and lowermost parts of the succession are made of the clastic rocks which comprise sandstones, fine-grained quartzites, siltsones, and red shales. The jasperoids are series of bedded, normally red cherts of massive appearance and sometimes brecciated (Junner, 1940; Jones, 1990; Osae et al., 2006). According to Junner (1940) and Jones (1990), some of the jasperoids, however, may have formed by metasomatic alteration of the clastic sediments, limestone and volcanics. The serpentinites are schistose to massive in nature and rich in chromite. The volcanic rocks consist predominantly of basalts, hawaiites, mugearite, and trachytes.

The BSU is characterized by interstratified volcanic and the sedimentary rocks which are believed to be coeval. Jones (1990) suggested that the volcanics and serpentinites are unrelated; the volcanics were probably erupted during a period of tension related to continental breakup at about 650 Ma, whereas the serpentinites mark a continental collision at about 500 Ma.

The sandstones tend to crop out in lens shaped bodies a few hundred meters to a few kilometers long. Junner (1990) proposed the deposition of the sandstones as alluvial fan deposits because of the lenticular shape of the sandstone bodies and paucity of sedimentary structures in the massive sandstones. The associated shales are red and contain desiccation cracks and ripple marks indicating shallow water or subaerial deposition. The clastic sediments are, therefore, of continental origin.

The BSU is considered as a tectonic and metamorphic lateral equivalents of the middle part of the Voltaian Group that has been dated 620–640 Ma (Grant, 1969; Affaton et al., 1980). However, K/Ar ages of three Buem volcanic specimens give a mean age of about 512 Ma (Jones, 1990), which is younger than the expected 650 Ma age for the deposition of the Buem Formation. This 500 Ma age coincide with metamorphic and metasomatic events that affected the Buem rocks after their deposition (Jones, 1990). Affaton et al. (1997), however, identified an earlier weak metamorphic imprint that is older than the Pan-African collision and may be coeval with the sedimentation age.

The geotectonic setting of the BSU is debated and various authors have given different interpretations: continental collision origin (e.g., Burke and Dewey, 1973), intracratonic origin (e.g., Clifford, 1972), continental rift origin (e.g., Attoh, 1990; Jones, 1990) and passive margin origin (e.g., Affaton et al., 1997).

2.3.2 TOGO STRUCTURAL UNIT

The rocks which form the north to northeast trending Togo Range consist of strongly tectonised phyllite, schist, quartzite and sandstones. These rocks are known as the Togo Structural Unit (Affaton et al., 1980). The contacts between the Togo and Dahomeyan to the east and the Buem to the west are thrust faults. The unit grades from east to west from phyllite and chlorite schist upwards into quartzite, and micaceous quartzite (Kesse, 1985). Grant (1969) indicated that serpentinites occur along the western contact and appear to be emplaced along thrust faults at the boundary with the BSU.

Different names have resulted from different authors for the rocks of this unit. Such names include Akwapimian (Kitson, 1928), Togo (Junner and Hirst, 1946), Togo Structural Unit (Affaton et al., 1980), Togo Series (Kesse, 1985) and Togo Tectonic Unit (Blay, 1991). However, the generally accepted name which is used by recent workers is Togo/Atacora Structural Unit (e.g. Affaton et al., 1980; Attoh et al., 1997). The Togo/Atacora Structural Unit is an irregular, fault-bounded belt of metamorphosed sediments that comprise the series of hills and ridges (Akuapem) which trend in a north northeast to south southwest from the Volta River towards the Ghana-Togo border and into northern Benin where it is called the Atacora Range (Kesse, 1985). The Togo Structural Unit marks the western limits of a very large area affected by the Pan-African thermotectonic event that peaked at about 600-550 Ma and whose effects extend right across Nigeria (Griffis, et al., 2002). Hoffman (1999) postulated that the Togo Structural Unit is a collisional belt and suture zone between the West African Craton and an eastern cratonic block that became welded together at a time the supercontinent of Gondwana was being created. Bordered to the east of the Togo Structural Unit is a generally low-lying area (Accra plains) underlain by high-grade, Dahomeyan metamorphic terrane.

The rocks of the Togo Structural Unit are highly deformed and metamorphosed and degree of metamorphism and deformation increase towards the southeast (Wright et al., 1985). Strong deformation and associated intense folds, fractures, joints and faults indicates a series of deformation of which the latest is related to the 600 Ma – 500 Ma Pan-African Orogeny event (Robertson, 1925; Crook, 1963; Kennedy, 1964; Grant, 1969). Along major faults, slices of higher grade metamorphic (Dahomeyan) and lenses of ultramafic and mafic units can be found. Previous dating of the Togo Structural Unit has been based on field relationships. Studies by Koert (1910) and Crook (1970), suggested the Togo Structural Unit to be younger than the

basement Dahomeyan. Studies by Mani (1978) and Blay (1991) also suggested that the Dahomeyan is older than the Togo Structural Unit because the Togo occurs as outliers in the Dahomeyan.

2.3.3 THE DAHOMEYAN STRUCTURAL UNIT

Kese (1985) indicated that the Dahomeyan rock units are up to 30 km wide and can be traced from Fete in the West of Accra to Age in the republic of Togo and beyond. Regional strike is NE with moderate dip to SE. The Dahomeyan Structural Unit covers 7000 km^2 of terrane in the southeastern corner of Ghana and continues towards the north and northeast into neighbouring countries such as Togo and Benin, and beyond (Hirdes and Davis, 2002). This structural unit is the easternmost rock unit in Ghana and differs significantly from other rocks in Ghana in that it is composed of high grade metamorphic rocks.

According to Holm (1974), the Dahomeyan Structural Unit consists of four lithologic belts of granitic and mafic gneiss. The mafic gneisses are relatively uniform oligoclase, andesine, hornblende, salite and garnet gneisses of igneous parentage and generally tholeiitic composition (Holm, 1974). The granite gneisses interlayer with the mafic gneiss and are believed to be metamorphosed volcaniclastic and sedimentary rocks. Persistent bands of nepheline gneiss in the system appear to be metamorphosed calc-alkaline igneous rocks (Holm, 1974). All of the gneisses have undergone at least two stages of penetrative deformation. The latest deformation is believed to be of Pan-African age (500-600 Ma) and is referred to as a "reactivation" of Birimian crust by Kennedy (1964). Fitches (1970), however, suggests that the metamorphism may be Eburnian (Proterozoic) in age.

A distinctive, but normal, lithology in the Dahomeyan is the "Kpong Complex", a calcareous rock which has been interpreted to be a carbonatite and associated alkali rocks within the suture zone (Attoh and Nude, 2008).

Geochronological studies made on the Dahomeyan showed it is Mesoproterozoic in age and has been involved in the Pan African tectonothermal event dated 600 ± 100 Ma (Alfaton et. al, 1991). The age of the Dahomeyan in Ghana has been a matter of considerable debate (Kitson, 1928; Junner, 1940; Roques, 1948; Kesse, 1985; Affatton et al., 2000; Hirdes and Davis, 2002). Kitson (1928), Junner (1940) and Roques (1948) considered the Dahomeyan gneisses to be Archean in age and thus as the oldest rocks in Ghana. However, Bonhomme (1962) based on geochronological data postulated that the Dahomeyan represent rejuvenated Paleoproterozoic rocks. Kesse (1985), Affaton et al. (2000) and Hirdes and Davis (2002) also associated the Dahomeyan gneisses with the Pan-African tectono-thermal event, implying that the rocks are late Neoproterozoic in age.

2.3.3.1 THE EXTERNAL NAPPES

The external nappes of the Dahomeyan Structural Unit consist of the augen gneisses (locally known in Ghana as the Ho gneiss) which represent the deformed edge of the WAC (Attoh et at., 1997, Attoh and Nude, 2008). Rocks of this nappe complex include augen and mylonitic gneisses, mostly hornblende-rich, sheared, overthrust the Togo unit. Doleritic and dioritic intrusives are common along contact zones with the Togo cover rocks.

The mylonitic granitoid gneiss unit of the external nappes is characterized by variably developed feldspar porphyroclasts. This protomylonitic granitoid unit, which represents the

2.1 Ga Ho gneiss, was thrust over the Togo structural units as is evident in tectonic windows such as the Kluma Hills, where the tectonic stacking can be inferred from the klippen of the Ho gneiss (Attoh and Nude, 2008).

Attoh et al. (2007) suggest that the eastern edge of the WAC is marked by an extensive ductile shear zone within which the granitoids have been transformed into mylonitic gneisses (Ho gneiss) and locally more highly sheared varieties which comprise ductile imbricate structures exposed in the Atacora eastern outliers. This shear zone is characterized by a shallow SE-dipping foliation that indicates NW verging thrust propagation (Attoh et al., 2007).

2.3.3.2 THE SUTURE-ZONE

At the east of the Ho gneiss (external nappes) is the suture zone of the Dahomeyan Structural Unit which marks the boundary between the authochthonous West African Craton and the exotic rocks of the Dahomeyan. This suture zone is well exposed from SE Ghana to NW Benin and consists of mafic and occasional ultramafic rocks, which display granulite and eclogite facies mineral assemblages (Attoh, 1998; Agbossoumondé et al., 2001; Hirdes and Davis, 2002, Agbossoumondé et al., 2004; Attoh and Morgan, 2004). This zone coincides with a prominent gravity anomaly that can be traced along the entire eastern margin of the WAC (Attoh et al., 2007 and references therein).

Distinctive mafic and ultramafic rock bodies can be traced for about 1000 km within the suture zone. These rocks are the high-pressure (HP) granulites gneisses referred to as the Shai Hills Gneiss in southeastern Ghana (Attoh and Morgan, 2004) and also include the ultrahigh-pressure gneisses of the Adaklu Hills also in southeastern Ghana. These bodies display

contrasting lithological and metamorphic features (Duclaux et al., 2006 and references therein). Granulites, eclogites and amphibolites are tectonically associated.

Along the suture zone, in SE Ghana, deformed alkaline rocks, magmatic carbonatite and ultrahigh-pressure (UHP) rocks occur (Attoh and Nude, 2008; Nude et al., 2009) in association with high-pressure granulites and eclogites of basaltic composition (Attoh and Morgan, 2004; Agbossoumondé et al., 2004). The presence of UHP rocks indicates subduction of the suture zone rocks to mantle depths during the Pan-African orogeny (Attoh and Nude, 2008; Agbossoumondé et al., 2013).

According to Attoh and Nude (2008), the dominant rock unit of the suture zone is composed of mafic granulites in which garnet megacrysts preserve a diagnostic microstructure of UHP metamorphism; it consists of a crystallographically controlled array of exsolved rutile rods in garnet. Metamorphic pressures estimated from Ti concentrations in the inferred precursor garnet indicate P >3 GPa, which requires subduction (and exhumation) of the suture zone rocks to and from mantle depths during collisional orogeny on the WAC margin (Attoh and Nude, 2008).

Within the suture zone extensive shearing has affected the mafic gneiss where it was thrust over the external nappes along a crustal-scale ductile shear zone (Attoh and Nude, 2008). Above this shear zone the granulite facies Shai Hills gneiss was partially retrogressed to garnet amphibolite.

Kinematic indicators and microstructures in the suture-zone nappes and the external zone indicate an early NW-thrusting followed by southerly nappe transport in the southern

Dahomeyides (Attoh, 1990; Castaing et al., 1993). These displacements produced the dominant NE-SW folding and superposed folds with ESE axial surfaces.

Attoh et al. (1997) indicated that the overall structure of the suture zone resulted from early east–west compression, which produced the north–south imbricate thrust slices followed by NNW-directed thrusting in the orogen. Thrust surfaces in the suture zone are characterized by low angle dips.

U-Pb analyses of zircon from the HP granulites by Attoh et al. (1991) gave an age of 610±2Ma which was interpreted as the time of peak metamorphism. Hirdes and Davis (2002) reported U-Pb analyses of zircon from the same HP garnet granulite unit with the youngest analysis yielding an age of 603±5Ma close to the time of peak metamorphism, while Affaton et al. (2000) published a zircon evaporation ($^{207}Pb/^{206}Pb$) age of 613±1Ma for the suture zone rocks in northern Togo. Hornblende separates from the mafic granulites yielded $^{40}Ar/^{39}Ar$ ages between 587 and 567 Ma, interpreted as the time of exhumation of the nappes (Attoh et al., 1997). These ages confirm HP metamorphism of the suture zone garnet granulites and eclogites around 603–613 Ma and exhumation through the hornblende blocking temperature of ∼600 ◦C by ca. 580–570 Ma (Hirdes and Davis, 2002). Thermobarometric calculations and phase equilibria considerations of the suture zone rocks at Shai Hills by Attoh (1998) suggest that the rocks preserve a record of: (1) prograde garnet crystallization during eclogite facies metamorphism as temperature increased to a maximum of about 600°C and pressure reached at least 18 kbar, followed by; (2) high-pressure granulite facies metamorphism when temperatures reached 800–900°C at about 14 kbar, resulting in partial melting to produce leucocratic veins, followed by; (3) decompression along a retrograde path down to about 700°C at about 10 kbar.

2.3.3.3 THE INTERNAL NAPPES

To the coterminous east and in tectonic contact with the suture zone rocks are the felsic gneisses and migmatites of the internal nappes of the Dahomeyide which represent the Benin-Nigeria basement. These granitoids to the east of the suture zone are postulated to be juvenile crust representing the arc terrane that formed during subduction and oceanic closure (Attoh et al., 2013).

Granitoid gneisses exposed east of the suture zone comprise the Accra Plains allochthon (Attoh et al., 1997) and have been subdivided into two units: (i) biotite migmatite and (ii) the Dzodze gneiss (to the east). The migmatite was intruded by synkinematic porphyritic- granitic gneiss with aplitic veins and was thrust over the suture-zone nappes. The prominent regional structure of the migmatitic gneiss is a shallow (20°-30°) SE-dipping foliation apparently developed during NW-thrusting (Attoh et al., 1997).

According to Attoh et al. (2013), two main types can be distinguished among the granitoid gneisses of the internal unit: (i) Dioritic gneiss characterized by hornblende as the main mafic mineral and occasional garnet and (ii) Migmatitic gneiss with biotite as the dominant mafic mineral. The migmatites also include highly-strained granitoids known as the straight gneiss with muscovite and are in tectonic contact with the suture zone rocks.

The straight gneiss forms just east of the suture zone and records U–Pb zircon ages ranging from 615 to 589 Ma (Attoh et al., 2013). This age range is similar to the metamorphic crystallization age of the suture zone rocks. On the other hand, Attoh et al. (2013) also recorded U-Pb zircon crystallization ages ranging from 2.19 to 2.14 Ga for the dioritic gneiss of the internal unit.

2.3.3.4 REVIEW ON GEOCHEMISTRY OF HP GRANULITE

The composition of the lower continental crust is of keen interest in geochemical models of the bulk earth and of the tectonic evolution of the continents. It is widely considered that high-pressure (HP) granulite facies rocks, which formed under lower crustal conditions, permit direct sampling and analyses of surface outcrops to estimate lower crust composition (e.g., Rudnick and Fountain, 1995) allowing evaluation of various models of the composition of the lower crust.

Geochemical investigations on high-pressure granulites carried out by Attoh and Morgan (2004) suggest that these rocks have preserved the geochemical imprints of their magmatic protoliths and display REE and trace element patterns quite similar to mafic lower crust composition. Moreover, they concluded that the HP granulites were derived from two types of tholeiitic magmas: dominantly island arc tholeiites (IAT) together with subordinate N-MORB tholeiites. The former show peculiar LREE enrichment with flat $[La/Yb]_N$ patterns where the latter are slightly depleted in LREE and have low $[La/Yb]_N$ relative to the lower crust and no europium anomaly.

Bernard-Grifiths et al. (1991) carried out geochemical investigations of eclogite facies and associated metamorphic rocks from the suture zone in Togo and reported REE concentrations in eclogites and garnet granulites. It was suggested that the REE variation patterns of the eclogites apparently reflected significant LREE loss, but in the case of the eclogitic rocks from the Kabye Complex in northern Togo, the REE patterns were compatible with a magmatic protolith typical of cumulate rocks. Bernard-Grifiths et al. (1991) also reported whole-rock Nd isotopic compositions of eclogite samples that yielded εNd values of ~ +7 for model age

(TDM) ~ 1150 Ma which they interpreted as evidence for depleted mantle source. U–Pb analyses of zircon separated from the eclogites in southern Togo were discordant with a lower intercept of ~ 640 ± 53 Ma. This age, together with Rb–Sr whole-rock and mineral age of 598 ± 12 Ma, suggest that metamorphic recrystallization occurred ca. 600 Ma, whereas the model age of 1150 Ma suggests that the mantle derivation of the protoliths of these rocks may have occurred significantly earlier (Attoh and Morgan, 2004 and references therein).

Geochronological and petrological studies of the suture zone mafic gneisses provide further constraints on the chronology of the tectonic and metamorphic record in the Dahomeyide orogen (Attoh et al., 1997). For example, zircon separated from mafic granulites in the Ghana segment of the suture zone yielded the concordant U–Pb age of 610 ± 2 Ma (Attoh et al., 1991) and this is interpreted as the peak metamorphic age, consistent with $^{40}Ar/^{39}Ar$ ages of hornblendes from amphibolites that indicate exhumation around 582–587 Ma following metamorphic peak ca. 610 Ma. Hirdes and Davis (2002) have also reported new U–Pb zircon and rutile ages which confirm peak metamorphism occurred ca. 600 Ma.

New geochemical data and interpretation of UHP granulite and eclogite from Adaklu will provide the opportunity to compare and confirm works already done in other portions of the suture zone like Shai and Lato Hills.

2.3.3.5 GEODYNAMIC SETTING

The context of geodynamic setting of the mafic-ultramafic rocks of the suture zone has been a subject of various interpretations. From the estimation of the crystallization conditions of various eclogitic assemblages of the suture zone in south Togo, Agbossoumondé et al. (2001)

proposed two units (lower and upper) which display different decompression paths. According to these authors, the upper unit underwent coeval decompression as the lower unit was transformed to granulite/high-pressure amphibolite-facies (8 ± 2 kbar; 720 ± 60°C), then to amphibolite (5 ±1 kbar; 560 ± 60°C) and finally greenschist facies conditions (3 ± 1 kbar; 475 ± 25°C). They proposed that the P-T evolutions of these eclogite assemblages support a dynamic change from subduction to continental collision during the formation of the Dahomeyides.

Moreover, the geochemical signature (E and T-MORB) of the protoliths of the Lato Hills eclogites, together with their close association with clastic sediments of continental origin, suggests an extension related setting, continental rift or narrow ocean (Bernard-Griffiths et al., 1991; Agbossoumndé, 1998).

In order to explain the existence of two types of metabasites in Togo, Agbossoumondé et al. (2004) proposed that the Agou massif corresponds to basic magmas emplaced and cooled at the base of an active continental margin whereas the eclogites reflect subduction of the passive margin of the WAC.

Agbossoumondé et al. (2013) proposed that the geochemical signatures of the parental magmas of the granulites of the Agou Igneous Complex (AIC) of the suture zone in southern Togo are consistent with an active continental margin environment. Major and trace element data including REE presented by Agbossoumondé et al. (2013) indicate that the Agou Igneous mafic rocks have a magmatic arc signature.

Geochemical data presented by Attoh and Morgan (2004) show that the high-pressure mafic granulites of the Pan-African suture zone have major and trace element concentrations and

patterns that are similar to those of the mafic lower continental crust. According to them, the suture zone mafic granulites consist largely of rocks with Island arc tholeiitic (IAT) affinities but also include suites of rocks with oceanic crust (N-MORB) geochemical signatures. This association of rock suites with IAT and N-MORB imprints suggests the existence of a subduction zone complex where oceanic crust may have formed in either a back-arc basin or intra-arc basin environment (Pearce et al., 1984).

Studies on the geodynamic setting of the suture zone rocks in West Africa is thus still required. Less work on the geodynamic setting on these mafic-ultramafic rocks of the suture zone has been carried out. All these few works carried out are mostly on the rocks in Togo with little or no work done on those in SE Ghana, precisely Adaklu. There is therefore the need to look into the petrology together with structures and geochemistry of these rocks in Adaklu (which is sandwiched between Shai and Lato Hills) in order to decipher the geodynamic setting and model of these rocks and compare to the previous works done on the Shai and Lato Hills.

CHAPTER THREE

METHODOLOGY

3.1 PRE-FIELD STAGE

3.1.1 Desk study

According to planned schedule, a desk study was carried out before reconnaissance and the main field work. Literature review was carried out to have the basic knowledge of the study area and also on previous works carried out in the area. Relevant literature such as articles as well as useful existing books about the study area were read and reviewed.

This stage included acquisition of topographical and regional geological maps as well as aeromagnetic data of the study area. These topographic/base maps and aeromagnetic data were digitized and processed respectively and studied so as to become very familiar with the area. This also aided in informing the strategies and methods that could be used in the main field stage and also for choosing a suitable site for setting up the base camp.

Acquisition of standard geological tools was done at this stage. During preparation prior to the main field stage materials such as the topographic maps, Global Position System (GPS), field notebooks, field boots, field kits, geological harmer, sample bags, dilute Hydrochloric acid (HCl), tape measure, camera and all other materials/tools needed for the field work were acquired and organized.

This stage included strategic planning for both main field and post-field stages and drawing of work schedules for the whole research work.

3.1.2 Aeromagnetic Data and Processing

The aeromagnetic geophysical survey data was obtained from the Ghana Geological Survey Department. The geophysical data was acquired in 1999/2000 by High Sense Geophysics Inc. of Canada at an altitude of 60 metres with flight line trending east to west spaced 400 m apart. The geophysical aeromagnetic image used for this work has already been processed to show total magnetic intensity (TMI) of the study area (Fig. 4.1). Options like minimum curvature, bi-directional gridding, tinning and kriging were used in gridding the magnetic data from the OASIS MONTAJ geophysical programme.

Gridding was the first step used to level the magnetic data. This method quality controlled the data by way of their display as enhanced images. The gridding provided smooth surfaces to the original point located data. This was done by using the minimum curvature and bi-directional line gridding tools from the Oasis Montaj 7.0 geophysical program.

Several enhancement tools and processes from the Geosoft Oasis Montaj software package were used to enhance the data to produce located profiles and grid versions in the form of images for the total magnetic intensity (Milligan and Gunn, 1997). These enhancement processes applied to the aeromagnetic data, Automatic Gain Control, first vertical derivative, reduction to the equator. The World Geodetic System (WGS) 84 Universal Transverse Mercator (UTM) Zone 30 coordinate system was used as the projection system for the processing with the units in metres. The datum used is WGS 84 (world). The limits used for the processing were:

Minimum X: 468500, Minimum Y: 663200, Maximum X: 583100 Maximum Y: 829100 with grid size of 100 metres.

Pre-processing by way of linear filtering process was done on the geophysical magnetic image to remove magnetic anomalies from the initial grid data based on the disparity in the average frequency content of the noise anomaly (Milligan and Gunn, 1997). This was done since irregularities from superficial sources have higher frequencies than anomalies from deeper sources. The linear filtering was done by running a series of Fourier transforms on the magnetic grid data set. The pre-processed magnetic grid data or image was reduced to the pole (Fig. 4.1) using inclination and declination values of -16.11 and -6.14 respectively. The data was also reduced to the equator. This makes the data easier to interpret without losing any geophysical meaning.

The first vertical derivative filter was also applied to magnetic field intensity data to aid in the enhancement of shallow geological structures from the data (Fig. 4.2). The first vertical derivative values of the magnetic field were computed directly from the gridded total magnetic field using fast Fourier transform. The second vertical derivative was applied to the total magnetic field to enhance near surface features, anomalies and to remove higher frequency from the image. This helped to mark out features with different susceptibilities. The vertical derivatives were important because lithologic contacts with contrasting magnetic susceptibilities are easy to delineate precisely.

3.2 FIELD WORK

The field work stage started with field reconnaissance which helped in self-familiarization to the field. During the reconnaissance stage all geological compasses were corrected, pace was checked and field orientation and positioning were also checked. The correction and setting of

the magnetic declination of the geological compass was done to ensure that the geographical north conforms to the grid north of the base map. The pace and compass method was used because it is one of the most efficient and cheaper methods used during the field mapping process. The compass was used alongside to give accurate direction of traverse while pacing. This method relies on the use of datum points which are reference points which can be located on the map and on the ground. From a known datum point, the number of steps taken is multiplied by an individual's pace to get the total distance covered to a location to the other. This helped to know the distance covered from one outcrop to the other.

The Global Positioning System (GPS) was also used to help in the traverse. The GPS showed the position in terms of WGS 84 georeferenced coordinates at any point in the field. The GPS was also the only tool which was used to take all geographical location of every outcrop encountered on the field. It also provided the records of traverse, distance from one station to the next and also the elevation of every station.

At every location of an outcrop or a station, self-positioning/orientation and taking of geographic location/coordinates were the first to be carried out. This was followed by macroscopic or mesoscopic observation and description of the rocks. This was done to review all obscure features which could not be seen when very closer observation of the outcrops was made. Then after hand specimen description of the rocks was also carried out. The description of the rocks was done with respect to colour, mineralogy, structures, size and location. It involved petrographic studies which comprised various systematic procedures taken at every outcrop. Petrographic description and recording of data and information into the field notebook and on and also maps were performed.

Structural observations, description, measurements and recording of data and information into notebooks and onto maps were then followed. Recognition, description and naming of various structures, rock units, and associated boundaries were also carefully done. Detailed description of all various structures present were made, followed by the measurement of attitudes of each structure. Most measurements done in the field were the structural and geometric measurements. The geological compass aided in the structural measurements. Structures measured on the field were foliations, joints, lineations, faults, fold axes, fold limbs, and other geological structures. In the structural measurements the main attitudes measured were the strike and dip of planar structures in the rocks and also trend and the plunge of lineations were also measured. For geometric measurement the surveyors' tapes and rulers were used. These measurements include measurement of the length and width of outcrops, the height of folds and the thickness of foliations and some mineral grains. All measurement data is recorded in the field note book. Taking photographs and making sketches of features accompanied with descriptions, measurements and interpretations were made. The features of which the photographs were taken were described in the notebook with the direction the photograph was taken.

Taking fresh, oriented, and representative samples was done by manual means. This was done with the help of the geological hammer. The kind of sampling strategy applied on the field was "Point Sampling" - where a single outcrop sample was taken manually from the outcrop at a particular spot in the rock exposure usually using geological hammer. Any sample taken was usually selected to represent the typical features of the geological material rather than the mass or volume. Oriented samples were taken by marking the structural attitudes of the samples before taking them. The samples were then knocked out from the outcrops with the help of the

geological hammer after which sample names were put on them with a permanent marker pen. The samples were put in the sample bags. All information and sampling data were entered into the field notebook. Sampling was purposely made for further petrographic and mineralogical study of the rock, for microscopic study and also for geochemical analysis of the rocks. A total of 45 representative samples were collected from 41 stations in the study area (Fig 4.3).

3.3 POST FIELD WORK

The post field stage of the research included thin-section preparation, petrographic studies/analyses, and preparation of samples for whole-rock geochemical analysis.

3.3.1 Thin Section Preparation

The 45 samples brought from the field were resampled to get 40 best representative samples for thin-section preparation and petrographical analysis at the Department of Earth Science Petrological Laboratory, University of Ghana.

These 40 rock samples were cut into smaller rectangular blocks (billets) with a diamond bladed rock saw. Surfaces of the rectangular blocks were ground flat and smoothened using silicon-carbide powder. The smoothened surface of the blocks were mounted on glass slides using Canada balsam. The other surfaces were polished and ground down with silicon carbide powder grade 80 until the rocks became thinner. Finer abrasives were progressively used as the section became much thinner. Six hundred (600) silicon carbide powder was used at the later stage of grounding until the thicknesses of the rocks were about 30 microns. Continuous

observation of interference colours of minerals like feldspar and quartz under the petrographic microscope helped in gauging the thicknesses of the sections.

The sections were then covered with a glass cover-slip cemented with Canada balsam after carefully clearing and scraping away excess cement. A total of 40 thin sections were produced and examined using an optical polarizing microscope for petrologic and microstructural analyses.

3.3.2 Petrographical Analyses

Quantitative and descriptive petrographic analyses of the 40 prepared thin sections were done with a petrographic/polarized microscope. These were done to help in the identification of minerals and microstructures to buttress the mesoscopic observations made on the field. Quantitative description of the thin section incorporated modal analysis, and textural analysis (including grain size, shapes, orientation, inclusions of mineral grains, mineral overgrowth and intergrowth textures as well as their associations).

The Pelcon Automatic Point Counter was used to determine the modal percentages of the minerals under the petrographic microscope. Photomicrographs were taken of each thin section examined using the Amscope software and its camera which was fixed to the microscope and a laptop.

The appropriate rock names were given to the different rocks encountered in the field after careful mesoscopic (hand specimen) observation and modal analysis of the rocks.

3.3.3 Whole Rock Geochemical Analyses

3.3.3.1 Samples Preparation

Twenty-six (26) representative and fresh and homogeneous samples were resampled from the 40 samples after petrographical studies for geochemical analysis. These 26 samples were cut into 6 cm by 4 cm by 2 cm rectangular blocks with a diamond bladed rock saw at the Department of Earth Science Petrological Laboratory, University of Ghana. The samples were labelled, packed in a box and transported to ALS Laboratory in Kumasi, Ghana for sample preparation. The samples were sent to ALS Laboratory in Vancouver, Canada where the geochemical analysis was carried out.

3.3.3.2 Analytical Techniques

Analytical techniques followed protocol of the procedures at ALS Laboratory. Major and trace elements analyses were carried out by Inductively Coupled Plasma-Atomic Emission Spectrometry (ICP-AES) and multi-elements fusion Inductively Coupled Plasma Mass Spectrometry (ICP-MS) respectively for the 26 prepared samples in Vancouver, Canada. Loss on ignition was determined at 100°C.

A mixture of about 0.200 g of prepared samples and lithium metaborate was fused in a furnace at 1025 °C for major elements analysis. The resulted melt was then cooled and dissolved in an acid mixture of nitric, hydrochloric and hydrofluoric acids. This solution was then analysed by ICP-AES for the major elements composition of the various rocks.

All procedures and protocols observed for the major elements analysis were also repeated for the trace elements analysis. However, the prepared samples for trace elements analysis weighed 0.100 g and the analysis was carried out with the ICP-MS.

Base metals were also analysed using the ICP-AES. A prepared sample of weight 0.25 g was digested with perchloric, nitric, hydrofluoric and hydrochloric acids. Dilute hydro chloric acid was then added to the residue and the solution was analysed by the ICP-AES.

Results obtained were corrected for spectral inter-element interferences (ALS laboratory). Precision is better than 2%.

3.3.3.3 Data Analyses

The results/data obtained from field work and laboratory work were compiled into tables, maps, graphs and diagrams.

These were done with the aid of computer software as MapInfo Professional 11.5, Delta graph, CorelDRAW X4, Petrograph (version 2 beta), Microsoft Excel 2013, Stereographic Projections (version 1.00) and Geochemical Data Toolkits (GCD kits 2.3).

MapInfo Professional 11.5 was used in the digitization of all the maps including the base and composite geological maps as well as the cross-section of the study area. Statistical analysis of the structures was done with the aid of the Stereographic Projections (version 1.00) and Microsoft Excel 2013.

CHAPTER FOUR

RESULTS

This chapter discusses the results of various observations made during the field work and laboratory work. The results are grouped into petrography, structures and geochemistry.

4.1 Results of Aeromagnetic Data

The processed aeromagnetic data obtained from the Ghana Geological Survey show the total magnetic intensity of the study area (Fig. 4.1). Total magnetic intensity image which has been reduced to pole and shading from northwest shows different shades of colours which give an indication of different magnetic signals displayed by the various lithologies in the study area. The area is largely characterized by low to high magnetic anomalies.

The first and second vertical derivatives helped in the enhancement of shallow geological structures (Fig. 4.2). All the structural lineaments which were enhanced by this technique have a unique north-east trend which confirms the general trend of the rocks in the area as observed during field mapping. The first vertical derivative increased the sharpness and visibility of structural grain in the magnetic grid data by emphasising higher amplitudes and higher frequencies. The sudden break in a magnetic intensity may be as a result of discontinuities or faults within the rock bodies. At southeastern corner of the first-vertical derivative image (Fig. 4.2) is the major shear zone between the mafic/ultramafic suture zone rocks and the migmatite gneisses of the internal unit of the Dahomeyide, east of the suture zone.

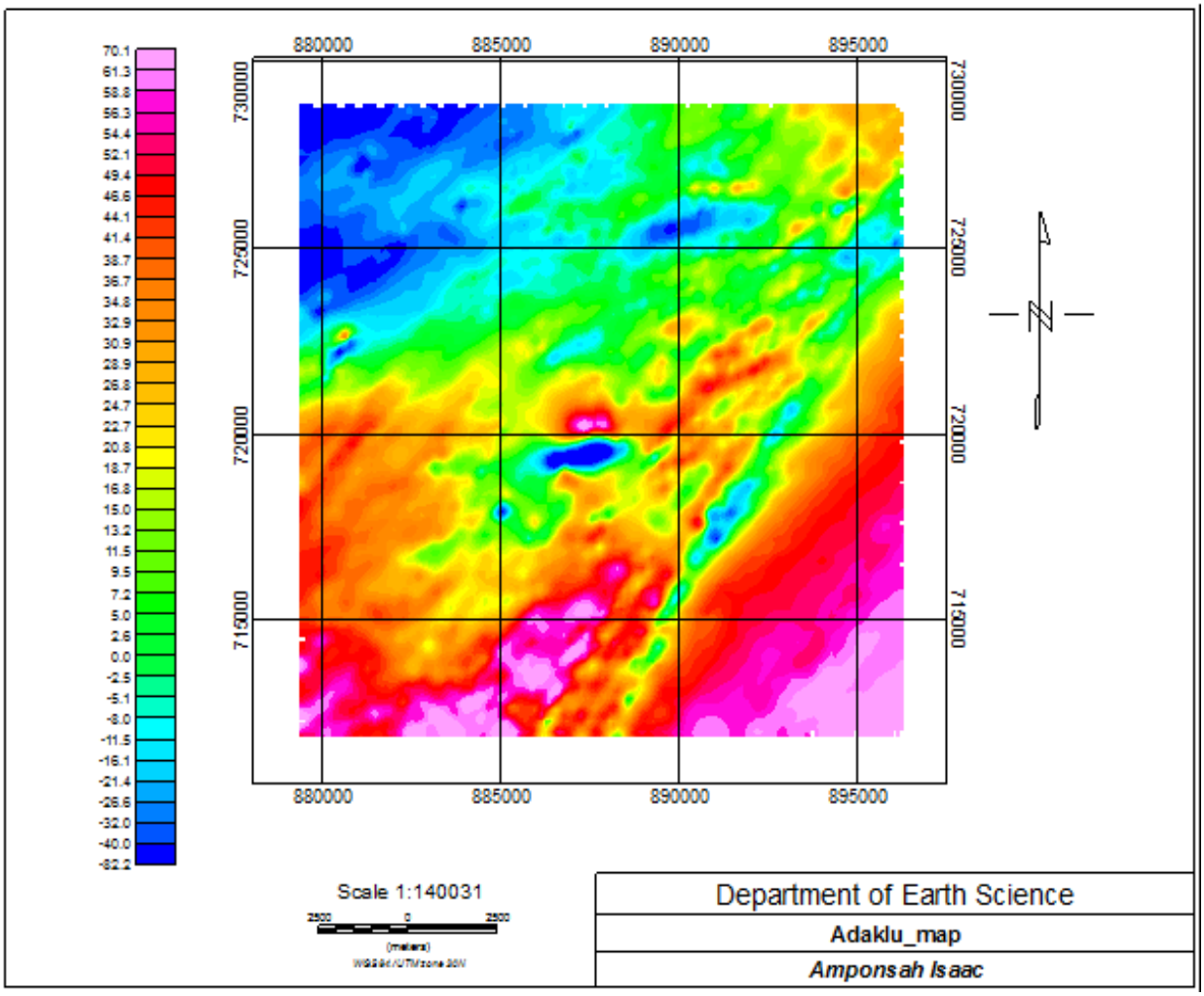

Fig. 4.1. Total magnetic intensity image of the study area which has been reduced to pole and shading from northwest. The unit for the colour bar is in nT. Different colours show different magnetic signals displayed by the various lithologies in the study area.

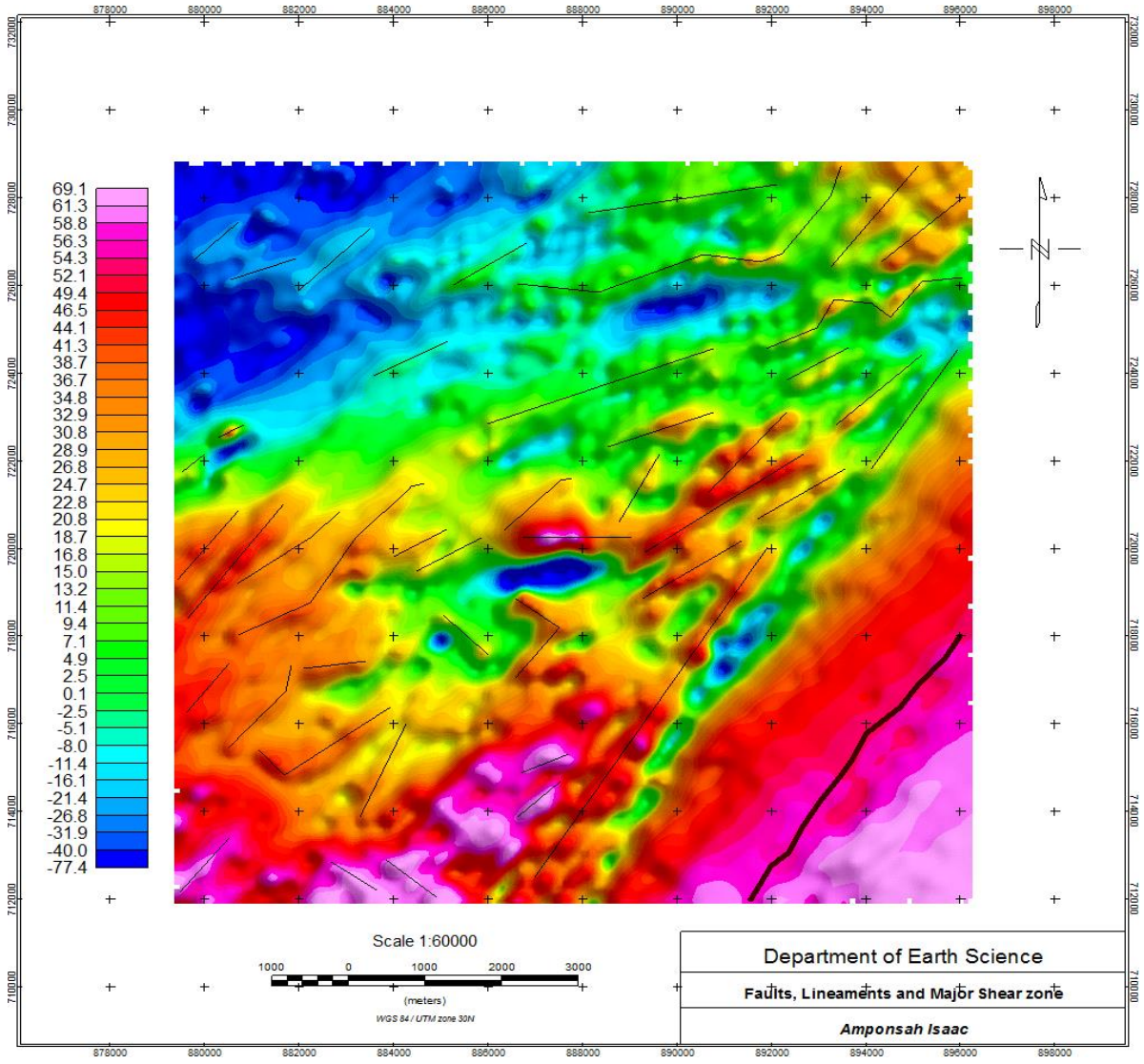

Fig. 4.2. First vertical derivative image of a reduce-to-pole data of the study area showing the various domains and lineaments within the study area. The figure also shows (at the southeastern corner) a major shear zone between the suture zone rocks and the migmatite gneiss of the internal unit of the Dahomeyide.

4.2 Field Relations

The outcrop map which shows various sample locations of the different rocks is shown in Fig. 4.3. The study area is characterized by garnet-rich and garnet-poor mafic/ultramafic rock bodies. These mafic/ultramafic rock bodies include different types of HP garnet-gneisses and eclogite as well as pyroxenite – the only igneous plutonic rock in the study area. From petrographic studies five different rocks were identified. These are the hornblende-garnet-pyroxene gneiss, hornblende-bearing gneiss (felsic gneiss), pyroxene-garnet-hornblende gneiss, eclogite and pyroxenite (Fig. 4.3). These rocks were classified based on their texture and mineral compositions from both mesoscopic and microscopic observations. The modal composition (abundances - %) of the minerals in the various rocks are shown in Table 4.1.

Lithologic contacts between the hornblende-bearing gneiss and the hornblende-garnet-pyroxene gneiss as well as the eclogite were observed at the SW of Abudai and at Torkor respectively. The hornblende-garnet-pyroxene gneiss is overlain by the hornblende-bearing gneiss at SW Abudai (Fig. 4.4). At Torkor the highly deformed and sheared hornblende-bearing felsic gneiss has under-thrust the ultramafic rock in the area (eclogite – Fig. 4.5). Rock types observed at the lithologic contacts are mostly sheared. There is also an inferred contact between the pyroxenite and hornblende-garnet-pyroxene gneiss between Sikaman and Helekpe (Fig. 4.3) as the pyroxenite observed at this location is sheared.

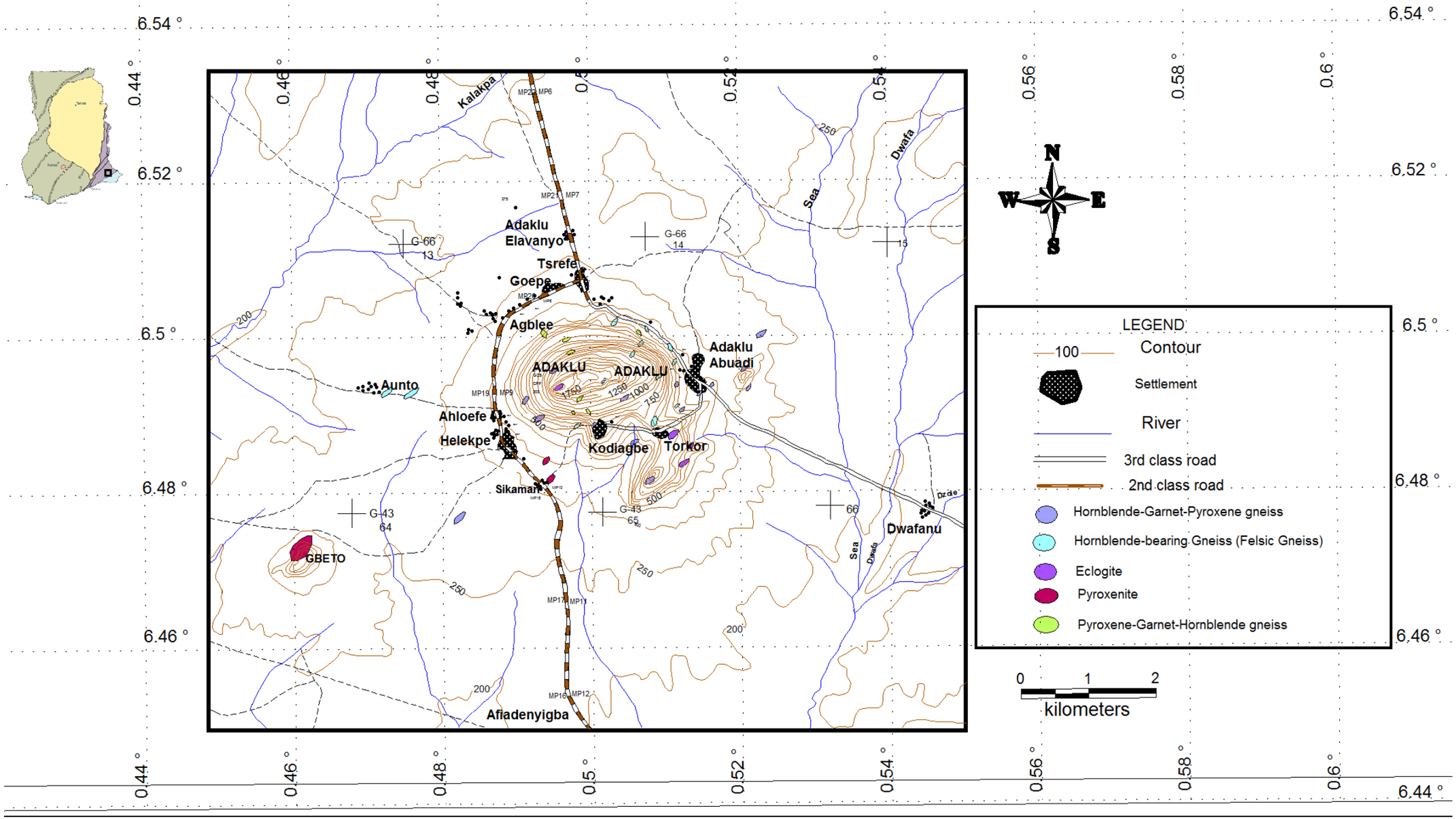

Fig. 4.3. Topographical map showing various outcrop/sample

Fig. 4.4. Lithologic contact between hornblende-bearing gneiss and hornblende-garnet-pyroxene gneiss at SW Abuadi (hornblende-garnet-pyroxene gneiss dips below the hornblende-bearing gneiss). Picture taken in SE direction.

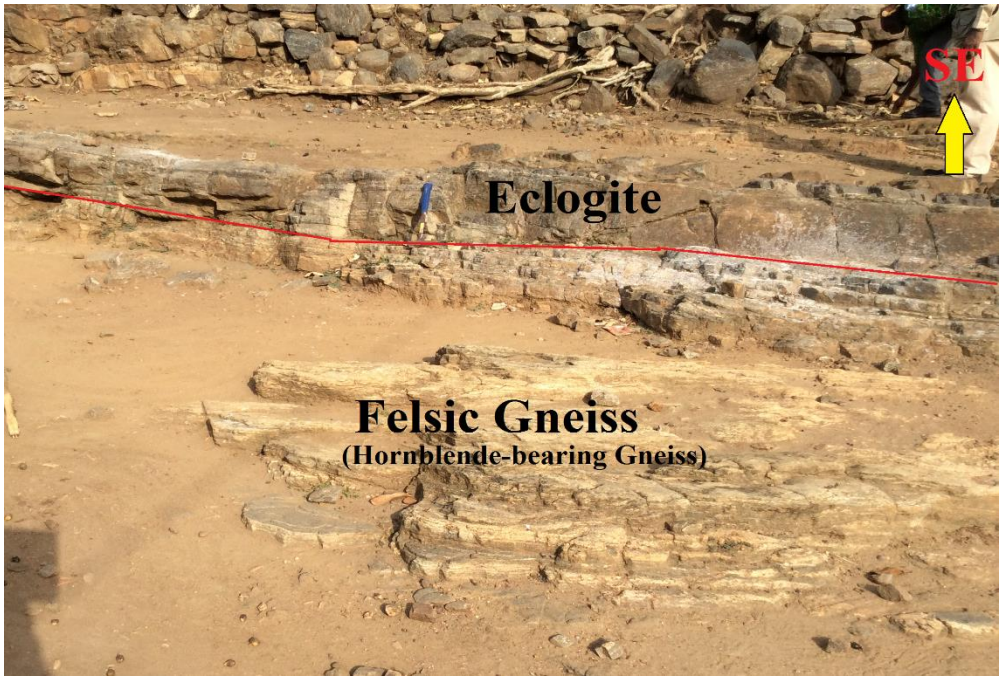

Fig. 4.5. Lithologic contact between the hornblende-bearing gneiss and eclogite at Torkor. The hornblende-bearing gneiss has under-thrust the eclogite. Both rocks are sheared. Picture taken in SE direction.

4.3 PETROGRAPHY

4.3.1 Hornblende-Garnet-Pyroxene Gneiss

This mafic gneiss is the dominant rock in the study area. It covers entirely every portion of the study area. Outcrops of this rock can be observed at a quarry south-east of Abuadi towards Dwafanu and Helekpe (Fig. 4.3). The rock was observed at stations IKE1, IKE2B, IKE2C, IKE5, IKE6, IKE9, IKE11, IKE12, IKE14, IKE18, IKE29, IKE33, and IKE37. The rock is dark-gray in colour with medium to coarse mineral grains (Fig. 4.6a). The rock is weakly foliated and banded and hence exhibits gneissic texture. It is a garnet-rich gneiss with numerous garnet porphyroblasts (Fig. 4.6b). Most conspicuous and characteristic of this group of rocks is the presence of garnet porphyroblasts, their size, orientation, distribution and abundance in which they occur in relation to the rock as whole as well as the other individual minerals. From hand specimens, the garnet crystals are subdivided according to size as minute to small (0.5-2 mm) being barely visible to visible, small (2-4 mm), medium (4-6 mm) and large (more than 6 mm). This notwithstanding, some porphyroblasts which are not all that rare were observed with a diameter size of about 50 mm or 5 cm. This rock has carbonate and quartz veins which run through mostly its joints (Fig. 4.41a, and 4.41b). Some garnet porphyroblasts are also retort-shaped. Hence the rock contains pre-tectonic to post-tectonic garnet grains.

The hornblende-garnet-pyroxene gneiss is composed primarily of plagioclase (albite and anorthite but dominantly anorthite), quartz, clino-pyroxene (diopside), hornblende, and garnet. These primary minerals have either been partially or completely replaced by secondary minerals like chlorite, epidote and calcite (Fig. 4.7a). The rock also contains scapolite which

occurs as an accessory mineral (Fig. 4.7b). The garnet porphyroblasts have inclusions of other minerals like pyroxene, hornblende, plagioclase and even quartz. The scapolite observed also contains some inclusions of pyroxenes. These inclusions in the porphyroblasts give the rock a poikiloblastic texture. Hence this gneiss exhibits gneissic and poikiloblastic textures with sutured to sub-sutured grain boundaries. The garnet porphyroblasts also exhibit rutile exsolution and fractures with lineated pre-kinematic grain inclusions and foliation is wrapped around garnets. Grains are somewhat stretched and elongated and are mostly anhedral to subhedral. Quartz grains are mostly polycrystalline and exhibit undulatory (undulose extinction). The calcite grains are also associated with the garnet grains (mostly developed around the garnet porphyroblasts) (Fig. 4.10a). Other textural features observed include corona textures around the garnet porphyroblasts and other embayment features – inclusions in garnet exhibit resolved and embayed textures (Fig. 4.8a, 4.8b, 4.9a and 4.9b). Chloritization and epidotization are the main alteration features observed under the microscope. Some pyroxene grains however have been partially or completely altered into hornblendes. Some deformational features are evident by some bent garnet porphyroblasts observed from the microscopic analysis (Fig. 4.10b).

Fig 4.6. Field photos of (a) dark-gray foliated and banded hornblende-garnet-pyroxene gneiss observed at a quarry east of Abuadi; (b) hornblende-garnet-pyroxene gneiss observed at Helekpe. The gneiss shows conspicuous garnet porphyroblasts and different sizes of garnet grains.

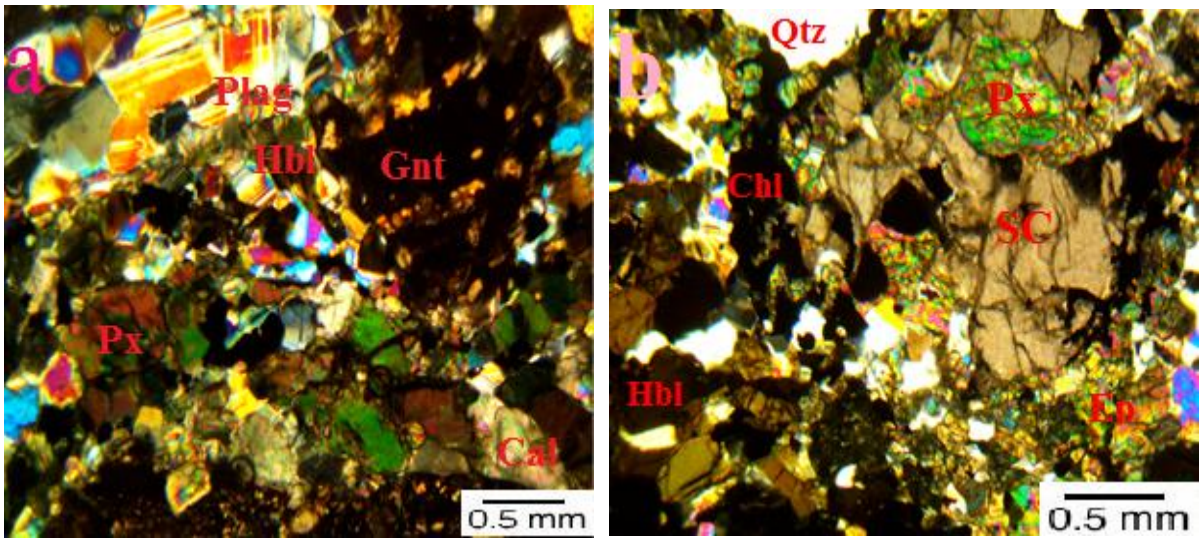

Fig. 4.7a and 4.7b. Photomicrograph of weakly foliated and banded hornblende-garnet-pyroxene gneiss composed of Px – pyroxenes (cliopyroxene – 30%), Gnt – garnet – 20%, Hbl – hornblende – 15%, Plag – plagioclase – 10%, Qtz – quartz – 10%, Sc – scapolite – 2%, Cal – calcite – 4%, Chl – chlorite – 5% and Ep – epidote – 3%. Scapolite contains inclusions of pyroxenes (a = XPL) and (b = XPL).

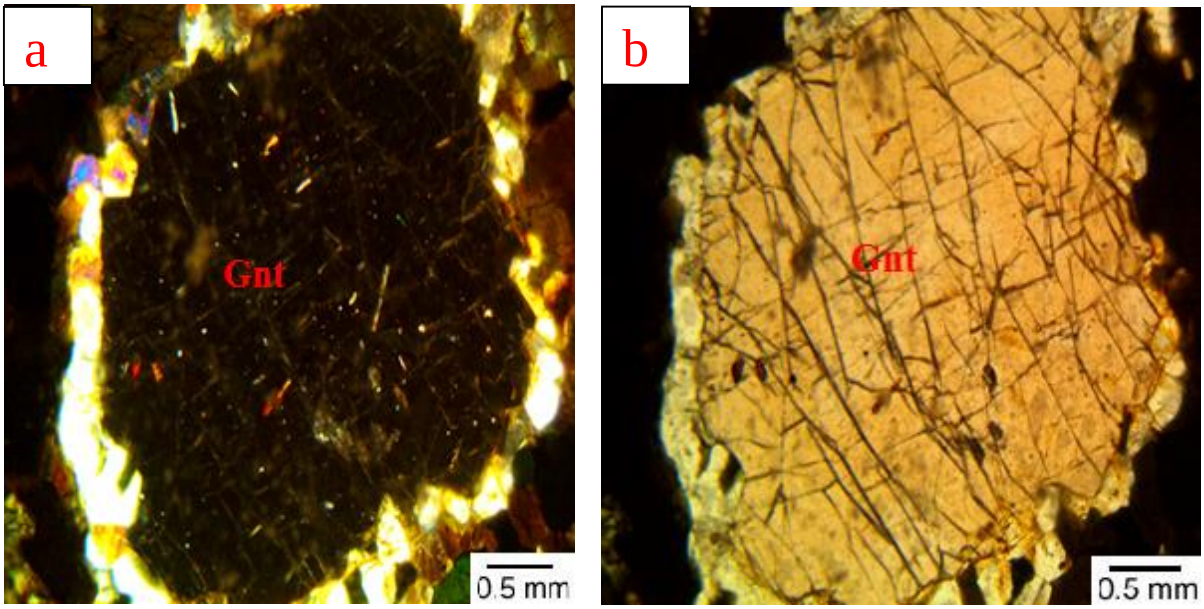

Fig. 4.8a and 4.8b. Corona texture observed under cross and plane polarized light around garnet porphyroblast exhibiting rutile exsolution. Around the garnet porphyroblast is an intergrowth of quartz which formed as a result of chemical reaction between garnet and pyroxene (a = XPL) and (b = PPL).

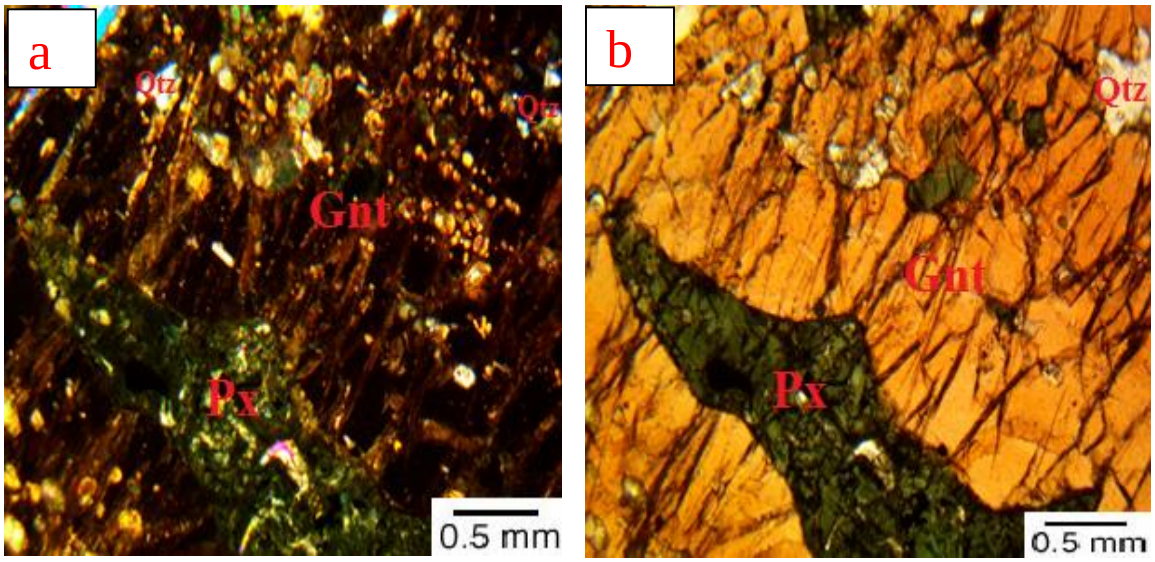

Fig. 4.9a and 4.9b. Photomicrograph of the hornblende-garnet-pyroxene gneiss showing resolved and embayed textures of mineral inclusions in garnet porphyroblast (a = XPL) and (b = PPL).

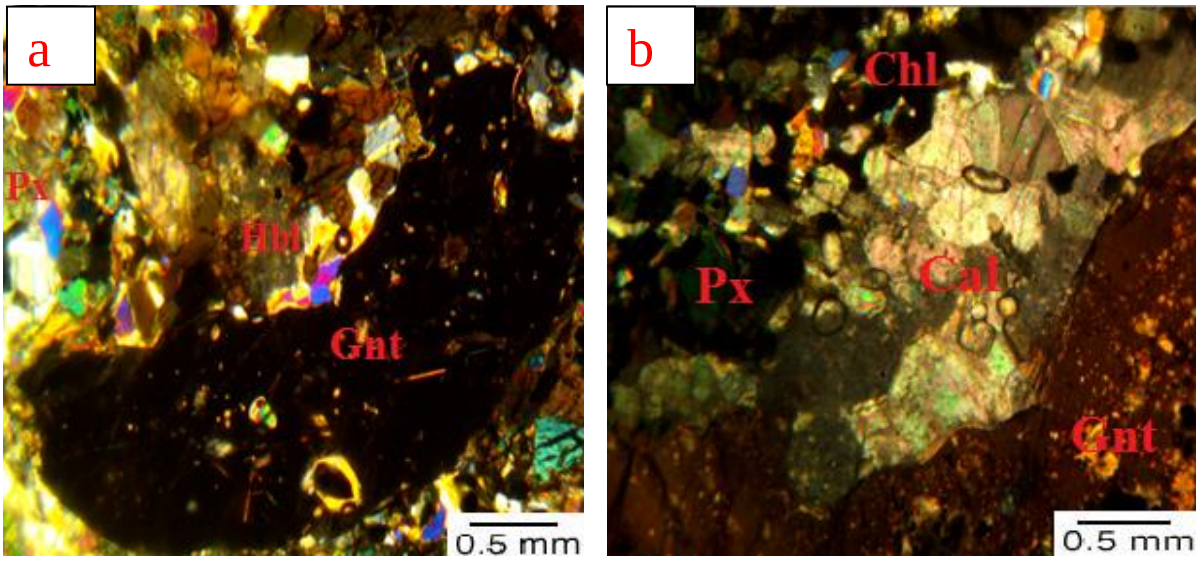

Fig. 4.10a & 10b. Photomicrograph of hornblende-garnet-pyroxene gneiss showing (a) bent garnet porphyroblast (Gnt) with inclusions of pyroxene and few smaller rods of rutile (XPL); (b) Calcite (Cal) grains associated with garnet porphyroblast (mostly observed around the garnet grains) – PPL.

4.3.2 Hornblende-bearing Gneiss

The hornblende-bearing gneiss is a felsic gneiss which is the second dominant rock. It outcrops at the central portion of the area – central to eastern portion of the Adaklu Inselberg and also at the west to north-west portion of the area (Fig.4.3). The rock was observed at stations IKE2, IKE4, IKE7, IKE15, IKE16, IKE17, IKE19, IKE20, IKE21, IKE22, IKE23, IKE24, IKE25, and IKE26. The rock is dark-gray with visible medium to coarse minerals (Fig. 4.11a). It is foliated and beautifully banded (exhibits gneissosity – Fig. 4.11a and 4.11b) and also shows flow texture. This rock is garnet-poor; nonetheless, it has very large garnet grains which can be of diameter of 6 cm scattered in the rock (Fig. 4.56c and 4.56d). Some of these garnet porphyroblasts have symmetrical and asymmetrical tails with inclusions of hornblende and quartz with foliation wrapped around them. This rock is strongly sheared and folded in some

areas like Torkor and has boudins of ultramafic rocks in it (Fig. 4.12a and 4.12b). The rock is deformed and folded in most places of the study area.

From microscopic analysis it was observed that this rock is banded, foliated, highly deformed and not very rich in garnet. Portions of this rock are highly milled and sheared and exhibit mylonitic texture with fine to medium grains (Fig. 4.13a and 4.13b). Minerals observed under the microscope are quartz, hornblende, plagioclase (albite), garnet, biotite and secondary alteration minerals like chlorite and sericites (Fig. 4.14a and 4.14b). Zircon is also an accessory mineral observed under the microscope (Fig. 4.15a and 4.15b). The minerals are stretched and highly strained with sutured grain boundaries and recrystallized grains. Quartz are mostly polycrystalline and exhibit undulose extinction. Garnet (micro-lithons) are medium to coarse grained, elongated and fragmented with foliation wrapping round them. Coarse grained garnet porphyroblasts have inclusions of quartz and hornblende. Hornblende and biotite are aligned in a preferred orientation along the foliation plane. Main alteration features include chloritization and sericitization. Some hornblende crystals have been partially or completely altered into chlorite and biotite (Fig. 4.17a). Albite (plagioclase) have been partially altered into sericites. Some biotites have also been altered into chlorites. Most biotites which have replaced the hornblendes exhibit pseudomorph of the hornblendes. Reaction rims of hornblende due to alteration was also observed (Fig. 4.17b). Pyroxenes in this rock have also been replaced by the hornblendes which also shows pseudomorph of the pyroxenes in some cases.

The hornblende-bearing gneiss is deformed and shows deformational features like micro-faults and micro-folds under the microscope (Fig. 4.16a and 4.16b). The major micro-fault exhibits

a drag displacement of adjacent micro-blocks of the rock indicating a frictional shear deformation along the fault causing folding as one block was dragged along the fault.

Fig. 4.11. Field photograph of hornblende-bearing gneiss showing (a) dark- gray colouration and penetrative planar foliation planes as well as; (b) beautiful alternating felsic and mafic bands (gneissosity).

Fig. 4.12 (a & b). Strongly sheared and deformed hornblende-bearing gneiss with boudins of ultramafic rock bodies at Torkor.

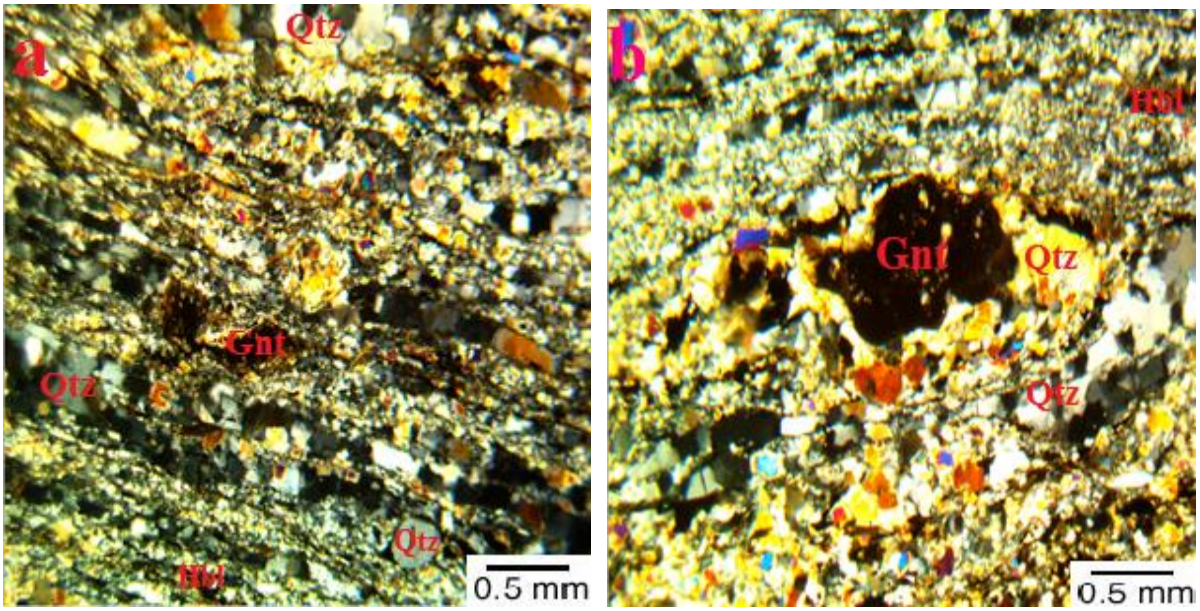

Fig. 4.13. Photomicrograph of highly sheared hornblende-bearing (felsic) gneiss showing mylonitic textures composed of fine to medium grains of Qtz – quartz (45%), Hbl – hornblende (13%), Gnt – garnet (9%). Minerals are milled and stretched. (a=XPL) and (b=XPL).

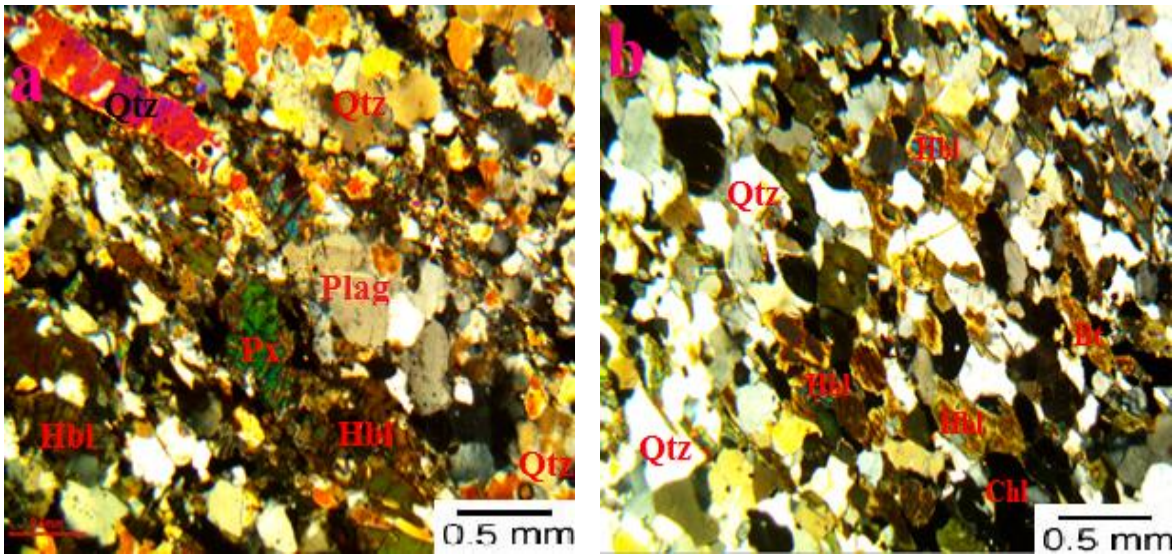

Fig. 4.14. Photomicrograph of the hornblende-bearing gneiss showing (a) medium to coarse grained portion of the rock with pyroxene (Px – 5%) partially and completely replaced by hornblende (leaving pseudomorph of pyroxene), plag-plagioclase (20%), ; (b) medium to coarse grains of Qtz-quartz (45%), Hbl-hornblende (13%), Bt-biotite (2%), and Chl-chlorite (5%). Hornblende grains have been altered to chlorite and biotite leaving pseudomorph of hornblende. (a=XPL, b=XPL).

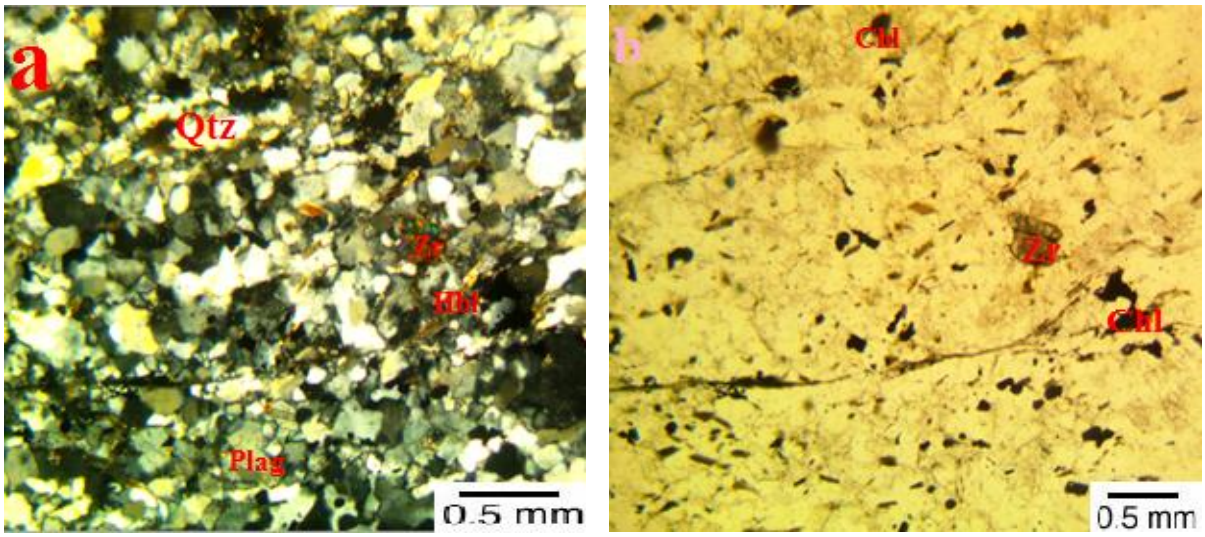

Fig. 4.15. Photomicrograph of hornblende-bearing gneiss showing (a) Hbl-hornblende, Plg-plagioclase feldspar, Qtz-quartz and rounded zircon (heavy mineral) as an accessory mineral; (b) Zircon and chlorite crystals (a=XPL) and (b=PPL).

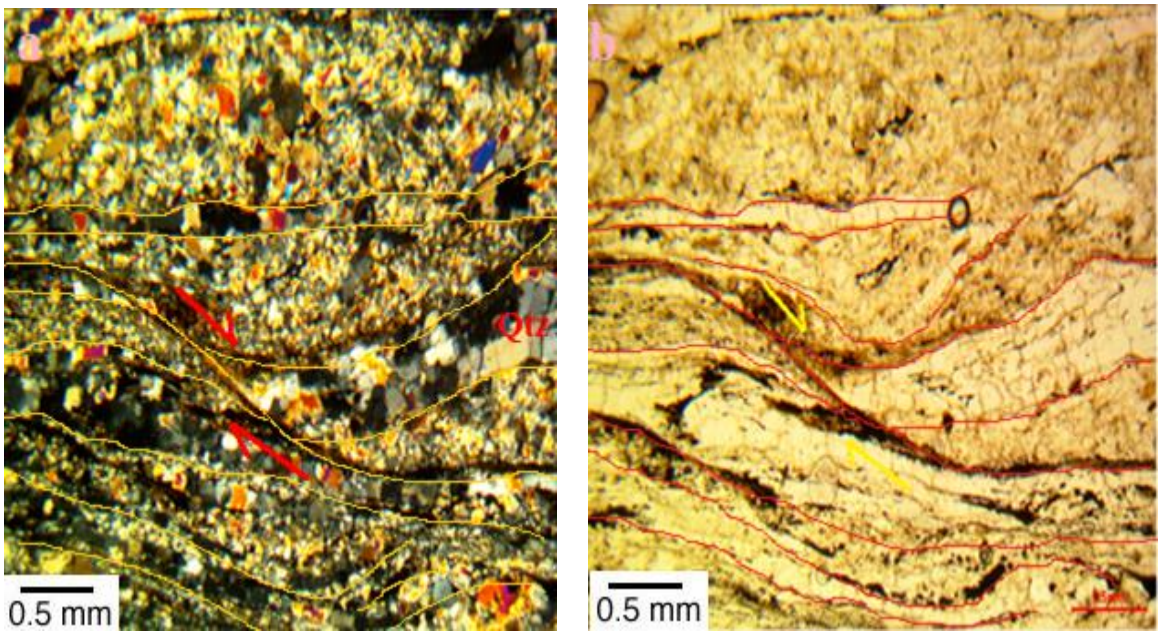

Fig. 4.16. Photomicrograph of the hornblende-bearing gneiss exhibiting high sense of deformation in the rock. These two photomicrographs show how sheared and milled the rock has undergone with deformational structures like micro-faults and micro-folds. Micro-blocks of the rock can been seen displaced along a frictional shear deformational plane causing folding as one block was dragged along the other (a=XPL) and (b=PPL).

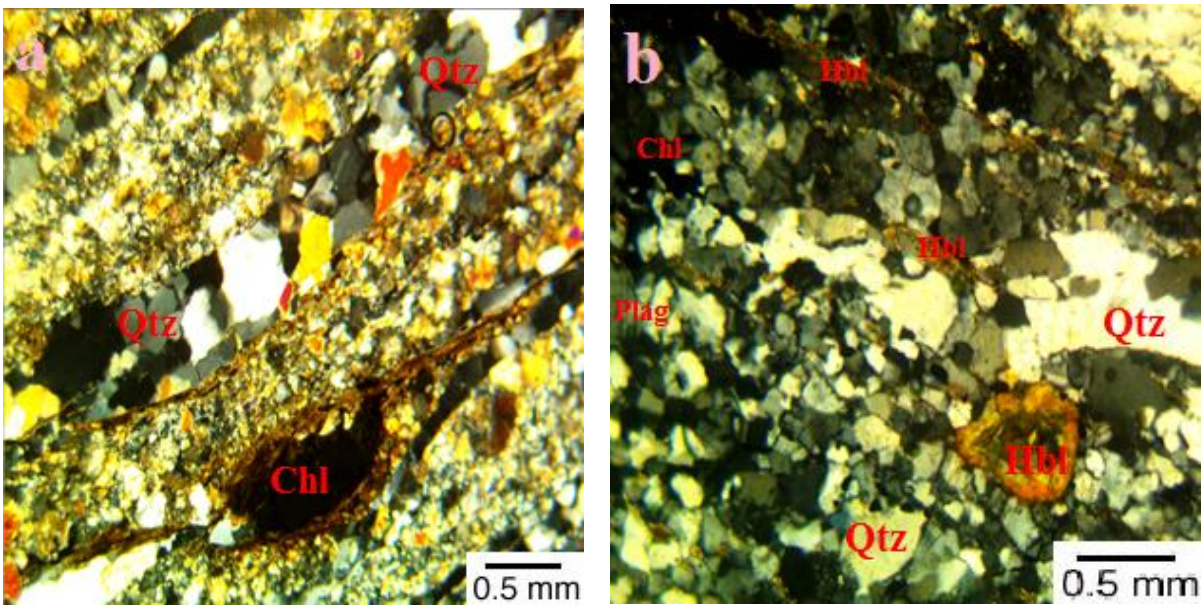

Fig. 4.17. Photomicrograph of hornblende-bearing gneiss showing (a) beautiful bands (mineral segregation) and chloritization from the alteration of hornblende. Chlorite and hornblende define foliation planes; (b) reaction rims of hornblende which is partially altered with pseudomorph of hornblende at the core (a=XPL, b=XPL).

4.3.3 Pyroxene-Garnet-Hornblende Gneiss

The pyroxene-garnet-hornblende gneiss occupies the central portion of the study area. It occupies the central through to the north-western portion of the Adaklu Inselberg (Fig. 4.3). This rock was observed at stations IKE30, IKE31, IKE32, IKE34, IKE35, IKE36 and IKE41.

From mesoscopic observation the rock is dark-gray, medium to coarse grained and contains hornblende, garnet, quartz, plagioclase, and a few pyroxenes (Fig. 4.18a). This rock is also foliated and banded, hence exhibits gneissosity (Fig. 4.18b). The rock has some joints (Fig. 4.19a and 4.19b), it is recrystallized with some quartz veins and also has garnet bands which have been displaced by some localized micro-faults (Fig. 4.18a). The rock is made of medium to coarser garnet grains. Fine to fairly medium garnets are mostly aligned with the felsic bands

whereas the coarser garnet grains (porphyroblasts) are scattered in the rock (Fig. 4.20a). Thickness of bands ranges from about 8 cm to few centimeters. This rock is affected by series of localized normal faults (Fig. 4.20b) which will be resolved in the next subchapter (section 4.4.4).

From microscopic observations, this rock is foliated and banded (exhibits gneissic texture – Fig. 4.21a and 4.21b). Minerals are medium to coarse grained and the rock is sheared and strained with fragmentations of mineral grains in some of the sections (Fig. 4.22a and 4.22b). Minerals observed are hornblende, garnet, quartz, plagioclase (dominantly albite), pyroxene (diopside) and secondary minerals like chlorite. The boundaries of quartz and plagioclase are mostly sutured, and quartz grains are polycrystalline. Minerals are stretched and elongated with the hornblendes dominantly aligned in a preferred orientation. Garnet porphyroblasts have inclusions of quartz, pyroxene and hornblende (Fig. 4.23a and 4.23b) and hence give the rock a poikiloblastic texture. Chloritization of the hornblendes is the main alteration feature observed though some of the few pyroxenes have been replaced by amphiboles with preserved pseudomorph of pyroxenes (Fig. 4.24a and 4.24b).

Fig. 4.18. Field photograph of the pyroxene-garnet-hornblende gneiss showing (a) dark-gray colouration, medium grains and quartz vein through it; (b) foliation and bands (exhibiting gneissosity).

Fig. 4.19. Pyroxene-garnet-hornblende gneiss displaying well-formed different set of joints which run through it. Joint sets in (b) are concordant and discordant to regional foliation plane of the rock.

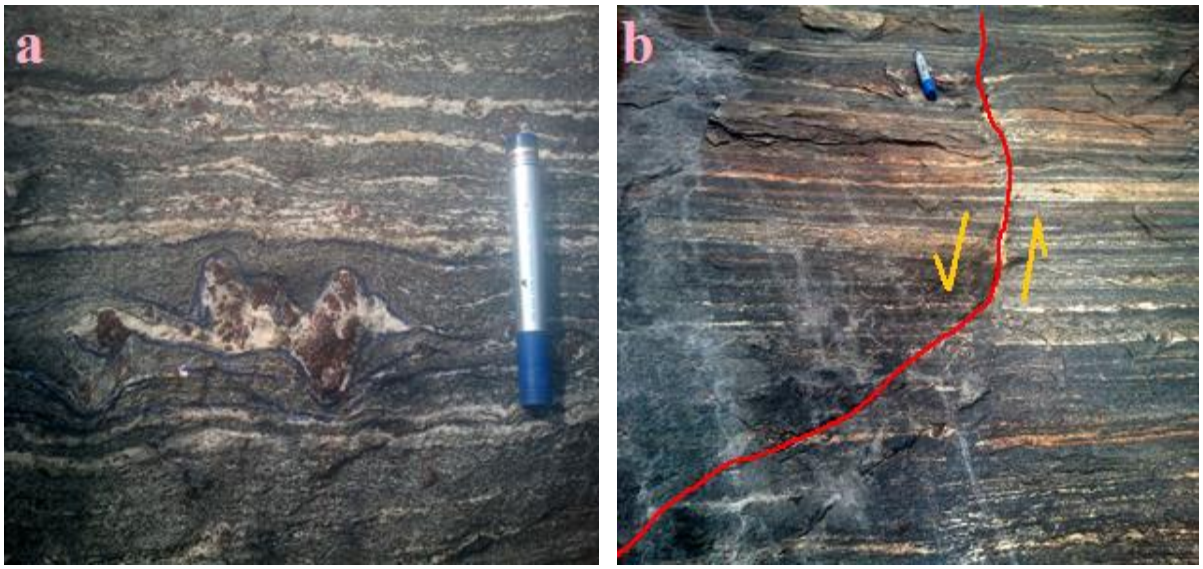

Fig. 4.20. Pyroxene-garnet-hornblende gneiss showing (a) fairly medium to coarse grained garnet crystals which are respectively aligned with the felsic bands and scattered in the rock; (b) a normal fault with refracted fault plane.

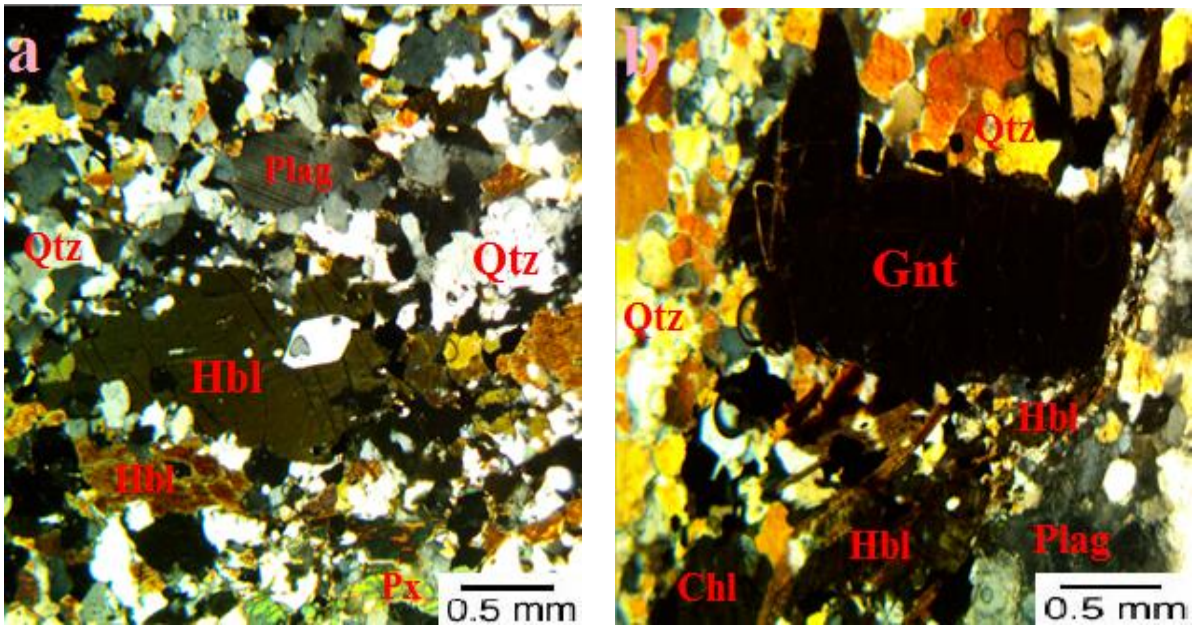

Fig. 4.21. Photomicrograph of pyroxene-garnet-hornblende gneiss exhibiting medium to coarse grains and strained mineral grains (Hbl-hornblende (40%), Gnt-garnet (20%), Pyx-Pyroxene (5%), Plg-plagioclase (10%), Qtz-quartz (20%), Chl-chlorite (5%) a=XPL and b=XPL.

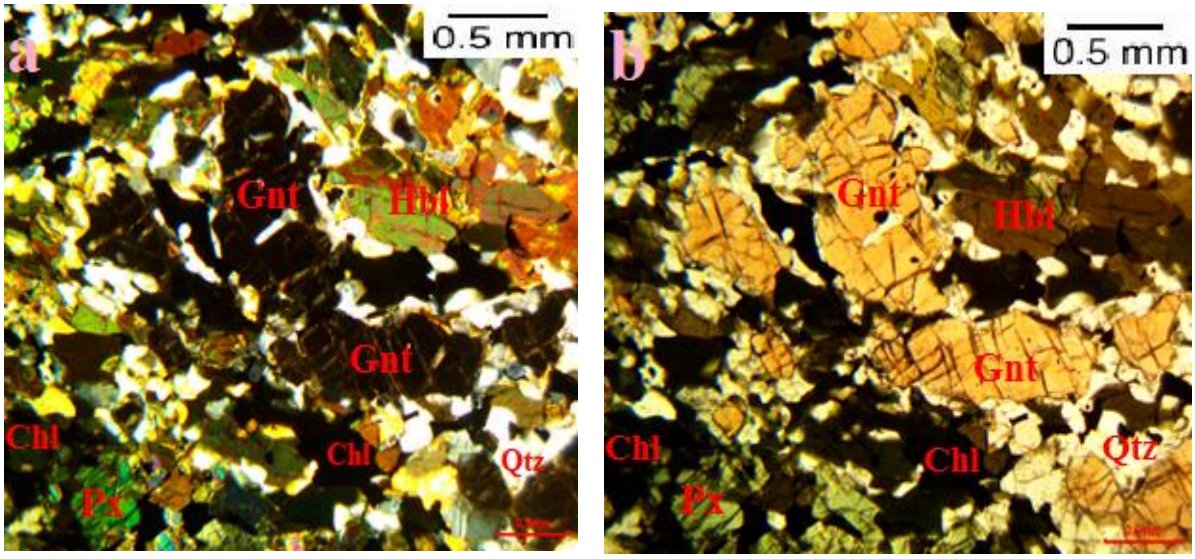

Fig. 4.22. Photomicrograph of pyroxene-garnet-hornblende gneiss showing sheared and fragmented mineral grains. Hornblende grains are partially or completely altered into chlorite. Boundaries of pyroxene at the down left corner is altered into chlorite. (a=XPL and b=PPL).

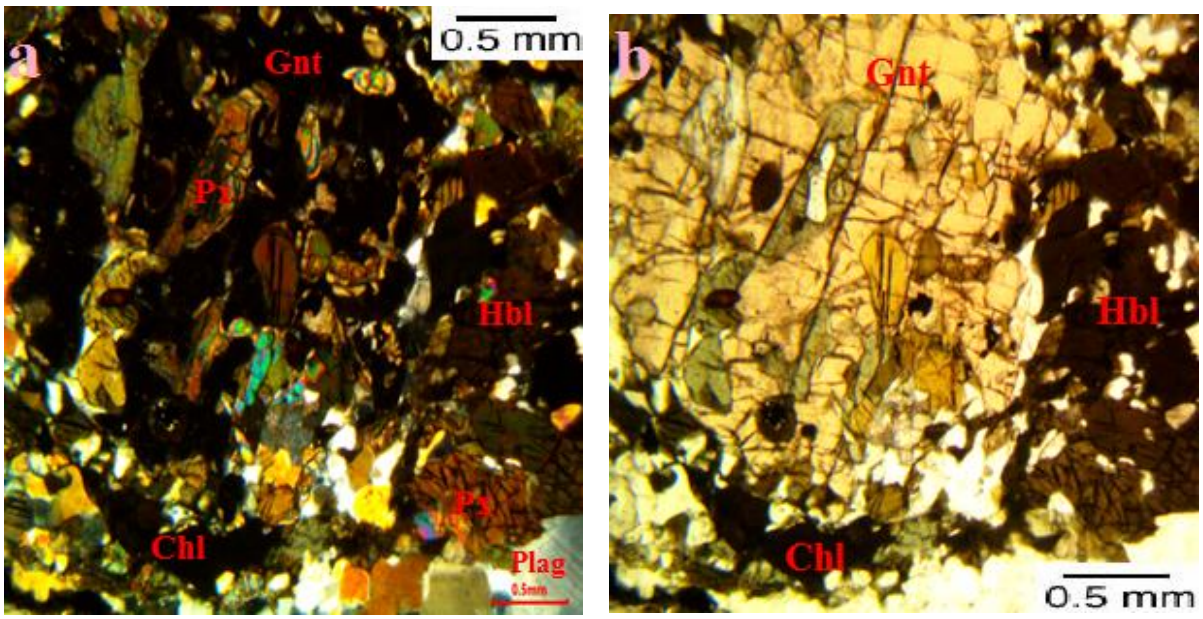

Fig. 4.23. Photomicrograph of pyroxene-garnet-hornblende gneiss displaying a garnet porphyroblast with fractures and inclusion of pyroxene, hornblende, quartz grains giving it a poikiloblastic texture (a=XPL and b=PPL).

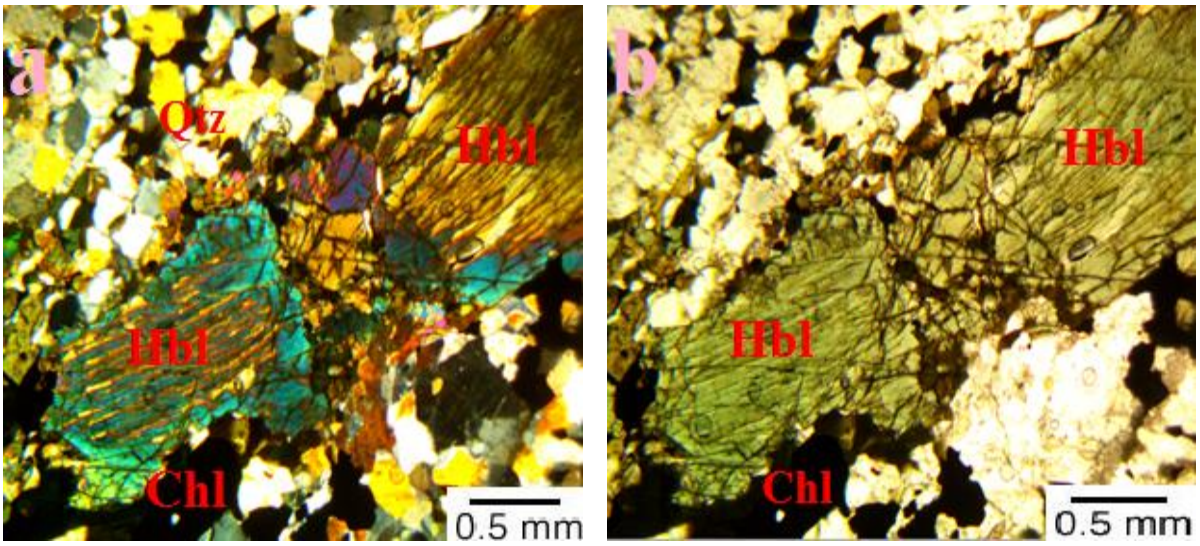

Fig. 4.24. Photomicrograph of pyroxene-garnet-hornblende gneiss displaying coarse fragmented grain of hornblende which has replaced a pre-existing pyroxene grain with the boundary altered to chlorite and core preserving pseudomorph of pyroxene (a=XPL and b=PPL).

4.3.4 Eclogite

This ultramafic rock (the eclogite) occurs as small lenses at the central portion of the study area (at the southeastern and western portions of the inselberg – Fig. 4.3). This rock was observed at stations IKE3, IKE8, IKE28 and IKE38. From mesoscopic observation in the field the rock is dark-green, and coarse grained. It is weakly foliated and banded (Fig. 4.25a and b) and it is composed of clinopyroxene and dark-red garnet (pyrope) with few plagioclase – anorthite (Fig. 4.26a and b). This rock has a lithologic contact with the hornblende-bearing (felsic) gneiss at Torkor where the former under-thrusts the ultramafic eclogite. Boudinage of the eclogite was observed in the hornblende-bearing gneiss (Fig. 4.12).

From microscopic analysis the rock has a sub-isotropic texture and it is dominantly made of clino-pyroxenes and pyrope garnets with few quartz and plagioclase (Fig 4.27a). Mineral

grains are anhedreal to subhedral. Garnets and pyroxenes have inclusions of pyroxenes and plagioclase respectively (Fig. 4.27b). The rock also exhibits corona texture around some garnet grains (Fig. 4.28a and b). This is a result of reaction between the garnets and pyroxenes along their boundaries leading to the development of quartz around the garnet.

Some pyroxenes have been partially altered into amphiboles with pseudomorph of pyroxenes preserved. Other alteration features (Fig. 4.29a and 4.29b) include chloritization and epidotization (all resulting from the alteration of pre-exiting pyroxenes).

Fig. 4.25. (a) Field observation of the eclogite at Torkor showing bands and weak foliations; (b) boulder of eclogite observed at Torkor displaying dark-green colouration.

Fig. 4.26. Dark-green eclogite displaying coarser pyrope garnet grains and sub-isotropic texture (dominantly made of clinopyroxene and garnet).

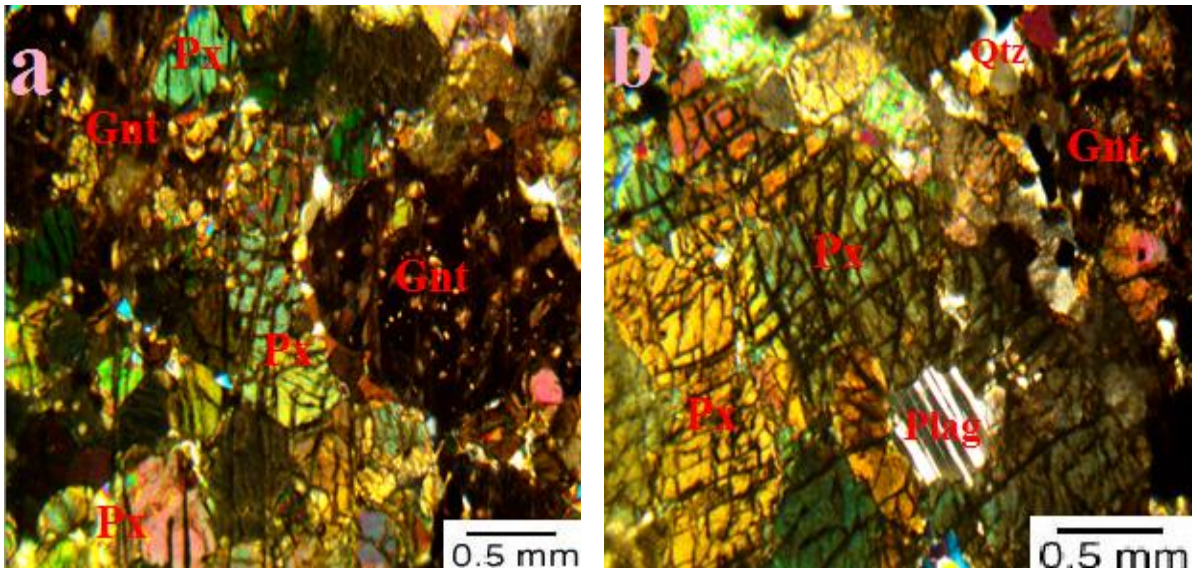

Fig. 4.27. Photomicrograph of eclogite displaying sub-isotropic texture and composed of Pyx-pyroxene (dominantly clinopyroxene – 57%), Gnt-Garnet (pyrope – 27%), Plg-plagioclase (5%) and Qtz-quartz (3%). Clinopyroxene displays inclusion of plagioclase in b. (a=XPL and b=XPL).

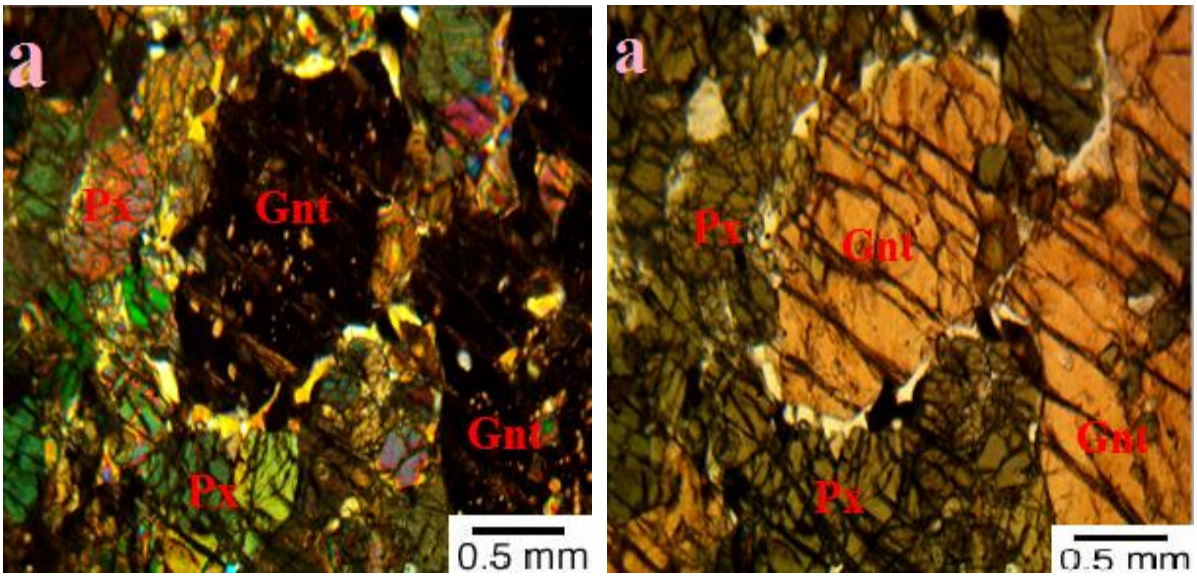

Fig. 4.28. Photomicrograph of eclogite displaying corona texture around garnets which resulted from the chemical reaction between garnet grains and the clinopyroxenes resulting in the development of quartz crystals around the garnet. Garnet grains have inclusions of pyroxene (a=XPL and b=PPL).

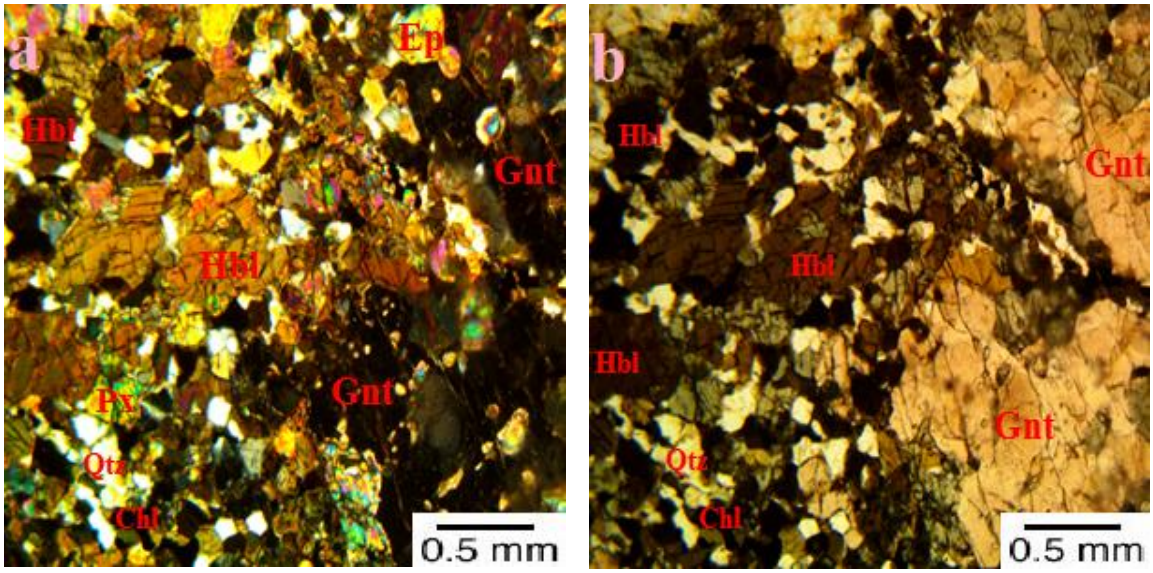

Fig. 4.29. Photomicrograph of eclogite showing partial and complete alteration of pyroxene to hornblende, chlorite and epidote (EP). a=XPL and b=PPL.

4.3.5 Pyroxenite

This is the ultramafic igneous plutonic rock in the study area. This rock occupies portion of the south-eastern foot of the inselberg at Sikaman (Fig. 4.30a) and also the whole Gbeto Hill at the south-western portion of the study area (about 4 km southwest of Sikaman – Fig. 4.29b) at stations IKE10 and IKE13 respectively. The pyroxenite observed on the Gbeto Hill has cumulative texture.

The rock is dark-green, massive, crystalline and weakly deformed (Fig. 4.30b). It is coarse grained. The rock is predominantly made of pyroxenes (clino-pyroxenes). In one instance few specks of garnet crystals were also noticed in a quartz vein through the pyroxenite at Sikaman. The coarse grained pyroxenes have clear regular somewhat parallel cleavages which cut across the mineral grains. Visible pyroxene crystals observed in the field display a stubby shape and square section. The rocks are weathered chemically with a lot of iron stains but are relatively intact physically. The pyroxenite is strongly sheared at the southwestern portion of the inselberg between Sikaman and Helekpe at the foot of the inselberg (Fig. 4.31a and b).

Petrographically, the rock is coarse grained, crystalline with sutured boundaries and has an isotropic textures (Fig. 4.32a). Minerals observed are clinopyroxenes, orthopyroxenes, and few olivine crystals (Fig. 4.32b). The rock also exhibits intergrowth of orthopyroxene and clinopyroxene with the host crystal (orthopyroxene) nearly at extinction with lamellae of clinopyroxenes (Fig. 4.33a, Fig. 4.33b and Fig. 4.34). Some of the pyroxenes have been partially altered to amphiboles.

Fig. 4.30. (a) Field observation of pyroxenite at Sikaman displaying conspicuously visible grained pyroxenes; (b) Weakly deformed pyroxenite observed on the Gbeto Hill displaying set of joints.

Fig. 4.31. (a) Field photograph of strongly sheared pyroxenite observed between Sikaman and Helepke at the southwestern foot of the inselberg; (b) Hand specimen of the sheared pyroxenite.

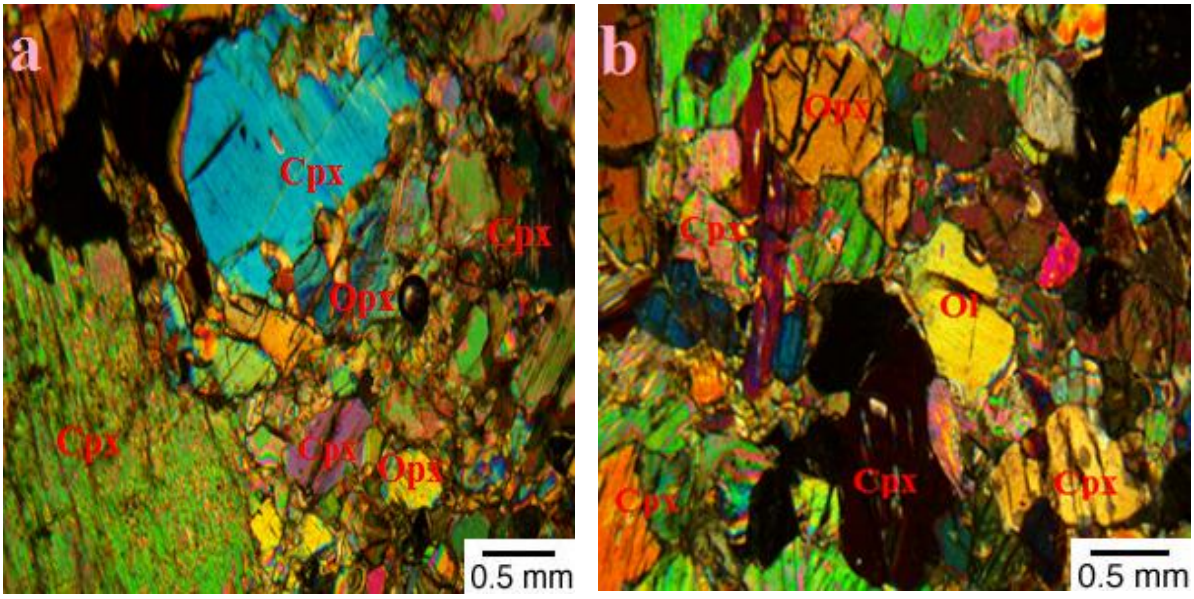

Fig. 4.32. Photomicrograph of pyroxenite displaying coarse grains of clinopyroxene (Cpx), orthopyroxene (Opx), and olivine (Ol). It is dominantly made of clinopyroxene. (a=XPL, b=XPL).

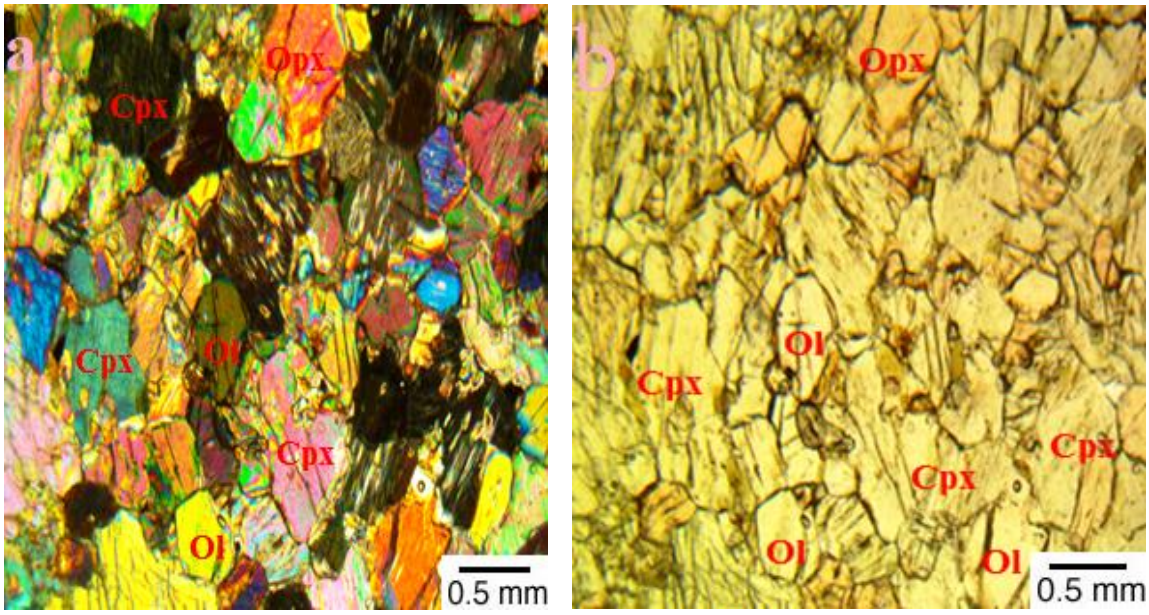

Fig. 4.33. Photomicrograph of pyroxenite exhibiting intergrowth of orthopyroxene and clinopyroxene with the host crystal (orthopyroxene) nearly at extinction and lamellae of clinopyroxenes. It also displays few olivine grains. (a=XPL and b=PPL).

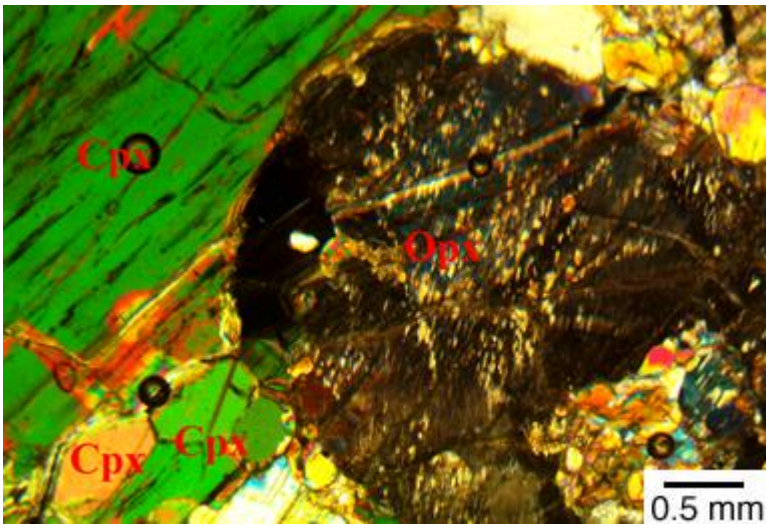

Fig. 4.34. Photomicrograph of pyroxenite exhibiting intergrowth of orthopyroxene and clinopyroxene. Orthopyroxene host lamellae of clinopyroxene. (XPL).

Table 4.1. Modal composition of the various classified rock types

	Modal Composition (%)				
Mineral	**Hornblende-Garnet-Pyroxene Gneiss**	**Hornblende-bearing Gneiss (felsic gneiss)**	**Pyroxene-Garnet-Hornblende Gneiss**	**Eclogite**	**Pyroxenite**
N	**12**	**15**	**6**	**3**	**4**
Quartz	10	45	20	3	-
Plagioclase	10	20	10	5	-
Pyroxene	30	5	5	57	95
Hornblende	15	13	40	5	3
Garnet	20	9	20	27	-
Scapolite	2	-	-	-	-
Olivine	-	-	-	-	2
Chlorite	5	5	5	3	-
Biotite	-	2	-	-	-
Epidote	3	-	-	-	-
Calcite	4	-	-	-	-
Zircon	-	1	-	-	-
Rutile	1	-	-	-	-

N = number of samples (40)

4.4 STRUCTURES

The various rocks in the study area display some level of deformational structures which were observed and analysed during the field work and also in thin sections during microscopic analysis. These structures include foliations and bands, joints, veins, faults, striations/lineation, folds, porphyroblasts (symmetrical and asymmetrical), boudinage, S-C structures, and lithologic contacts. These structures have been statistically analysed and their probable cause and relations have been established. Most of these structures were used as kinematic indicators and aided in resolving deformational directions in the field. The general distribution of these structures in the area is shown on the composite geological map (Fig. 5.1).

4.4.1 Foliations and Bands

The mafic/ultramafic and felsic gneisses show various degrees of foliations which usually mark the first phase of deformation (D_1). These foliations exhibit planar penetrative fabrics observed both at the mesoscopic and microscopic scales in the granulite gneisses and mylonitic gneisses. The granulitic gneisses exhibit fairly weak foliation planes as coarsened grains and porphyroblasts cut across the planes, hence destroying them (Fig. 4.35), whereas the mylonitic gneiss exhibits strong foliation planes. These rocks are also banded showing segregation of mafic and felsic mineral assemblages (Fig. 4.36). Hence, gneissosity is the typical foliation displaced by the gneisses in the study area (foliations, developed bands and visible grains).

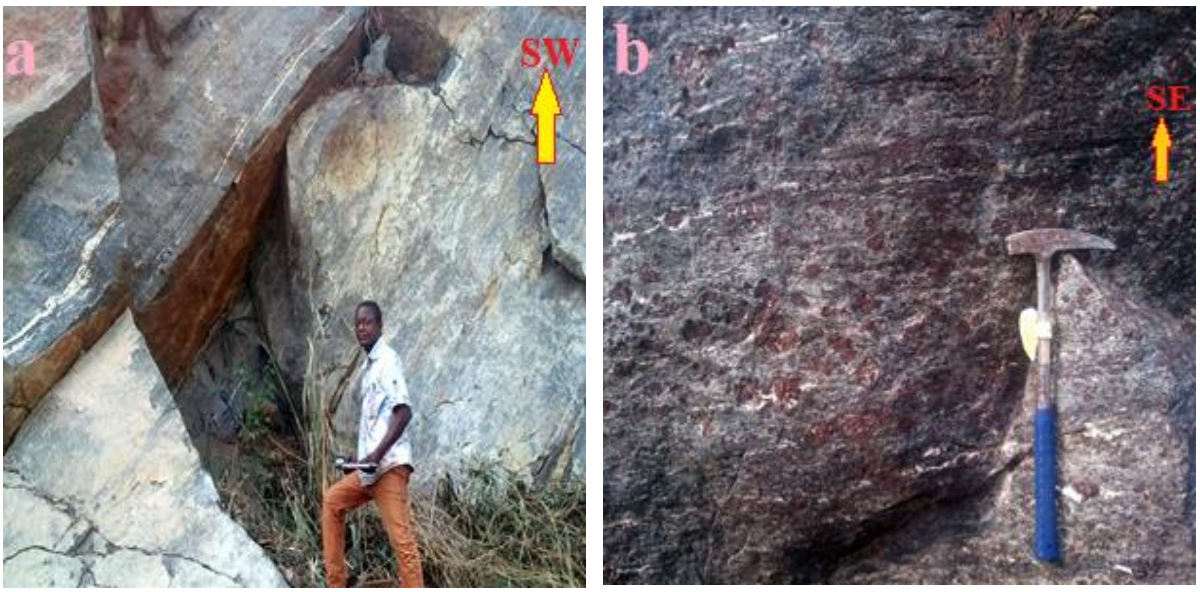

Fig. 4.35. Hornblende-garnet-pyroxene gneiss displaying (a) sub-vertical foliation in a quarry at Abuadi; (b) very gentle foliation plane at Helekpe. The rock is composed of visible coarse grains which cut across foliation. Pictures taken in the SW and SE directions respectively for a and b.

Fig. 4.36. Hornblende-bearing gneiss displaying weak foliation and beautiful bands (segregation of mafic and felsic minerals). Pictures taken in the SE and NE directions respectively for a and b.

The rocks have moderate to gentle foliation planes. Thicknesses of foliations and bands range from 0.2 to 0.5 and 3 to 8 centimeters respectively. The mean strike for foliations in the study area is 035° (NE) and an average gentle dip of 23° SE (Fig. 4.37a). Poles to planes plotted mostly around the center and away from the periphery (Fig. 4.37a). However, some localized outcrops in different portions deviate from the regional strike of these rocks. Some strike in the NE with NW dip direction and others have a NW strike with SW dip directions (at the NW and SW portion of the inselberg respectively). Most of the rocks have gentle dips with relatively average to high density of deformation (Fig. 4.37b).

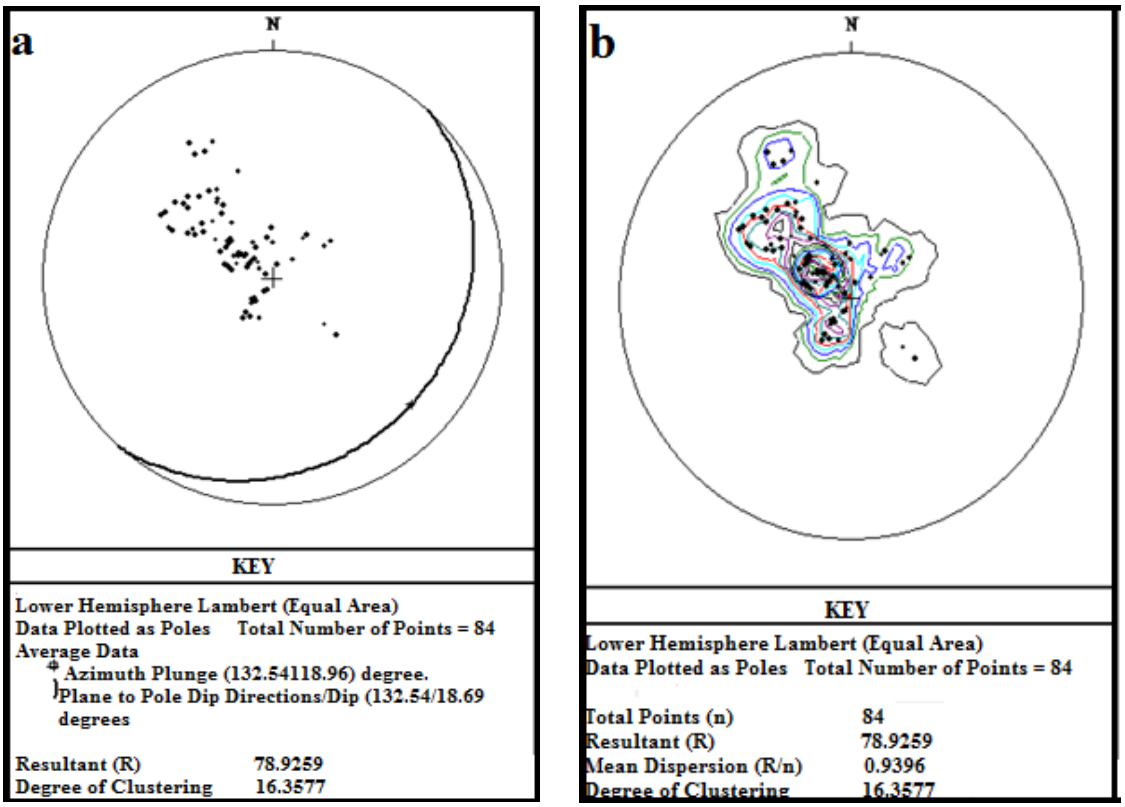

Fig. 4.37. Lower hemisphere stereographic projection (a) plot of poles to foliation planes; (b) plot of contours for equal areas showing intensity and density of deformation. The contours depict a NW-SE polarity of deformation. Lambert Stereo Net type.

4.4.2 Joints

The different rocks display various joint sets, some of which are concordant and others discordant to regional foliation plane (parallel or perpendicular to the strike of foliation surfaces of the exposed rocks). Hence the two main joint sets observed in the area are the NE-SW set of joints and the NW-SE joint sets. These two joint sets intercept orthogonally (Fig. 4.38). Discordant joints have an average strike of 310° with a mean dip of 54°, and the mean strike of concordant joints is 050° with a mean dip of 46°. Hence joint planes are relatively steeper than foliation planes and average intensity/density in the area (Fig. 4.40). The pyroxenite observed on the field is also weakly deformed and affected by some similar joints sets (Fig 4.39).

Fig. 4.38. Parallel and perpendicular joint sets intercept orthogonally in the hornblende-bearing gneiss at Torkor. (Picture taken in the direction of dip). Picture taken in the SE direction.

Fig. 4.39. Pyroxenite outcrop on the Gbeto Hill exhibiting some joint sets. Picture taken in the Eastern direction

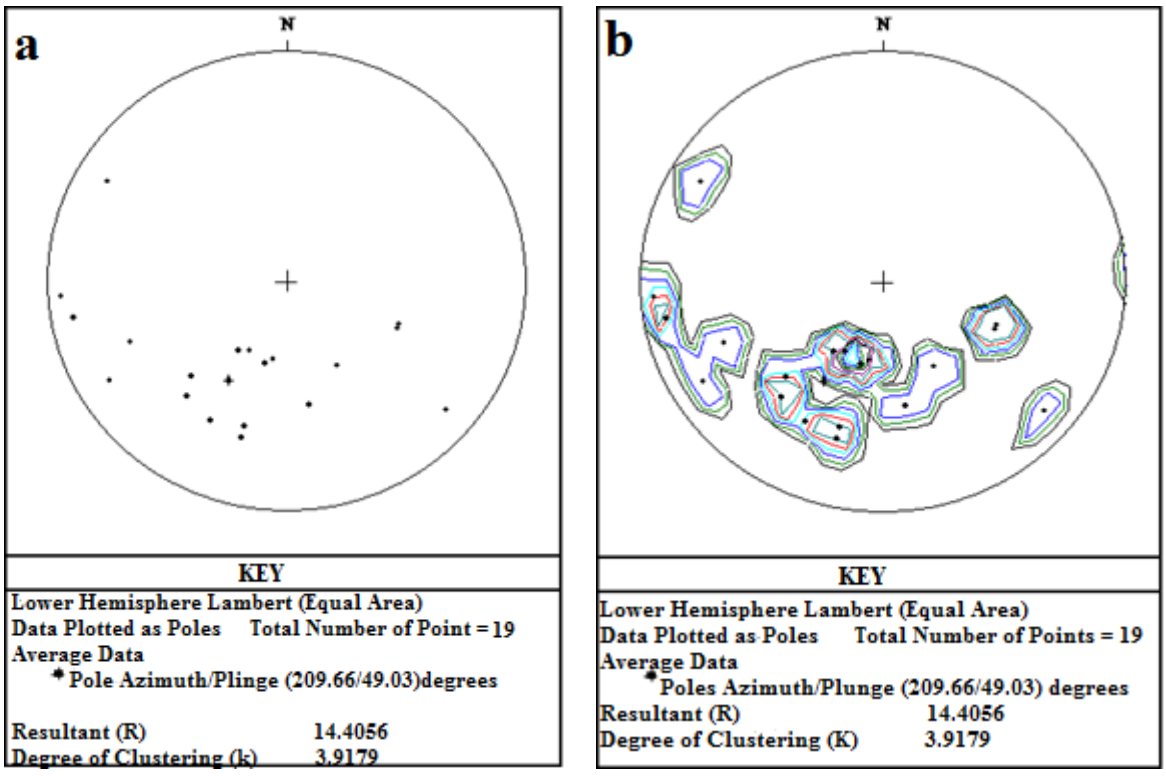

Fig. 4.40. Lower hemisphere stereographic projection (a) plot of poles to joint planes; (b) plot of contours for equal areas showing intensity and density of deformation. Lambert Stereo Net type.

4.4.3 Veins

Veins found are mostly associated with the gneisses in the area. The veins observed are calcite (carbonate), plagioclase and quartz veins which have filled joint planes in the rock (Fig. 4.41a and 4.41b). The quartz and calcite veins range in thickness from 1mm to 3 cm and 4 cm to 8 cm respectively. Most quartz veins have been affected by cross cut of later veins and others are displaced by localized micro-faults.

Fig. 4.41. (a) Calcite (carbonate) and plagioclase veins observed in the hornblende-garnet-pyroxene gneiss in a quarry at Abuadi. (b) Quartz veins observed in the hornblende-garnet-pyroxene gneiss. These veins have been cross-cut by other veins and some have been displaced.

4.4.4 Faults

The area has been affected by series of normal faults (micro faults), most of which were observed around southern foot of the inselberg. All the faults observed around Kodiagbe are normal faults (hanging blocks moved down relative to foot blocks) which have locally displaced the pyroxene-garnet-hornblende gneiss in the area in a sinistral sense of movement. All the normal faults observed in this area have the same sense of frictional shear deformation (sinistral sense) and their planes have a mean strike of 020° NE and a steeper mean dip of 64° NW. Displacements are usually in order of few centimeters and occasionally spotted elastic stretching of foliation or mineral bands along the plane in the direction of movement (Fig. 4.42).

The major fault (Fig. 4.42) in the area has a plane which strikes at 040° NE and dips at 50° NW with a displacement of 35 cm. This rock (pyroxene-garnet-hornblende gneiss) has been affected by series of normal faults which have a listric behaviour (Fig. 4.43a, 4.43b and 4.44) and also a drag fold. The drag fold was observed to be affected by a later normal fault with the same sense of deformation (Fig. 4.45). One of these normal faults displays a refracted plane as the plane intercepts different foliation planes in the rock (Fig. 4.46). The refracted plane is steeper above and becomes gentle at deeper depths.

A graben was also observed in the hornblende-bearing gneiss at the eastern portion of the inselberg in Abuadi (Fig. 4.47). The northern block of this fault has been rotated to meet the southern block on top of the graben, closing the gap created by the fault with the displaced block between them. The displacement of this block is about 1m. Generally, the faults have

sub-vertical planes (steep planes) and have same sense of frictional shear deformation (Fig. 4.48).

Fig. 4.42. Major normal fault in the pyroxene-garnet-hornblende gneiss observed around Kodiagbe displaying sinistral sense of movement. (Fault plane strikes at 040° NE and dips at 50° NW with a displacement of 35cm). Picture taken in the NE direction.

Fig. 4.43. Pyroxene-garnet-hornblende gneiss at Kodiagbe displaying series of normal faults all exhibiting sinistral sense of deformation (Fault plane strikes at 025° NE and dips at 50° NW with a displacement of 5cm for both a and b). Pictures taken in the northern direction.

Fig. 4.44. Pyroxene-garnet-hornblende gneiss at Kodiagbe exhibiting listric normal faults with a sinistral sense of deformation. Picture taken in the northern direction.

Fig. 4.45. Pyroxene-garnet-hornblende gneiss displaying a normal fault with refracted fault plane. Picture taken in the northern direction.

Fig. 4.46. Drag fold affected by a later normal fault. Picture taken in the northern direction.

Fig. 4.47. Hornblende-bearing gneiss displaying a graben with rotated blocks. Picture taken in the western direction.

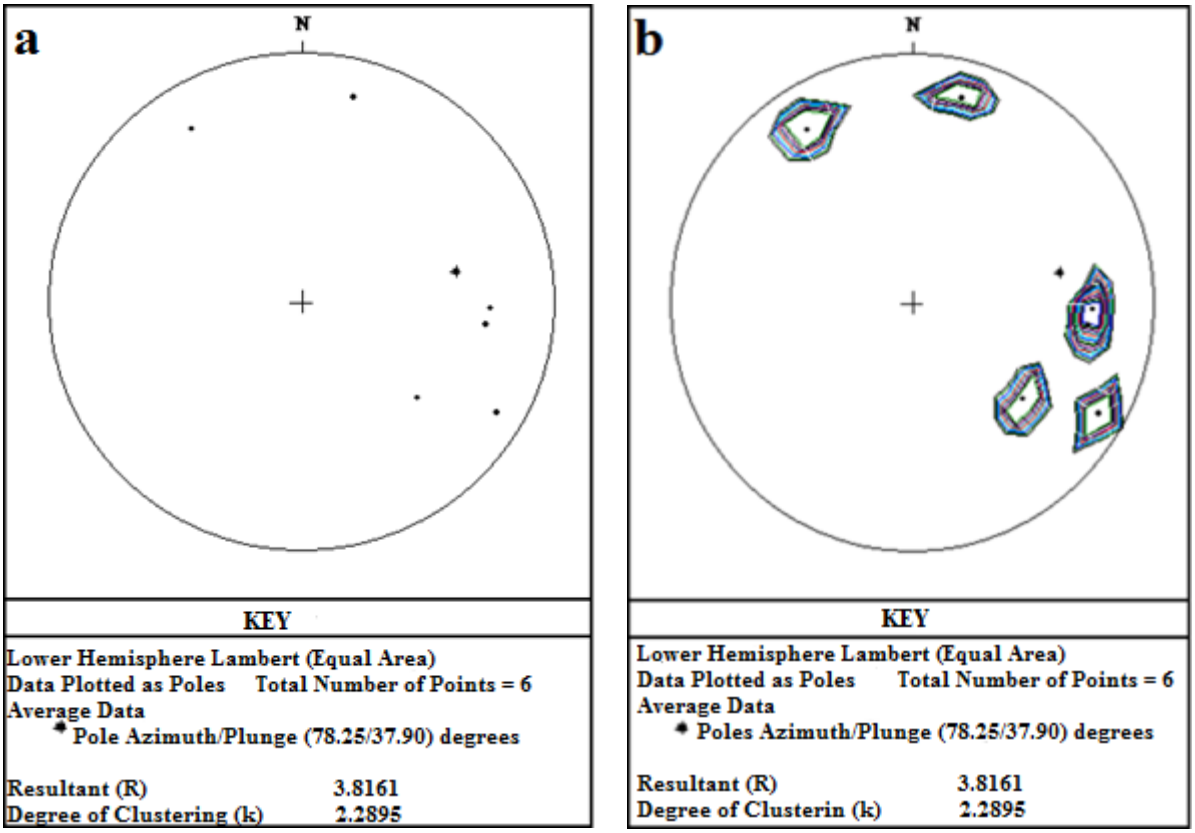

Fig. 4.48. Lower hemisphere stereographic projection (a) plot of poles to fault planes; (b) plot of contours for equal areas showing intensity and density of deformation. Lambert Stereo Net type.

4.4.5 Folds

The various folds observed include kink- recumbent folds, drag folds and monocline with majority of these being hosted in the mafic and felsic gneisses in and around the inselberg. The recumbent folds (Fig. 4.49a, and b) occur in the hornblende-bearing gneiss which outcrops in the Torkor. They have horizontal axes and horizontal axial plane. The fold axes trend in the SE direction in the direction of dip of the rock. The hornblende-beraing gneiss which hosts the recumbent folds in Torkor is strongly sheared and deformed with tight and symmetrical recumbent folds. An opened fold in simple sheared rotated hornblende-bearing gneiss at

Abuadi was also observed (Fig. 4.50a). A probable fold was inferred in Kodiagbe village located at the base of the inselberg. The well layered rocks outcropping in the middle of the village are in two parts noticeably dipping away from each other in different directions (Fig. 4.50b). The distance between these two parts is about 4 m-6 m. The crest line along which these two parts meet is eroded and destroyed leaving a bare stretch between them. These two parts are suspected to be the opposing limbs of a big fold in the study area (Fig. 4.50c) with a NNE-SSW trend of inferred axis. This inferred fold has one limb striking at 84°NE and dipping at 15°SE and the other limb striking at 300°NW and dipping at 10°NE. Hence this fold is an asymmetrical upright fold.

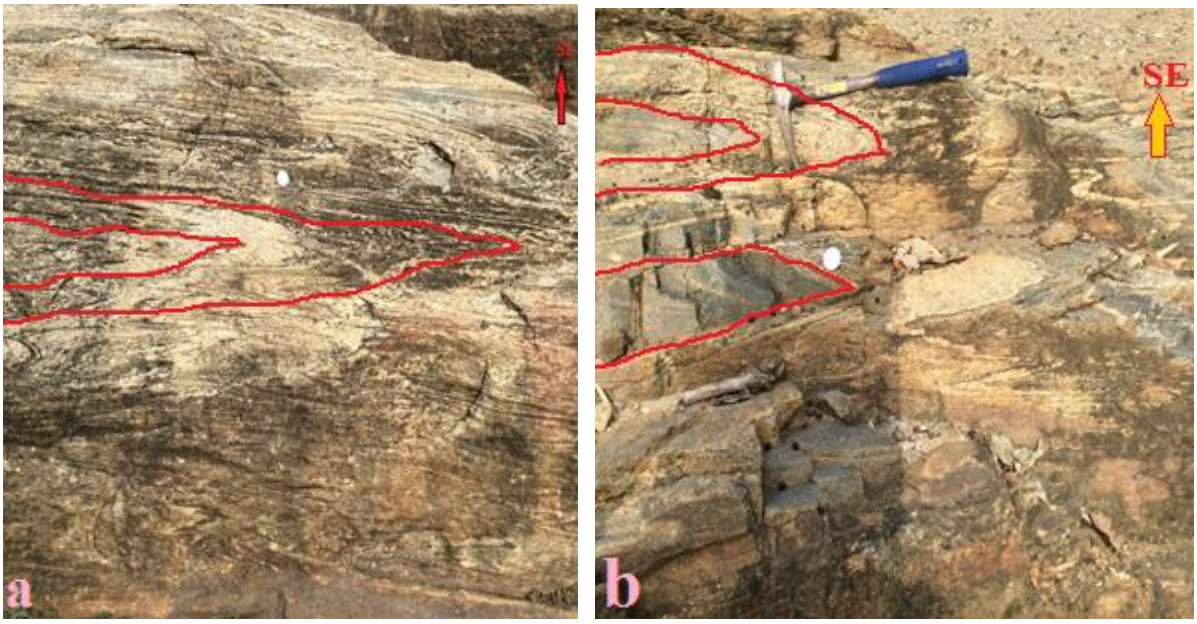

Fig. 4.49 (a & b). Strongly deformed and shear hornblende-bearing gneiss observed in Torkor displaying recumbent folds with a SE axial trend. Pictures taken in the SE direction.

Fig. 4.50. (a) Opened fold and rotated hornblende-bearing gneiss at Abuadi; (b) Inferred fold in mafic gneiss at Kodiagbe; (c) Limbs of inferred asymmetrical fold at Kodiagbe dipping in opposing directions at 10°NE and 15°SE directions. Pictures taken in the SW, W and E directions respectively for a, b and c.

4.4.6 Boudinage and S-C Structures

Boudins were observed in areas where the rock are strongly sheared and some of the boudins were used to resolve the sense of shearing. These boudins were observed in the strongly sheared hornblende-beraing gneiss at Torkor and also the sheared pyroxene-garnet-hornblende gneiss around Kodiagbe.

The hornblende-bearing gneiss at Torkor contains S-C structures and boudins of the ultramafic rocks which were believed to come from the eclogite which has a contact with this rock at this village (Fig. 4.51 and 4.52). According to Sibson (1983), S-plane of S-C structures is the foliation plane and C-plane is 'cisaillement', shear-plane. The S-C structures together with the boudins (Fig 4.51 and 4.53) observed in the hornblende-bearing gneiss at Torkor helped to resolve the sense of shearing. It was observed that these boudins have over and under-thrust each other in the NE-SW direction in a dextral (clockwise) sense of movement. These inferred rotated boudins contain relict foliation planes of strike 320° NW and dip 70° SW (foliation of country rock is 010° NW and dip of 16° SE) as represented in Fig. 4.51.

The strongly sheared pyroxene-garnet-hornblende gneiss at Kodiagbe also exhibits some beautiful stretched, compressed and rotated boudinage (Fig. 4.54). From careful observations it was resolved that these boudins in this area had been subjected to an extensional period of deformation and a later compressional period. The compression resulted in the boudins under-thrusting each other in a NW-SE direction at a sinistral (anti-clockwise) sense of shearing.

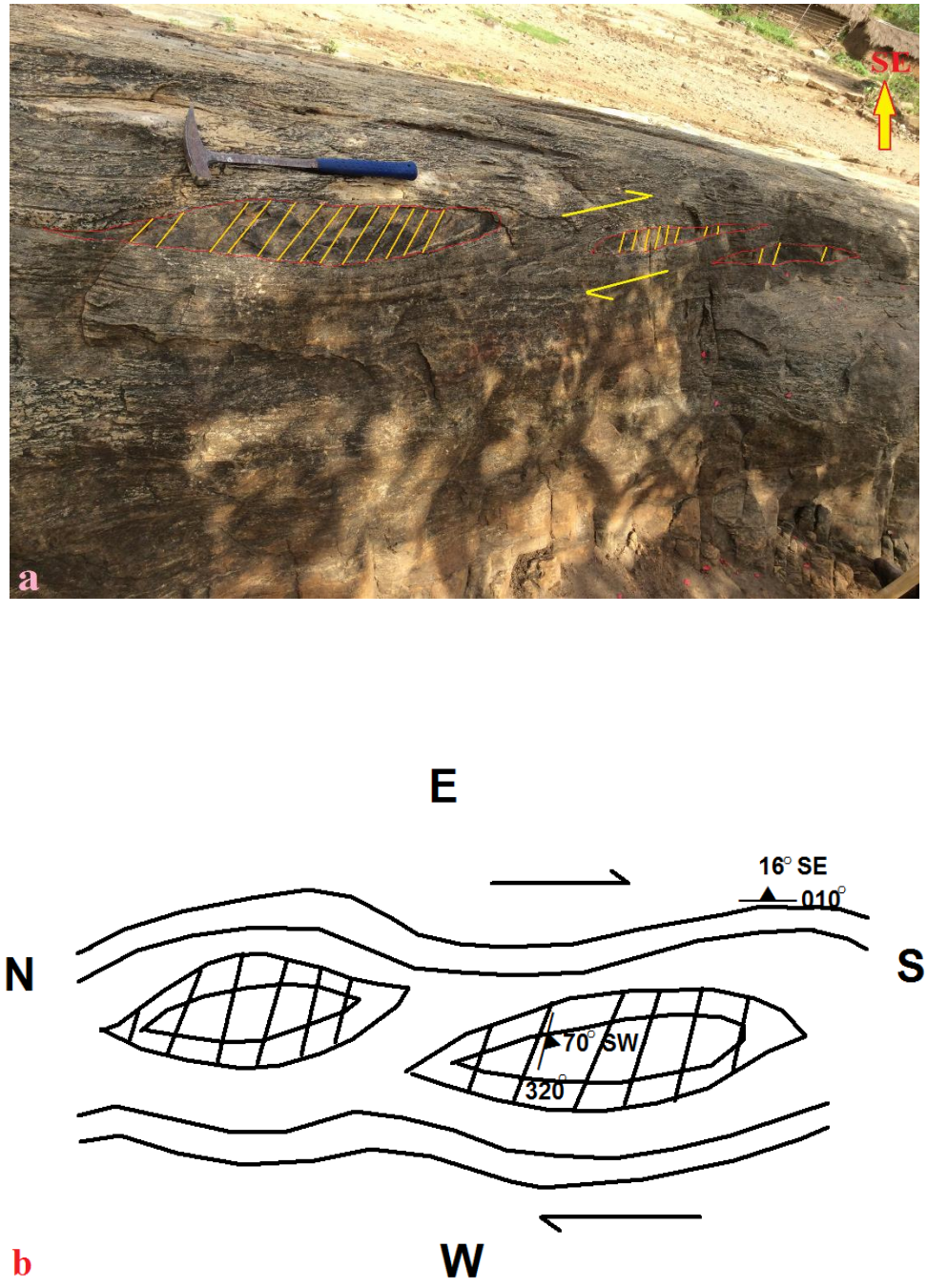

Fig. 4.51. (a) Field observation of rotated boudins with relict foliation texture in hornblende-bearing gneiss at Torkor. Picture taken in the SE direction; (b) Sketch of the boudins with relict foliation texture observed at Torkor with resolved sense of shearing (dextral) and attitudes of relict foliation and foliation of country rock.

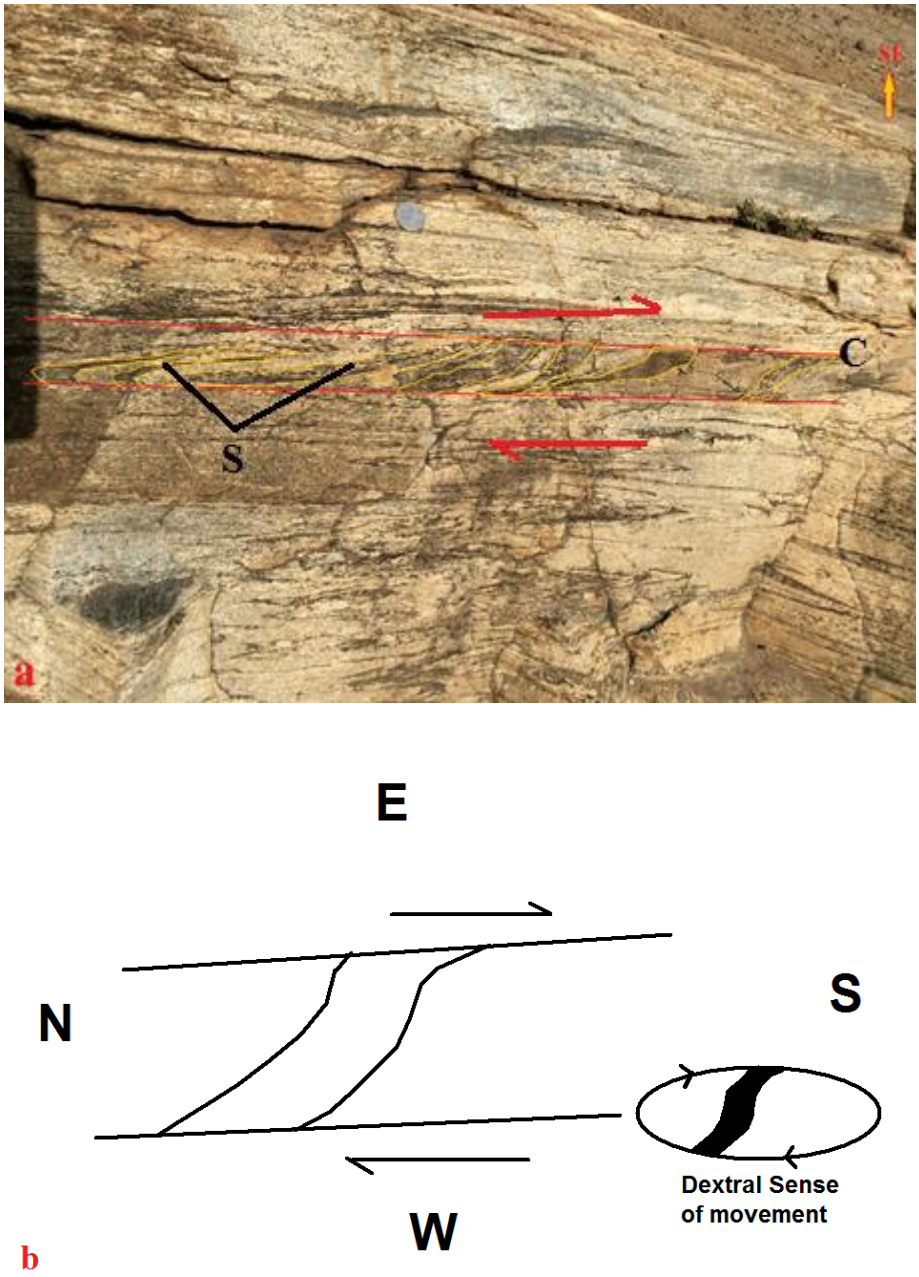

Fig. 4.52. (a) Field observation of S-C structures in the hornblende-bearing gneiss at Torkor. S-plane is defined by quartz, plagioclase, hornblende and garnet ribbons, show reduction in width (and grain size) as they are deflected into higher strain C-planes. Picture taken in the SE direction; (b) Sketch and resolved sense of shearing which resulted in the formation of the S-C structures in the rock.

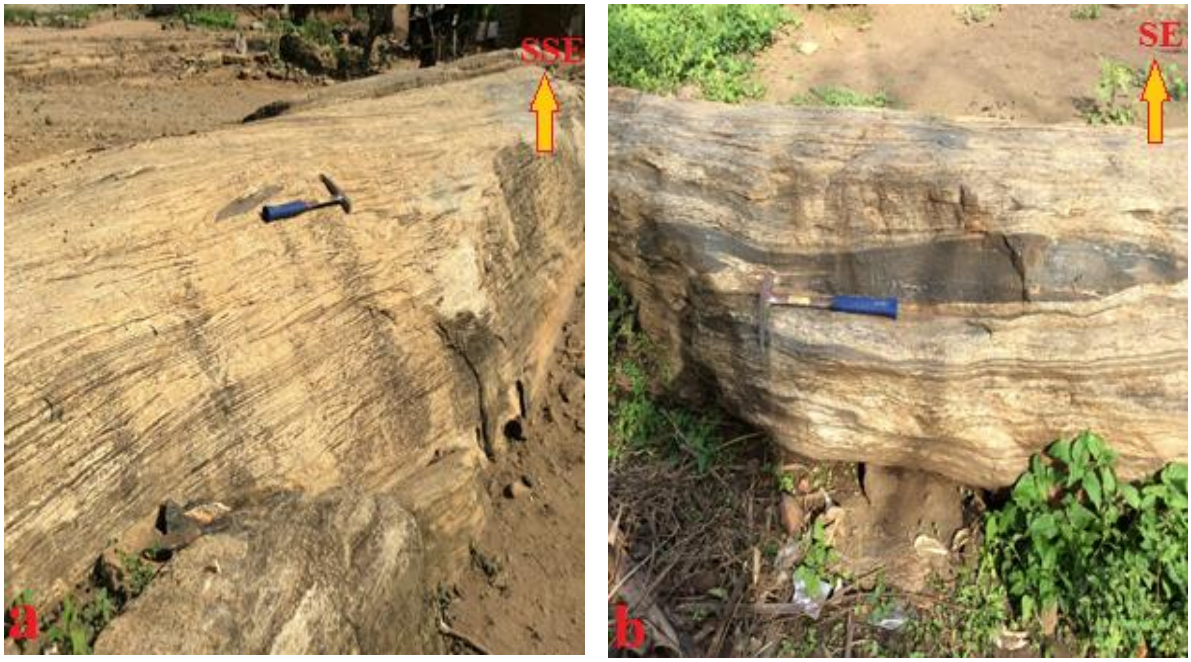

Fig. 4.53. Boudins of ultramafic rocks observed in the hornblende-bearing gneiss at Torkor. The boudin in 'b' was observed closer to the contact between the garnet-hornblende gneiss and the eclogite. Pictures taken in the SSE and SE directions respectively for a and b.

Fig. 4.54. Stretched, compressed and rotated boudin observed in the pyroxene-garnet-hornblende gneiss at Kodiagbe over and under-thrust in the NW-SE direction (Sinistral sense of movement). Picture taken in the NE direction.

4.4.7 Slickenlines

Slickensides were observed in Torkor where the lithologic contact of the hornblende-bearing gneiss and the eclogite (hornblende-bearing gneiss under-thrust the eclogite at Torkor). The under-thrusting movement of the hornblende-bearing gneiss created these slickensides. Slickenlines which trend at 070° NE and plunge at 18° were observed on the slickenside and the rock has a strike of 036° NE and dips at 32° SE (Fig. 4.55). From the measurements made polarity was determined and these structures also exhibit a dextral sense of shearing.

Fig. 4.55. Slickenside with various slickenlines observed closer to the lithologic contact between the ultramafic rock and the hornblende-bearing gneiss at Torkor. This rock also displays parallel set of joints. Picture direction is NW.

4.4.8 Garnet Porphyroblasts

Many symmetrical and asymmetrical garnet porphyroblasts were observed in the mafic and felsic gneisses (Fig. 4.56). The asymmetrical garnet porphyroblasts are spiral in shape (retort-shaped) and have asymmetrical tails. They were used as kinematic sense indicators and hence also aided in resolving the sense of deformation in the area. These asymmetrical porphyroblasts which were observed are syntectonic. Hence, it was resolved that these garnet porphyroblasts were also deformed by the first deformational phase (D_1) which affected the area and resulted in the regional foliations in the area. These asymmetrical garnet porphyroblast observed in the different rock types exhibit dextral sense of deformation. Due to inclusion patterns which mimic the structure in the rock at the time of growth, these porphyroblasts were valuable source of information on local tectonic and metamorphic evolution, in special cases also as shear sense indicators.

Fig. 4.56. Spiral-shaped asymmetrical garnet porphyroblasts observed in the (a) hornblende-garnet-pyroxene gneiss and (b) garnet-hornblende gneiss. Both porphyroblasts exhibit dextral sense of deformation. (c & d) Symmetrical garnet porphyroblasts with symmetrical tails observed in the hornblende-bearing gneiss. Foliation wrapped around porphyroblasts.

4.5 Whole Rock Geochemistry

Tables 4.2 and 4.3 represent the major and trace element data for 26 rock samples from the study area. Twelve (12) of these are samples (i.e., IKE1, IKE1B, IKE2C, IKE6, IKE9, IKE14, IKE14B, IKE18, IKE29, IKE33, IKE33C and IKE37) are mafic granulites (hornblende-garnet-pyroxene gneiss), 5 of the samples (IKE2, IKE20, IKE22, IKE25 and IKE25B) are felsic gneisses (hornblende-bearing gneiss), 4 of them (IKE30, IKE31B, IKE32 and IKE35) are intermediate gneisses (pyroxene-garnet-hornblende gneiss), 3 of them (IKE3, IKE3B and IKE38) are eclogite and 2 of the samples (IKE10 and IKE13) are pyroxenites.

4.5.1 Major Elements Concentration

4.5.1.1 Hornblende-Garnet-Pyroxene Gneiss

This is a garnet-rich mafic gneiss which dominates the study area. This rock is characterized by SiO_2 content of 45.7-53.1 wt%, TiO_2 of 1.34-2.08 wt%, Al_2O_3 of 14.9-17.25 wt%, Fe_2O_3t (for total Fe content) of 11.25-14.35 wt%, MnO of 0.15-0.26 wt%, MgO of 4.63-8.96 wt%, CaO of 8.3-14.2 wt%, Na_2O of 2.32-4.72 wt%, K_2O of 0.09-0.58 wt% and P_2O_5 of 0.15-0.43 wt% (Table 4.2). The hornblende-garnet-pyroxene gneiss has a low Mg# of 51; Mg# = [Mg/ (Fe+Mg)] x100.

4.5.1.2 Hornblende-bearing Gneiss

The hornblende-bearing gneiss shows slight variations in the major elements composition. The rock has relatively higher SiO_2 content than the mafic granulite gneiss. The rock is

characterized by SiO_2 content of 58.4-74.9 wt%, TiO_2 of 0.28-1.53 wt%, Al_2O_3 of 11.65-15 wt%, Fe_2O_3t (for total Fe content) of 2.59-9.65 wt%, MnO of 0.04-0.25 wt%, MgO of 0.29-2.29 wt%, CaO of 1.2-4.93 wt%, Na_2O of 3.43-5.78 wt%, K_2O of 0.39-2.72 wt% and P_2O_5 of 0.04-0.67 wt% (Table 4.3). The rock has a relative high K_2O content (averagely >1wt %) and Na_2O content (>1wt %). This felsic gneiss has very low Mg# of 25.

4.5.1.3 Pyroxene-Garnet-Hornblende Gneiss

This rock also shows slight variation in the major elements composition. The rock is characterized by SiO_2 content of 47.3-69.8 wt%, TiO_2 of 0.49-1.93 wt%, Al_2O_3 of 14.05-15.15 wt%, Fe_2O_3t (for total Fe content) of 4.6-13.9 wt%, MnO of 0.12-0.28 wt%, MgO of 1.63-6.87 wt%, CaO of 2.73-13.45 wt%, Na_2O of 2.37-5.19 wt%, K_2O of 0.3-1.42 wt% and P_2O_5 of 0.12-0.85 wt% (Table 4.3). This rock is an intermediate gneiss with low Mg# of 48.

4.5.1.4 Eclogite

The eclogite is characterized by SiO_2 content of 45-45.8 wt%, TiO_2 of 1.71-2.04 wt%, Al_2O_3 of 14.9-15.95 wt%, Fe_2O_3t (for total Fe content) of 13.45-13.95 wt%, MnO of 0.2-0.22 wt%, MgO of 7.34-9.11 wt%, CaO of 11.5-12.4 wt%, Na_2O of 2.13-2.55 wt%, K_2O of 0.23-0.34 wt% and P_2O_5 of 0.19-0.37 wt% (Table 4.3). The eclogite has Mg# of 55.

4.5.1.5 Pyroxenite

This igneous plutonic rock of the study area is characterized by SiO_2 content of 51.5-54.4 wt%, TiO_2 of 0.18-0.47 wt%, Al_2O_3 of 3.16-6.01 wt%, Fe_2O_3t (for total Fe content) of 8.24-8.45 wt%, MnO of 0.16-0.18 wt%, MgO of 16.65-23 wt%, CaO of 11-17.2 wt%, Na_2O of 0.34-0.65 wt%, K_2O of 0.01-0.03 wt% and P_2O_5 of 0.01 wt% (Table 4.3). This is ultramafic rock whose SiO_2 content must be <45wt% but in this situation this rock has relatively higher SiO_2 content (52-54wt %), hence this ultramafic rock has additional intake of some SiO_2. Notwithstanding, this ultramafic rock has low TiO_2, high Fe_2O_3t, high MgO and CaO. The rock has low K_2O content and Na_2O. It has a very high Mg# of 82.

Table 4.2. Major and trace elements composition of the hornblende-garnet-pyroxene gneiss

Sample	IKE1	IKE1B	IKE2C	IKE6	IKE9	IKE14	IKE14B	IKE18	IKE29	IKE33	IKE33C	IKE37
Major elements (wt%)												
SiO_2	47.4	46.5	46.9	47.1	46.7	45.9	46.1	53.1	48.3	45.7	46.3	48.2
TiO_2	1.74	2.08	2.04	1.34	1.74	1.79	1.75	1.62	1.34	1.96	1.85	1.6
Al_2O_3	16.55	15.5	15.8	15.4	17.25	15.3	15.7	15.1	15.5	14.95	15.15	15.7
Fe_2O_3	11.25	13.45	14.35	13	13	13.05	13.1	12.35	10.65	13.55	13.5	11.75
MnO	0.16	0.22	0.21	0.21	0.18	0.16	0.17	0.26	0.18	0.19	0.17	0.15
MgO	5.22	7.26	7.4	7.92	6.24	6.49	6.35	4.63	6.79	7.33	7.16	8.96
CaO	14.2	12.85	10.3	13.35	12.95	13.25	13.8	8.3	12.75	11.95	12.45	9.96
Na_2O	2.56	2.32	3.24	2.45	2.61	2.55	2.48	4.72	2.91	2.85	2.84	3.73
K_2O	0.09	0.22	0.58	0.28	0.18	0.16	0.11	0.54	0.41	0.24	0.2	0.46
P_2O_5	0.23	0.25	0.3	0.15	0.22	0.22	0.23	0.43	0.16	0.2	0.2	0.18
LOI	0.41	0.46	0.46	0.45	0.26	0.27	0.24	0.46	0.69	0.29	0.42	0.73
Total	99.88	101.2	101.64	101.74	101.42	99.23	100.12	101.58	99.77	99.32	100.34	101.52
Mg#	47.90	51.68	50.53	54.69	48.74	49.63	48.90	42.62	55.81	51.73	51.24	60.17
Trace elements (ppm)												
Cs	0.49	0.78	<0.01	<0.01	0.01	0.03	0.05	<0.01	0.01	0.03	0.06	0.01
Rb	0.6	1.1	2.3	1	0.6	2	2.1	1.8	2.1	1.1	1.2	2.4
Ba	11.6	49.5	125.5	48.2	28.1	23.8	25.5	151.5	114.5	36.4	43.3	132.5
Th	0.26	0.42	0.26	0.64	0.27	0.35	0.43	0.41	0.63	0.64	0.18	0.07
Ta	0.2	0.2	0.2	0.1	0.2	0.3	0.3	0.3	0.1	0.3	0.2	0.2
K	747.12	1826.29	4814.76	2324.36	1494.23	1328.21	913.14	4482.70	3403.53	1992.31	1660.26	3818.60
La	5.2	5.4	7.9	6.5	6	5.6	6.4	16.8	5.9	5.4	4.9	4.5
Ce	15.9	16.9	20.6	15.8	16.2	15.9	17.8	37.9	14.7	15.8	15.3	14.4
Pr	2.71	2.91	3.2	2.4	2.63	2.59	2.77	5.64	2.19	2.64	2.6	2.37
Nd	14.7	16.1	17.8	11.5	14.3	13.6	14.6	26.9	12	14.5	15.2	13.2
Sm	4.48	5.13	4.98	3.46	4.25	4.6	4.46	7.42	3.57	4.87	4.62	4.06
Eu	1.54	1.75	1.64	1.16	1.46	1.43	1.49	2.06	1.18	1.55	1.69	1.45
Gd	5.64	6.81	5.87	4.17	5.41	5	5.4	8	4.73	6.32	5.61	4.68
Tb	0.86	1.18	0.98	0.63	0.91	0.82	0.95	1.25	0.78	1.01	0.93	0.73
Dy	5.57	6.7	5.83	4.69	5.65	5.32	5.65	8.15	4.65	6.75	5.93	4.5
Ho	1.15	1.41	1.18	0.95	1.16	1.09	1.09	1.67	1	1.41	1.18	0.94
Er	3.33	3.9	3.54	2.59	3.35	3.04	3.15	4.67	2.71	4.17	3.23	2.7
Yb	2.94	3.9	3.2	2.46	2.96	2.66	2.8	4.41	2.43	3.55	3.28	2.15
Lu	0.45	0.58	0.5	0.38	0.49	0.42	0.46	0.66	0.39	0.59	0.47	0.32
Sr	269	203	251	216	307	260	272	304	264	217	227	330
Hf	3.1	3	2.7	1.8	2.9	3.1	2.8	4.3	2.3	3.2	3.9	4.3
Zr	119	113	112	69	117	113	110	171	79	119	164	188
Ti	10431.3	12469.6	12229.8	8033.3	10431.3	10731.05	10491.25	9711.9	8033.3	11750.2	11090.75	9592
U	0.12	0.13	0.11	0.14	0.09	0.12	0.16	0.14	0.24	0.06	0.08	0.05
Nb	3.7	3.1	4.3	1.9	4	4.5	4.8	5.2	2.2	4.3	3.3	3.5
Y	30.2	35.1	31.6	23.5	30.2	27	30	42.3	25.9	35.3	31.1	22.4
Sc	40	42	44	39	41	41	41	31	37	43	41	34
Cr	290	360	170	330	320	410	440	100	300	430	430	230
Ni	122	209	62	162	137	179	168	22	146	169	186	142
Co	43	59	41	53	55	53	49	28	44	55	54	48
V	290	334	403	299	317	329	333	301	280	320	336	303
Ta	0.2	0.2	0.2	0.1	0.2	0.3	0.3	0.3	0.1	0.3	0.2	0.2
P	1003.86	1091.15	1309.38	654.69	960.21	960.21	1003.86	1876.78	698.34	872.92	872.92	785.63
Pb	<2	<2	<2	<2	<2	<2	<2	<2	<2	<2	<2	<2
Zn	86	105	99	102	97	104	97	126	81	106	108	77
Tm	0.45	0.59	0.48	0.38	0.47	0.4	0.48	0.68	0.41	0.61	0.45	0.34

Table 4.3. Major and trace elements composition of the Hornblende-bearing gneiss, Pyroxene-Garnet-Hornblende Gneiss, Eclogite and Pyroxenite.

	Hornblende-bearing Gneiss					Pyroxene-Garnet-Hornblende Gneiss				Eclogite			Pyroxenite	
Sample	IKE2	IKE20	IKE22	IKE25	IKE25B	IKE30	IKE31B	IKE32	IKE35	IKE3	IKE3B	IKE38	IKE10	IKE13
Major elements (wt%)														
SiO_2	74.9	70.3	58.4	74.2	74.3	51.3	69.8	47.3	59.6	45.8	46.2	45	51.5	54.4
TiO_2	0.28	0.6	1.53	0.29	0.31	1.93	0.49	1.65	0.9	2.04	1.99	1.71	0.47	0.18
Al_2O_3	11.65	14.9	15	14	14.05	14.05	14.8	15.15	15	15.35	15.95	14.9	6.01	3.16
Fe_2O_3	2.59	3.8	9.65	2.82	2.85	13.9	4.6	13.05	7.59	13.95	13.9	13.45	8.24	8.45
MnO	0.14	0.07	0.25	0.04	0.05	0.28	0.26	0.2	0.12	0.2	0.23	0.22	0.16	0.18
MgO	0.41	0.96	2.29	0.29	0.39	5.05	1.63	6.87	5.11	9.11	7.34	9.2	16.65	23
CaO	1.43	2.93	4.93	1.2	1.37	8.62	2.73	13.45	6.17	11.5	12.25	12.4	17.2	11
Na_2O	3.43	5.67	5.78	5.28	5.41	4.39	5.19	2.37	3.37	2.13	2.15	2.55	0.65	0.34
K_2O	2.72	0.82	0.39	2.64	2.31	0.56	1.36	0.3	1.42	0.34	0.26	0.23	0.03	0.01
P_2O_5	0.07	0.17	0.67	0.04	0.07	0.85	0.12	0.22	0.21	0.26	0.37	0.19	0.01	0.01
LOI	0.36	0.23	0.24	0.25	0.5	0.28	0.53	0.56	1.76	0.37	0.34	0.58	0.27	0.07
Mg#	23.87	33.35	31.98	16.92	21.33	41.85	41.25	51.05	57.15	56.40	51.13	57.54	80.01	84.36
Trace elements (ppm)														
Cs	0.22	0.01	0.02	0.01	<0.01	0.02	0.04	0.07	0.1	0.01	0.04	<0.01	0.02	<0.01
Rb	46.8	3.4	1.1	28.8	23.7	2.1	15.7	2.8	29.3	2.9	3.7	0.9	0.6	0.2
Ba	804	578	220	681	680	130	485	97.1	768	67.2	113	24.5	52.4	7.2
Th	5.03	1.93	0.74	5.97	3.48	0.49	1.78	0.65	1.5	0.33	0.58	0.17	0.1	<0.05
Ta	0.2	0.2	0.3	0.1	0.1	0.1	0.1	0.2	0.2	0.2	0.3	0.2	<0.1	<0.1
K	22579.54	6807.07	3237.51	21915.43	19176	4648.73	11289.77	2490.39	11787.85	2822.44	2158.34	1909.30	249.04	83.01
La	35.3	32.5	19.7	40.7	33	13.9	20.3	7.6	20.7	5.4	11.3	4.2	1	0.6
Ce	74.8	70.6	46.9	87.3	70.9	33.1	44.7	19.4	48.1	16.2	28.9	13.5	3.8	2.1
Pr	9.45	8.61	6.69	10.7	8.93	4.68	5.69	2.83	6.49	2.63	4.72	2.38	0.72	0.37
Nd	40.3	37.2	32.4	43.9	37.5	24.1	25.6	14.2	28.8	14.5	23.8	14.4	4.9	2.4
Sm	9.04	7.41	8.69	9.22	8.51	6.73	6.07	4.12	6.95	4.81	5.96	4.46	1.83	0.79
Eu	1.52	1.53	3.44	1.41	1.36	2.02	1.66	1.41	1.45	1.47	1.92	1.52	0.49	0.25
Gd	7.99	6.84	10.25	8.79	8.13	7.95	6.78	5.23	6.05	5.79	6.74	5.7	1.98	0.83
Tb	1.39	1.01	1.64	1.4	1.31	1.22	1.17	0.9	0.88	1.01	1.14	0.94	0.3	0.13
Dy	8.8	5.94	9.48	7.88	7.22	6.84	7.7	5.52	4.7	5.96	6.55	6.3	1.74	0.79
Ho	1.9	1.22	1.86	1.56	1.42	1.39	1.82	1.13	0.81	1.27	1.36	1.33	0.32	0.17
Er	6.22	3.55	5.6	4.17	4.27	3.9	5.89	3.33	2.19	3.58	3.84	3.81	0.96	0.49
Yb	6.67	3.23	5.41	3.94	3.98	3.12	6.7	2.91	1.56	3.21	3.45	3.55	0.7	0.44
Lu	1.09	0.55	0.83	0.63	0.59	0.5	1.11	0.47	0.21	0.5	0.53	0.55	0.11	0.06
Sr	138	408	269	178	240	296	265	280	306	209	326	238	54.5	25.1
Hf	7.3	7.2	4.9	9.1	7.1	2.3	5.9	2.5	2.3	3.1	3.5	3	0.6	0.2
Zr	271	266	186	349	272	83	246	85	88	122	135	110	13	5
Ti	1678.6	3597	9172.35	1738.55	1858.45	11570.35	2937.55	9891.75	5395.5	12229.8	11930.05	10251.45	2817.65	1079.1
U	0.3	0.14	0.25	0.5	0.39	0.15	0.4	0.2	0.3	0.12	0.24	0.13	<0.05	<0.05
Nb	9.1	5.7	6.2	5	4.7	2.8	4.3	3	8	4	5.6	3.6	<0.2	<0.2
Y	55.6	32.1	53.4	39.5	38.1	35.1	46.8	29.7	22.2	32.8	35.7	33.5	8.4	4.3
Sc	10	11	19	5	5	31	10	39	18	41	40	40	61	44
Cr	10	10	10	30	20	30	30	440	110	310	370	340	1580	3040
Ni	2	6	<1	3	6	22	9	173	49	139	155	153	432	479
Co	<1	3	9	1	2	27	6	51	25	51	47	50	55	59
V	7	25	72	6	12	350	51	345	155	383	364	303	297	159
P	305.52	741.98	2924.28	174.58	305.52	3709.91	523.75	960.21	916.57	1134.80	1614.90	829.27	43.65	43.65
Pb	15	6	<2	8	6	4	6	<2	<2	3	<2	<2	<2	2
Zn	73	36	84	33	34	128	216	99	109	99	98	90	35	50
Tm	0.99	0.51	0.84	0.61	0.62	0.5	0.93	0.48	0.28	0.49	0.58	0.54	0.13	0.05

4.5.2 Trace Elements Geochemistry

The Rare Earth Elements (REEs), transition metals and incompatible trace element concentrations for the hornblende-garnet-pyroxene gneiss, hornblende-bearing gneiss, pyroxene-garnet-hornblende gneiss, eclogite and pyroxenite are presented in Tables 4.2 and 4.3.

4.5.2.1 Rare Earth Elements (REEs)

The REE data and total REE (∑REE) content bring a distinction among the 5 different suite of rocks in the study area. The total REE (∑REE) for the rocks is high in the hornblende-bearing gneiss, hornblende-garnet-pyroxene gneiss, pyroxene-garnet-hornblende gneiss and eclogite, and low in the pyroxenite. The total REE content for the hornblende-garnet-pyroxene gneiss range from 56.34 to 126.21 ppm, 153.73 to 222.21 ppm for the hornblende-bearing gneiss, 69.53 to 136.12 ppm for pyroxene-garnet-hornblende gneiss, and 63.18 to 100.79 ppm for the eclogite and that for the pyroxenite is in the range 9.47 to 18.98 ppm. Chondrite-normalized rare earth element (REE) variation diagrams of the rocks were plotted and compared with lower crust, N-MORB, E-MORB and OIB (Fig. 4.57).

Chondrite-normalized REE variation-diagrams were plotted for the different rocks types. The HP mafic granulite (hornblende-garnet-pyroxene gneiss) which dominates the study area show moderate enrichment in light rare earth elements (LREE) with $(La/Sm)_N$ values between 0.66 and 1.42 (Fig. 4.57a). It also shows weak depletion in heavy rare earth elements (HREE) with a very weak negative Eu anomaly (Eu/Eu*=0.82-1.02). This rock is moderately enriched in Ce, Nd and Sm. It has a slight negative Eu anomaly and relatively low Yb concentration and a flat HREE pattern (Fig. 4.57a). The REE pattern exhibited by this rock mimics that of N-

MORB. It is also most likely that HREE depletion exhibited by this rock is a characteristic of mantle source (Shirey and Hanson, 1984; Stern et al., 1989). Ratios of $(Gd/Yb)_N$ are virtually in the range of >1 to <2 indicating the chondrite normalized HREE patterns are nearly flat.

Comparatively, the hornblende-bearing gneiss shows high LREE-enrichment ($(La/Sm)_N$=1.43-2.78 and $(La/Yb)_N$=2.46-6.96) pattern and nearly flat depleted HREE pattern (Fig. 4.57b). The REE patterns are characterized by a very strong negative Eu anomaly (Eu/Eu*=0.48-0.66) though one sample shows a very weak positive Eu anomaly (Eu/Eu*=1.11). The REE pattern exhibited by this rock also in some way mimics that of the lower crust and the E-MORB. The rock is enriched in Ce, Nd, and Sm and relatively low in Yb content. Ration of $(Gd/Yb)_N$ is in the range 0.97-1.80 indicating the chondrite normalized HREE pattern is nearly flat.

Relatively the pyroxene-garnet-hornblende gneiss also shows moderate LREE-enrichment ($(La/Sm)_N$=1.30-2.10) and a nearly flat and depleted HREE with a moderate negative Eu (Eu/Eu*=0.68-0.93) anomaly (Fig. 4.57c). This pattern is also similar to that of lower crust. The pattern shows enrichment in Ce, Nd, Sm and depleted Yb content. Ratio of $(Gd/Yb)_N$ is in the range of 0.82-2.05, indicating a nearly flat HREE chondrite normalized pattern, though one sample shows a relative gentle slope pattern ($(Gd/Yb)_N$=3.13).

The eclogite however, displays LREE depletion and a moderate HREE-enrichment (Fig. 4.57d). Out of three samples plotted, two samples show strong depletion in LREE ($(La/Sm)_N$=0.59-0.71) with a relatively moderate enrichment in HREE, whereas one sample

displays moderate enrichment in LREE ($(La/Sm)_N$=1.19) with a relative depletion in HREE. The REE patterns display weak negative Eu anomaly (Eu/Eu*=0.85-0.93). Averagely, this rock displays depletion in LREE and a flat HREE-enrichment. The REE pattern of this rock is similar to that of the N-MORB.

The pyroxenite of the study area however displays a quite complex and contrasting REE pattern (Fig. 4.57e) compared to the HP gneisses and eclogite. The REE patterns for this rock display a steep slope for the LREE depletion and a relative gentle one for the HREE. This rock shows extremely low LREE ($(La/Sm)_N$=0.34-0.48) pattern but enriched in Nd and Sm and also a weak enrichment in the HREE ($(La/Yb)_N$=0.92-0.96). The rock displays weak negative Eu anomaly (Eu/Eu*=0.77-0.94). This rock exhibits N-MORB-like REE pattern (closer to the primitive source).

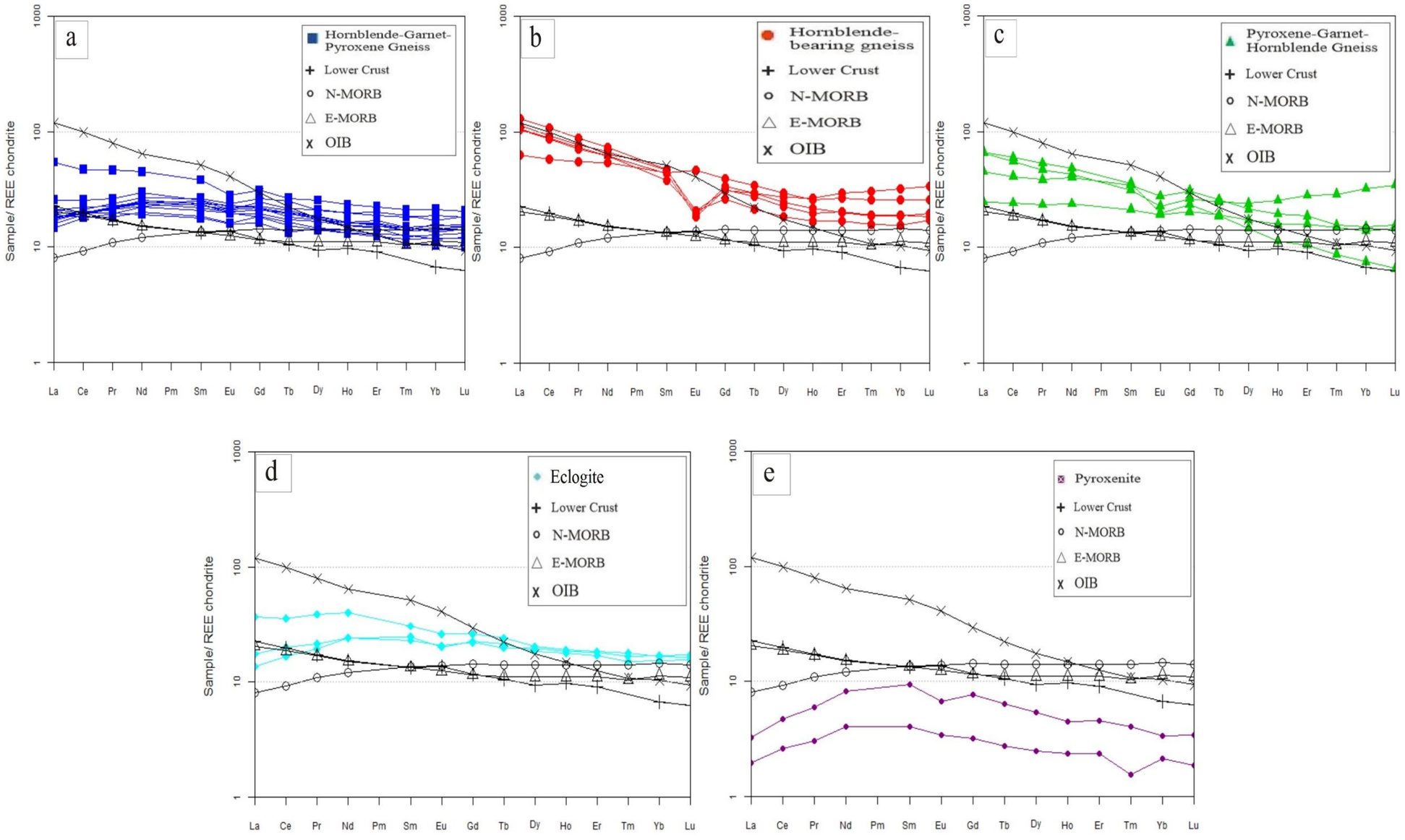

Fig. 4.57. Chondrite-normalized plots of the REE composition of the rock in the study area (a) hornblende-garnet-pyroxene gneiss; (b) hornblende-bearing gneiss; (c) pyroxene-garnet-hornblende gneiss; (d) eclogite and (e) pyroxenite. REE chondrite-normalize (Boynton,1984) plot and values for Lower Crust values from Rudnick and Fountain, 1995, N-MORB, E-MORB and OIB values from Sun and McDonough, 1989.

4.5.2.2 Transition Elements

Transition elements reported by the geochemical analysis are chromium (Cr), vanadium (V), scandium (Sc), zinc (Zn), cobalt (Co) and nickel (Ni). Concentrations of these transition elements in the mafic/ultramafic rocks are higher than those in the felsic and intermediate gneisses. There are no significant variations in the Co concentrations in the mafic/ultramafic rocks but concentration is lower in the felsic gneiss. The Co concentrations for the hornblende-garnet-pyroxene gneiss range from 28 to 59 ppm, 47 to 51 ppm for the eclogite, 55 to 59 ppm for the pyroxenite, 6 to 51 ppm for the pyroxene-garnet-hornblende gneiss and <1 to 9 ppm for the hornblende-bearing gneiss.

Nickel content ranges from 22 to 209 ppm in the hornblende-garnet-pyroxene gneiss, 139 to 155 ppm in the eclogite, 432 to 479 ppm in the pyroxenite, 9 to 173 ppm in the pyroxene-garnet-hornblende gneiss and <1 to 6 ppm in the hornblende-bearing gneiss. The Cr content in the hornblende-garnet-pyroxene gneiss has a range of 100 to 440 ppm, 310 to 370 ppm in the eclogite, 1580 to 3040 ppm in the pyroxenite, 30 to 440 ppm in the pyroxene-garnet-hornblende gneiss and 10 to 30 ppm in the hornblende-bearing gneiss. The vanadium concentrations in hornblende-garnet-pyroxene gneiss, eclogite, pyroxenite, pyroxene-garnet-hornblende gneiss and hornblende-bearing gneiss are in the range of 280 to 403 ppm, 330 to 338 ppm, 159 to 297 ppm, 51 to 350 ppm and 6 to 72ppm respectively. There is no significant difference in Sc concentrations in the mafic/ultramafic rocks; (31 to 44 ppm in hornblende-garnet-pyroxene gneiss, 40 to 41 ppm in eclogite and 44 to 61 ppm in pyroxenite). Sc concentration in the pyroxene-garnet-hornblende gneiss ranges from 10 to 39 ppm and very low in the felsic hornblende-bearing gneiss (5 to 19 ppm).

4.5.2.3 Incompatible Trace Elements

Figure 4.58 show primitive mantle-normalized (Sun and McDonough, 1989) incompatible elements plot of the mafic/ultramafic rocks and felsic gneisses compared with the lower crust, N-MORB, E-MORB and OIB.

Primitive mantle-normalized incompatible element patterns of the hornblende-garnet-pyroxene gneiss (Fig. 4.58a) display selective depletion in Cs, Rb and K and moderately enriched in Ba. Though more samples show depletion in Cs others show moderate Cs-enrichment. The primitive mantle-normalized incompatible shows depletion in Th and Nd relative to La. This rock shows strong depletion in selective highly incompatible elements (large ion lithophile elements – LILE) than the high field strength elements (HFSE). Hence the pattern displays enrichment in the HFSE relative to the LILE. Though enriched in Hf and Zr contents the pattern is almost flat for the HFSE. For the heat-producing elements (HPE), the primitive mantle-normalized incompatible element patterns display depletion in the Th and moderate concentrations in in K and U. The patterns exhibited by this rock is similar to that of lower crust and N-MORB (Fig. 4.58a).

Primitive mantle-normalized incompatible element patterns of the hornblende-bearing gneiss show depletion in Cs and Rb with positive peaks for K and Ba (Fig. 4.58b). The patterns display depletion in Ta, Ti and P and also enrichment in Zr and Hf contents. The rock also displays depletion in the HPE Th and U and has a positive peak for K (Fig. 4.58b). This rock hence shows characteristics of middle to lower crustal composition.

The pyroxene-garnet-hornblende gneiss also shows primitive mantle-normalized incompatible element patterns similar to those of the lower crust (Fig. 4.58c). This rock shows selective

depletion of strong incompatible elements (LILE) Cs, and Rb with moderate Sr content and also moderately depleted in the HPE Th and U with moderate K content. It also shows a positive peak for Ba and depleted in Ta and Ti.

Figure 4.58d shows a primitive mantle-normalized incompatible element patterns for the eclogite. The eclogite samples display strong depletion in Cs and Rb, moderate K content and positive peak for Ba as well as a weak depletion in Ta (Fig. 4.58d). It also shows depletion in Th with moderate U content. This rock shows a strong LILE depletion relative to the HFSE. The patterns show relatively flatter and HFSE-enrichment as compared to a steep LILE-depletion. This pattern mimics that of the N-MORB (Fig. 4.58d).

Figure 4.58e shows primitive mantle-normalized incompatible element patterns of the pyroxenite compared with the primitive mantle, N-MORB, E-MORB, OIB and lower crust. Primitive mantle-normalized incompatible element patterns of the pyroxenite rock (Fig. 4.58e) are similar to those of the N-MORB and primitive mantle. The rock displays selective depletions (negative peaks) in Cs, Th, Nb, K, P and Zr as well as positive peaks for Ba, U, Ta, and Eu. The Primitive mantle-normalized incompatible element patterns of this rock is complex relative to the other rocks of the study area as this rock shows selective depletion and enrichment in both LILE and the HFSE. Averagely it is depleted in LILE and enriched in HFSE. Concentrations of most of the incompatible trace elements plot closer to the primitive mantle, hence this plutonic rock could be a cumulate from a primitive mantle source.

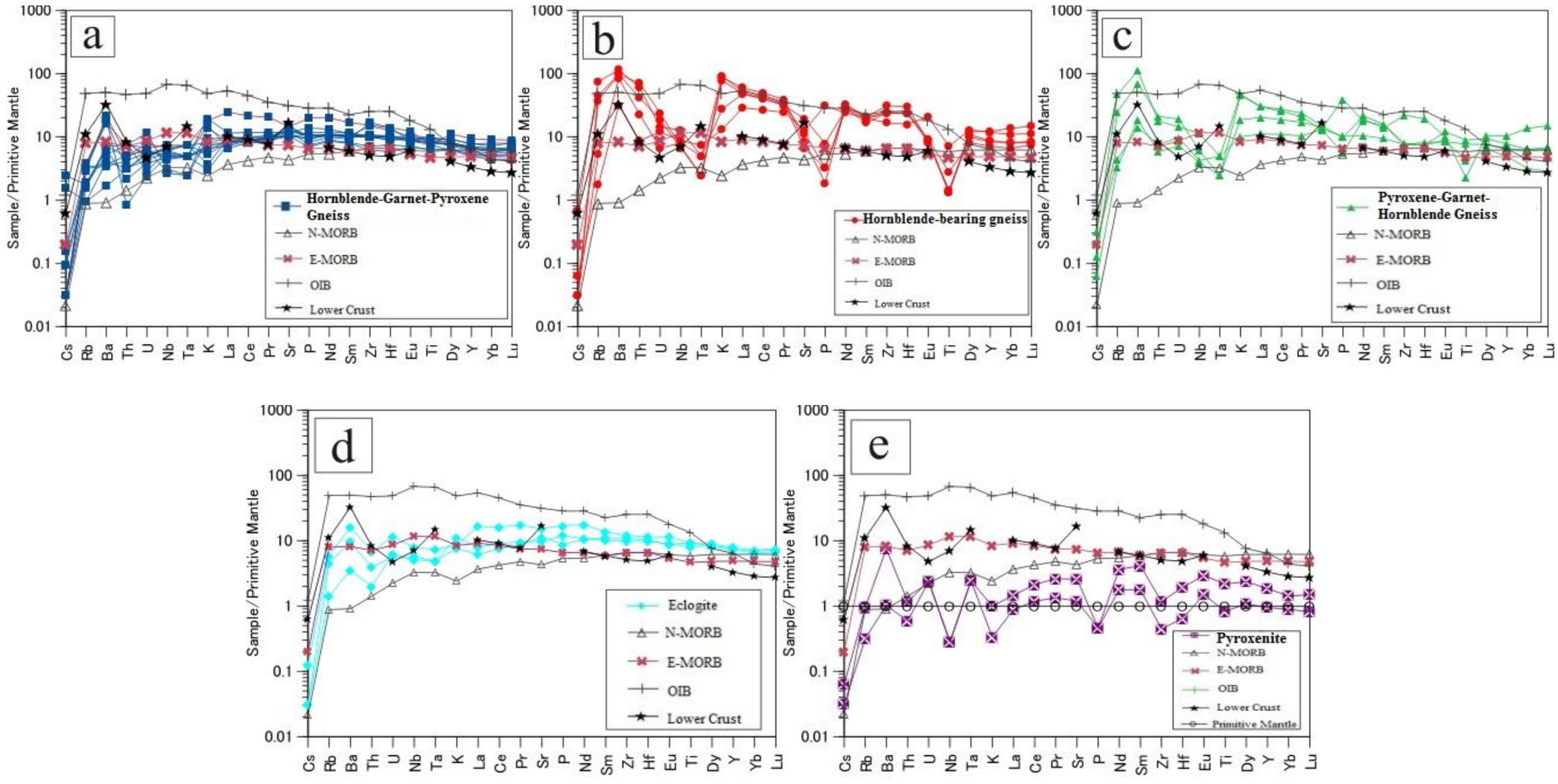

Fig. 4.58. Primitive mantle-normalized plots of the incompatible trace element composition of the rock in the study area (a) hornblende-garnet-pyroxene gneiss; (b) hornblende-bearing gneiss; (c) pyroxene-garnet-hornblende gneiss; (d) eclogite and (e) pyroxenite. Normalizing values for Lower Crust values from Rudnick and Fountain, 1995, values for Primitive mantle, N-MORB, E-MORB and OIB from Sun and McDonough, 1989.

CHAPTER FIVE

DISCUSSION

Discussion of the results is based on the textural, mineralogical and chemical compositions, structural and petrographic analysis, interpretation of geochemical data and field relationships.

5.1 HP and UHP Metamorphism

The new petrological data obtained from field and from microstructural analysis suggest that these HP/UHP mafic/ultramafic rocks of the Dahomeyide suture zone were possibly formed from the Pan-African subduction complex. The distinctive features of these HP/UHP granulites are the occurrence of scapolite, and relatively high modal abundance of garnet (20 vol %) with exsolved rods of rutile. The mineral assemblage of the granulites helped to group them into garnet-diopside-rich granulite (hornblende-garnet-pyroxene gneiss), garnet-hornblende-rich granulite (pyroxene-garnet-hornblende gneiss), both of which have the same compositional amount of garnet (20%). The garnet-diopside-rich granulite has mineral proportions of 20% garnet, 30% diopsidic-pyroxene, 15% hornblende, 10% plagioclase, 10% quartz, 2% scapolite, 4% calcite, 5% chlorite, 3% epidote and 1% rutile. The garnet-hornblende-rich granulite also has mineral proportions of 20% garnet, 40% hornblende, 5% pyroxene, 10% plagioclase, 20% quartz and 5% chlorite. The hornblende-bearing gneiss which is also a HP rock is felsic in composition with mineral assemblage of 45% quartz, 20% plagioclase, 5% pyroxene, 13% hornblende, 9% garnet, 5% biotite, 2% epidote and 1% zircon. The eclogite is an UHP ultramafic rock composed of 27% pyrope-garnet, 57% diopsidic-

pyroxene, 5% hornblende, 5% plagioclase, 3% quartz and 3% chlorite. Field distribution of these HP/UHP mafic/ultramafic and felsic gneisses and associated ultramafic plutonic rock (pyroxenite) is shown in Fig. 5.1 with SW-NE and NW-SE cross-sections. The pyroxenite and eclogite occur as pockets of lenses on the map and the granulites dominate the area.

Small rods of rutile exsolution which have filled cracks and fractures within the subhedral-euhedral garnet porphyroblasts of the mafic granulites indicate UHP metamorphism (Fig. 4.8a and b). Attoh and Nude (2008) also noted this microstructure clearly in samples from Shai Hills and they also attributed the presence of the exsolved rutile rods to UHP metamorphism.

From the various mineral assemblages in the different rocks it can be deduced that metamorphic facies of rocks range from eclogite-to granulite-to amphibolite-to- greenschist facies. High-pressure (HP) granulite facies rocks dominate the study area. The eclogite facies is marked by garnet and diopside-rich clinopyroxene; granulite facies is marked by clinopyroxene, garnet, scapolite, plagioclase and hornblende assemblages; amphibolite facies is marked by hornblende, plagioclase and few garnet mineral assemblages; and the greenschist facies assemblage is marked by chlorite, epidote and quartz. Progressive subduction of the rocks to mantle depth at high pressure/low temperature conditions led to eclogitization (prograde metamorphism) of the rocks and later exhumation of these rocks resulted in retrograde metamorphism. The HP/UHP mafic/ultramafic rock assemblage therefore preserved retrograde assemblages under granulitic-amphibolitic-to greenschist facies conditions.

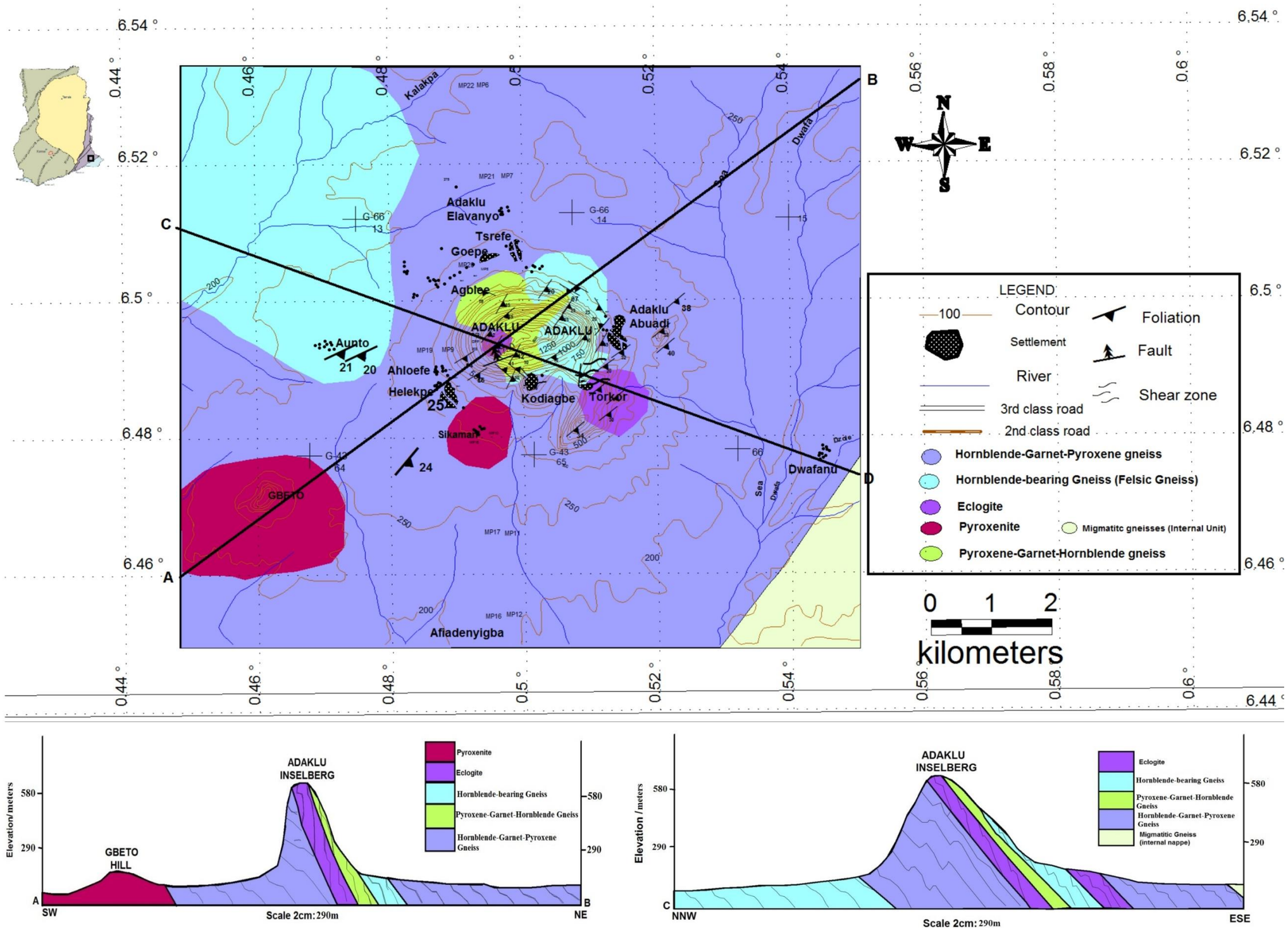

Fig. 5.1. Composite geological map of the study area with cross-sections through SW-NE and NW-SE portions of the area.

Gradual stages of prograde basalt/gabbro-to-eclogite and retrograde transformations are preserved by the disequilibrium textures of incomplete reactions within the granulites and eclogites. Corona textures observed around garnet grains in the eclogite and granulite from the thin section analysis (Fig. 4.28 and 4.8) suggest that chemical equilibrium in these rocks has not been attained. Chemical reaction between the garnets and the pyroxenes resulted in the formation of quartz around the garnets in the eclogite and suggests a solid-to-solid net transfer reaction in the rock. Alteration and secondary minerals like chlorite, epidote, sericite and calcite observed in most of the rocks during microscopic analysis confirms retrograde metamorphism of these rocks.

Some garnet porphyroblasts observed on the field (Fig. 4.56a to 4.56d) were very helpful in timing metamorphism and deformation of rocks in the study area. Both pre-tectonic and syn-tectonic garnet porphyroblasts were observed in the HP granulite and felsic gneisses. The internal foliations (S_i) of pre-tectonic garnet porphyroblasts are straight and external foliations (S_e) have been wrapped around the porphyroblast (Fig. 4.56c and 4.56d). For the syn-tectonic garnet porphyroblasts they have characteristic spiral and flattened or folded S_i and mostly have asymmetrical tails (Fig. 4.56a and 4.56b). The rocks at Adaklu have therefore experienced polyphase tectonic and metamorphic history.

Calcite grains are also present in the granulite samples which were taken from a quarry in Adaklu Abuadi (Fig 4.10b) and the calcite grains are mostly associated with the garnets. Wickham et al. (1994) published that regional alteration of the crust associated with major shear zones provides direct evidence for mantle-derived magmatic CO_2 rich fluid mobility. In this case localized carbonate alteration of silicate rocks was involved with the growth of calcite and perhaps other carbonate minerals which have replaced preexisting silicates. During this

metasomatic process, ankerites which probably recrystallized to the calcites was generated close to equilibrium with the silicate minerals at higher temperatures of about 500°C (Wickham et al., 1994). The calcite later formed within the rocks at much lower temperatures by recrystallization of the ankerites, possibly during later stage infiltration of H_2O-rich fluids. Hence carbonate alteration of this type often located along major shear zones, may represent a lower temperature mid-crust manifestation of the deeper level CO_2 infiltration. The carbonates which occur as secondary minerals might have also resulted from hydrothermal alteration during metamorphic processes.

The occurrence of HP metamorphic rocks and eclogite in this area of the suture zone suggests paleo-subduction processes. Agbossoumondé et al. (2001) also suggested paleo-subduction processes for the suture zone HP metamorphic rocks and eclogite at southern Togo.

From field observations, compositional, microstructural and textural analyses, it can be inferred that all the gneiss are from a magmatic source origin (basaltic/gabbroic). Their basaltic or gabbroic parentage was subducted to deeper depth (mantle depth) and recorded prograde garnet crystallization during eclogite facies metamorphism at relatively higher pressure / lower temperature conditions which was later followed by HP granulite facies metamorphism and then later decompression along a retrograded path at low temperature and pressures which was accompanied by partial melting to generate the felsic components of the gneisses. Hence these gneisses of the same parentage have been differentiated by metamorphic processes (metamorphic differentiation) and partial melting, as the felsic gneiss contains relicts of the mafic granulitic rocks. Attoh (1998) has suggested that the rocks of the suture zone preserve a record of prograde garnet crystallization during eclogite facies metamorphism as temperature increased to a maximum of ~600°C and pressure reached at least 18kbar followed by HP

granulite facies metamorphism when temperature reached 800-900°C at 14kbar, resulting in partial meting to produce felsic components and then later followed by decompression along a retrograde path down to ~700°C at 10kbar.

The pyroxenite which probably occurred in a later stage is weakly deformed and weakly metamorphosed.

5.2 Deformation and Structures

Adaklu falls within the suture zone of the Dahomeyide orogenic belt and hence has recorded long periods of multiple deformation events. The various structures observed resulted from different episodic deformational events which affected the area.

The tectonic foliations (S_1 tectonites) observed are dominantly exhibited by all the mafic/ultramafic garnet-bearing and felsic gneisses in the area. The Lambert stereographic plots (Fig. 4.37) for foliations show that these gneisses strike averagely in the NE-SW direction and also show relatively gentle dip in the SE direction. Nonetheless there are various localized deviations of the strike and dip directions of foliation planes in the study area. These deviations are due to a probable inferred opened asymmetrical upright fold (F_1) which has affected the area. Evidence of F_1 was observed in Kodiagbe where the limbs of this fold were observed to be dipping in different directions and at different angles. From field observations the inferred fold axis for F_1 trends in the NNE-SSW direction.

In thin section analysis S_1 foliation is defined by elongated grains of minerals such as quartz, amphiboles, and some garnets. S_1 foliation marks the first phase of deformation (D_1) in the

area, which was caused by compression and shearing. F_1 was also caused by the same compressional deformation event D_1. Hence S_1 and F_1 were both caused by D_1 deformational event. From field observation and careful analysis the axial plane of F_1 is sub-parallel to the S_1 foliation planes (S_1 strikes in NE-SW and axial plane of F_1 strikes in NNE-SSW direction).

From field evidences and microstructural analysis, D_1 deformation divulges dextral sense of shear deformation. This was resolved with the aid of some kinematic indicators such as the retort-shaped asymmetrical garnet porphyroblasts which were observed in the field. These asymmetrical porphyroblasts are syn-tectonic (were also affected by D_1) and exhibit dextral sense of deformation. D_1 deformation in the NW-SE direction caused the progressive spiral and flattened or folded internal foliation (S_i) of the porphyroblasts. The spiral patterns of inclusion within the porphyroblasts is interpreted as a result of the porphyroblast being rowed by shear along the foliation plane as the garnets grew (Winter, 2001).

The area later experienced an extensional D_2 deformational event which is evident by the numerous normal faults, listric faults, graben and a normal drag fold which were observed around Kodiagbe in the pyroxene-garnet-hornblende gneiss (south of the inselberg – Fig. 4.42 to 4.47). These normal faults (Ft_1) mimic each other. The faults planes of these normal faults strike in the NE direction and dip steeply in the NW direction. They all exhibit sinistral sense of shear deformational movement. On the field it was observed that Ft_1 was affected by another extensional deformation Ft_2 (Fig. 4.46). This is also evident by the normal drag fold (Ft_1) at Kodiagbe which has been cross-cut by another normal fault (Ft_2) as shown in Fig. 4.44. Hence faulting was initiated first by the first extensional deformation, followed by shear deformation along the fault causing the drag fold (Ft_1) as one block was dragged along the other. This drag fold (Ft_1) was then later affected by the Ft_2 extensional frictional shear deformation event.

Similarly both Ft_1 and Ft_2 have planes which strike in NE with steep dips in the NW all divulging a sinistral sense of frictional shear deformation (D_2). Hence the second deformational event as observed on the field and thin section is characterized by a sinistral sense of deformation. This extensional event (D_2) is also evident by a stretched and rotated boudin in the pyroxene-garnet-hornblende gneiss (Fig. 4.54). From observation this boudin was stretched by the extensional deformation and also later compressed in a sinistral sense causing the stretched boudin to over-thrust and under-thrust each other in the NW-SE direction. The compression and rotation of this boudin can be attributed to localized compressional perturbations which affected the rocks in the area. Hence the extensional D_2 deformational event was accompanied by a localized compressional event.

The study area was again affected by a last shear and compressional deformation event (D_3). This deformational event is strongly manifested by the strongly sheared hornblende-bearing gneiss which outcrops at Torkor. This rock is strongly sheared and has some boudins and S-C structures (Fig. 4.51 and 4.52) as well as tight symmetrical recumbent folds (Fig. 4.49). Shearing and compressional activities created these boudins and caused them to over-thrust each other in a dextral sense of shearing (Fig. 4.51). Compressional deformation event D_3 also resulted in the formation of F_2 folds which are tight recumbent folds with both horizontal axes and axial planes. Axes of the recumbent folds trend in the SE direction. These F_2 folds have hence overprinted the F_1 folds in the area. The S-C structures in this rock also helped to confirm the dextral sense of shearing (Fig. 4.52) which resulted from the D_3 deformational event.

After a period of relaxation all the rocks in the study area experienced some periods of dilation which resulted in the formation of the parallel orthogonal joint sets which affected all the rocks in the area including the pyroxenite. The pyroxenite is therefore weakly deformed as it displays

these joint sets and also strongly sheared at its contact with the pyroxene-garnet-hornblende gneiss between Sikaman and Helekpe (Fig. 4.31). These joints have steep dips and cross-cut the S_1 foliations in the study area.

From field observation and microstructural analysis, it was observed that portions of the pyroxene-garnet-hornblende gneiss and hornblende-bearing gneiss at the south and east of the inselberg display mylonitic textures in some locations. These mylonitic gneisses show a marked reduced and milled grains (most of which are fragmented). Tullis and others (1982) indicated that mylonitic rocks show a marked reduction in grain size by predominantly crystal-plastic deformation mechanisms. These gneisses in the area exhibit both brittle and crystal-plastic deformation, also known as the brittle-ductile transition zone deformation. According to Sibson's conceptual model (1977; 1983) deformation in rocks which are characterized by brittle-ductile deformation usually occurs at depth of about 7-15 km.

In summary, the area is interpreted to have undergone three main phases of deformation; D_1, D_2, and D_3 based on the structures discussed above. The D_1 event was a transpressional event which produced the penetrative S_1 foliations observed in the rocks which is sub-parallel to the axial plane and axis of fold F_1. D_1 is characterized by dextral sense of deformation. D_2 is marked by a dominant extensional event which resulted in the normal faults (Ft_1 and Ft_2) of the area and the stretched and compressed boudins in the hornblende-garnet gneiss. D_2 is also marked by a subordinate compressional event which is evident by the thrusting of the boudins. D_2 is characterized by sinistral sense of deformation. D_3 which is the last of the main phases of deformation (dextral sense) was a compressional event which is evident in the hornblende-bearing gneiss at Torkor. D_3 resulted in the formation of the recumbent folds F_2 which have over-printed F_1. These three deformation events confirm with a typical convergent boundary

deformation at an arc tectonic setting which starts with collision, extension and a final collision (transtension) which are all represented by the D_1, D_2 and D_3 respectively. After a period of relaxation all the rocks in the study area including the pyroxenite experienced a period of dilation which resulted in the formation of the joint sets.

5.3 Chemical Alteration and Metamorphism

During late and/or post-magmatic alteration and metamorphism, the major elements such as Si, Na, K and Ca and some of the trace elements including Cs, Rb, Ba and Sr are easily mobilized (Pearce, 1975, Schiano et al., 1993 and Dampare et al., 2008). It is therefore very necessary to assess the effect of chemical alteration and/or metamorphism on the samples before attempting any petrogenetic and tectonic setting interpretations. Therefore, it is very important to depend on trace elements, such as high-field strength elements (HFSE), rare earth elements (REE) and transition elements when rocks are altered, for their petrogenesis and tectonic setting interpretation. This is because the HFSE, REE and transition elements maybe immobile during alteration and metamorphism of basaltic and more evolved rocks (Pearce and Cann, 1973; Floyd and Winchester, 1975; Holm, 1985). These elements are characterized by intermediate charge/radius (Z/r) values such that they do not readily form soluble hydrated cations (low Z/r), complex anions (high Z/r) or chloride complexes in fluids (Pearce, 2014). Only relatively fluid-immobile trace elements, such as the rare earth elements (REE) and high field strength elements (HFSE), can be applied to reconstruct compositions of the basaltic and gabbroic precursors (e.g., Möller et al., 1995; John et al., 2003). Several studies by some workers (like Griffiths and Cornichet, 1985; Brunsmann et al., 2001) have however proved

that the light-REE (LREE) are mobilized during high pressure/low temperature metamorphism and this casts doubt on their usefulness for determining protolith compositions.

Figure 5.2 shows a binary plot of loss on ignition (LOI) against SiO_2 concentrations in all the analysed rocks of the area. Dominant rocks of the study area contain very low LOI and moderate to high SiO_2 contents. LOI content in the hornblende-garnet-pyroxene gneiss is < 1 wt%, < 0.5 wt% in the hornblende-bearing gneiss, < 2 wt% in the pyroxene-garnet-hornblende gneiss, < 1 wt% in the eclogite and also < 0.5 wt% in the pyroxenite. According to Dampare et al. (2008) an inverse relation between SiO_2 and LOI may suggest the remobilization of SiO_2 during alteration and/or metamorphism. In a plot of LOI versus SiO_2 (Fig. 5.2) the rocks show a diffuse pattern relation with SiO_2. This coupled with low LOI content in these rocks and diffuse relation with SiO_2 may suggest very weak to moderate alteration of the rocks. On the outcrop and thin section, calcite, chlorite, sericite and epidote were observed indicating alteration features.

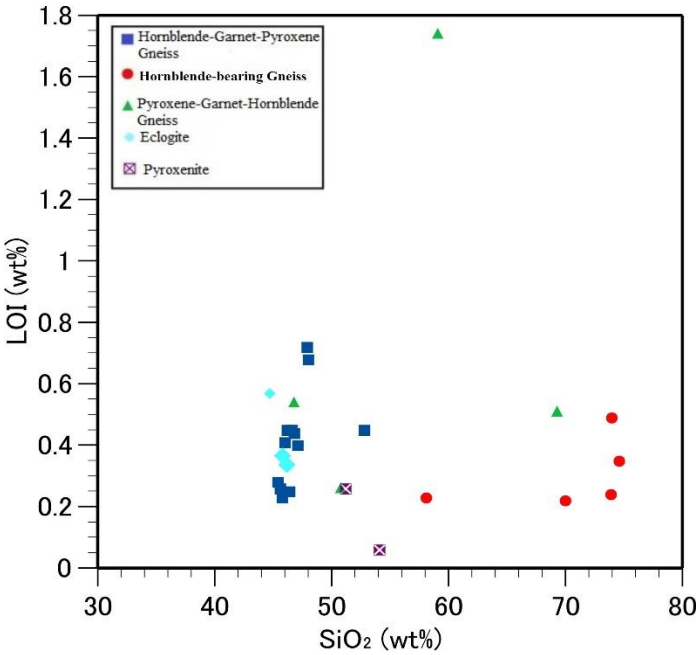

Fig. 5.2. A binary plot of LOI versus SiO_2

Considering all these, conclusion can be made that the rocks in the study area might have undergone weak alteration. The ultramafic pyroxenite from the study area also shows weak alteration and from the geochemical data it shows relatively high SiO_2 concentration than a normal ultramafic rock. This may be probably caused by some intake of SiO_2 during possibly hydrothermal alteration.

To make very certain of the use of the HFSE and especially the REE (since Pearce, 2014; Humphris and Thompson, 1978 and Whitford et al., 1988 observed some mobility of REE (especially LREE) during hydrothermal alteration) for petrogenetic and tectonic setting interpretations a plot of LOI versus Nb/La or Th/La were plotted for the rocks (Fig 5.3a and 5.3b). The lack of correlation between LOI and Nb/La or Th/La suggests that the primary Th–Nb–LREE concentrations in the rocks have not been disturbed by alteration or metamorphism.

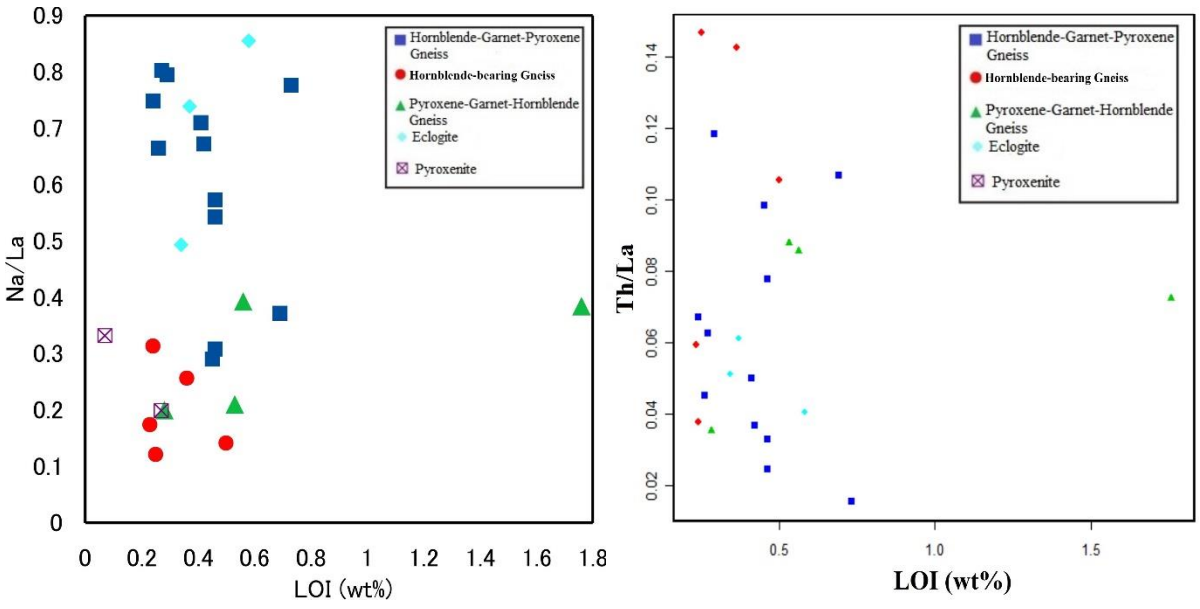

Fig. 5.3: A plot of LOI versus (a) Nb/La and (b) Th/La. The diffuse trend suggests no effect of alteration on the primary Nb, Th and the REEs.

5.4 Classification and Possible Protoliths of the Gneisses

Petrographical investigations based on the texture, composition and microstructure of the rocks have revealed that the rocks in the study area hornblende-garnet-pyroxene gneiss, hornblende-bearing gneiss (felsic gneiss), pyroxene-garnet-hornblende gneiss, eclogite and pyroxenite.

The analysed samples were plotted in the classification diagrams of Cox et al., (1979) for both volcanic and plutonic rock (Fig. 5.4a and b). From Fig. 5.4a and b the mafic gneiss (hornblende-garnet-pyroxene gneiss) plot in the fields of gabbro/basalt, and basaltic andesite. The pyroxene-garnet-hornblende gneiss plots in the fields of gabbro/basalt, andesite/diorite and granite. The hornblende-bearing gneiss (felsic gneiss) plots in the andesite/diorite and granite fields. The gneisses in are subalkaline/tholeiitic in composition and show basic to ultrabasic composition (Fig. 5.4). The eclogite plots closer to the ultrabasic and basic boundary in basaltic/gabbroic fields.

Considering these classification plots it can therefore be inferred that the mafic granulitic gneisses have basaltic/gabbroic protolith, the intermediate gneisses have andesitic protolith and the felsic gneisses also have andesitic to granitic protolith.

A Plot of Zr/Ti versus Nb/Y by Pearce, (1996) was also plotted for these rocks. In this diagram (Fig 5.5) the mafic gneisses plot in the basaltic and basaltic-andesite fields whereas the felsic gneiss plot mostly in the dacites field. Most of the rocks studied show subalkaline/tholeiitic affinity and the felsic gneisses plot in the calc-alkaline series (Fig. 5.56).

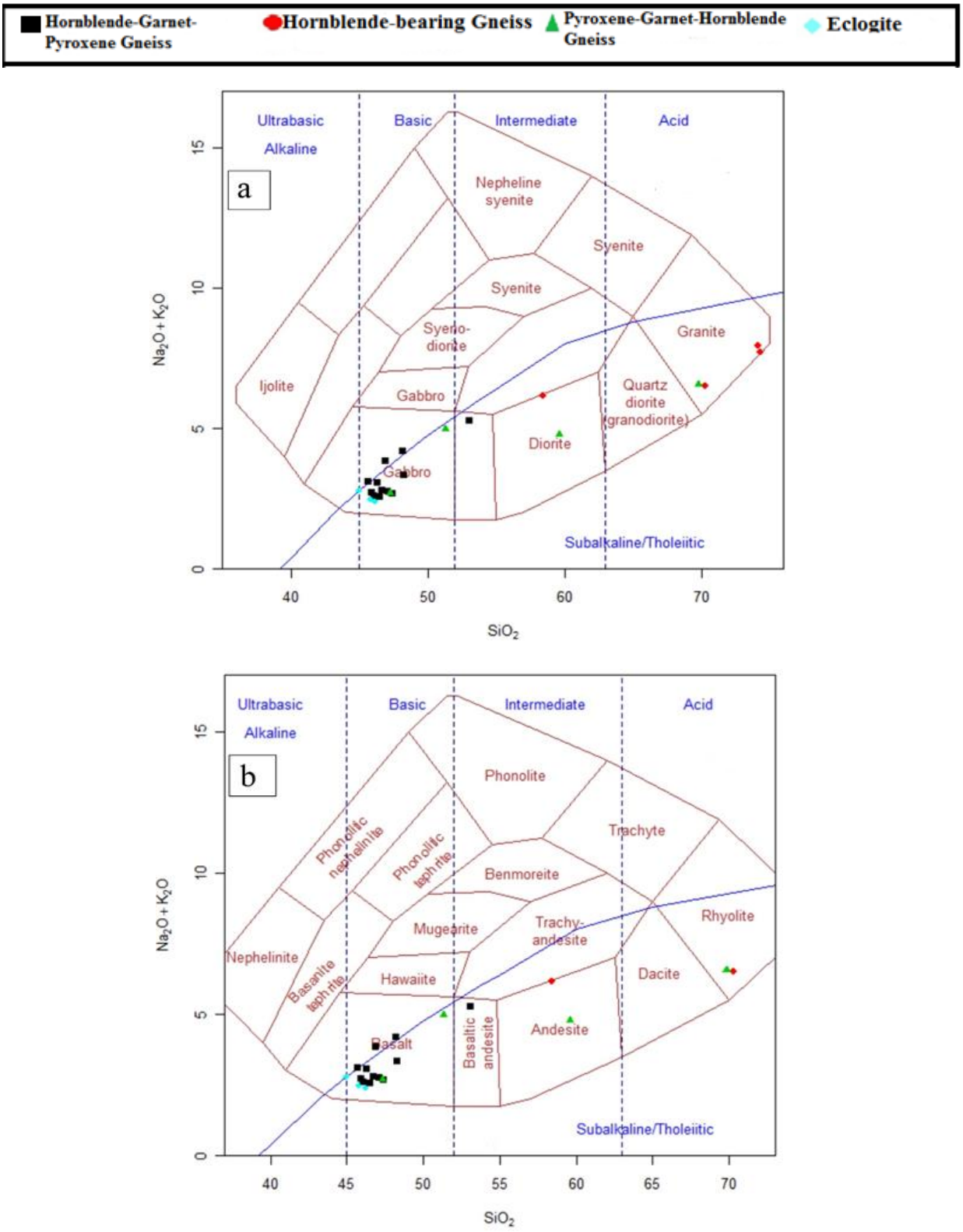

Fig. 5.4: Geochemical classification of the analysed rocks using TAS diagrams of SiO_2 versus Na_2O+K_2O after Cox et al. (1979) for (a) for plutonic rocks and (b) volcanic rocks.

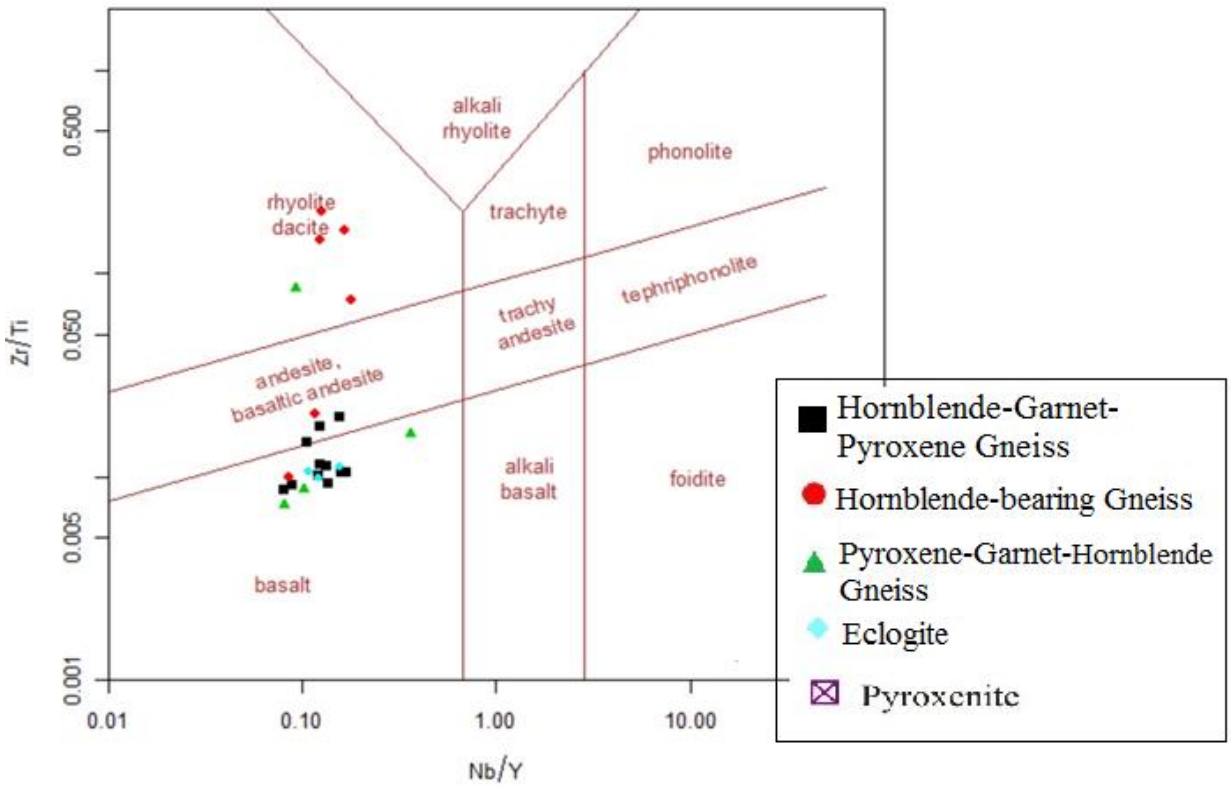

Fig. 5.5. Plot of Nb/Y versus Zr/Ti for the rocks (after Pearce, 1996). All rock plot in the subalkaline region (basaltic to dacitic in composition).

5.5 Petrogenesis

5.5.1 Magma type

Winter (2001) indicated that primary magmas have Mg# >65, Cr >1000 ppm and Ni >400-500 ppm. The mafic and felsic gneisses and the eclogite (from Table 4.2 and 4.3) have Mg# between 25 and 55 and this may suggest that these rocks are not from primary magma and that they are evolved magmas in which their primary magma might have undergone some degree of fractionation. On the other hand, the pyroxenite of the study area has Mg# of 82, Cr content >1000 ppm and Ni content > 400 ppm, suggesting that this rock is from a primary magma. The

evolution of these mafic gneisses and the eclogite was also tested using the AFM diagram (Fig 5.6).

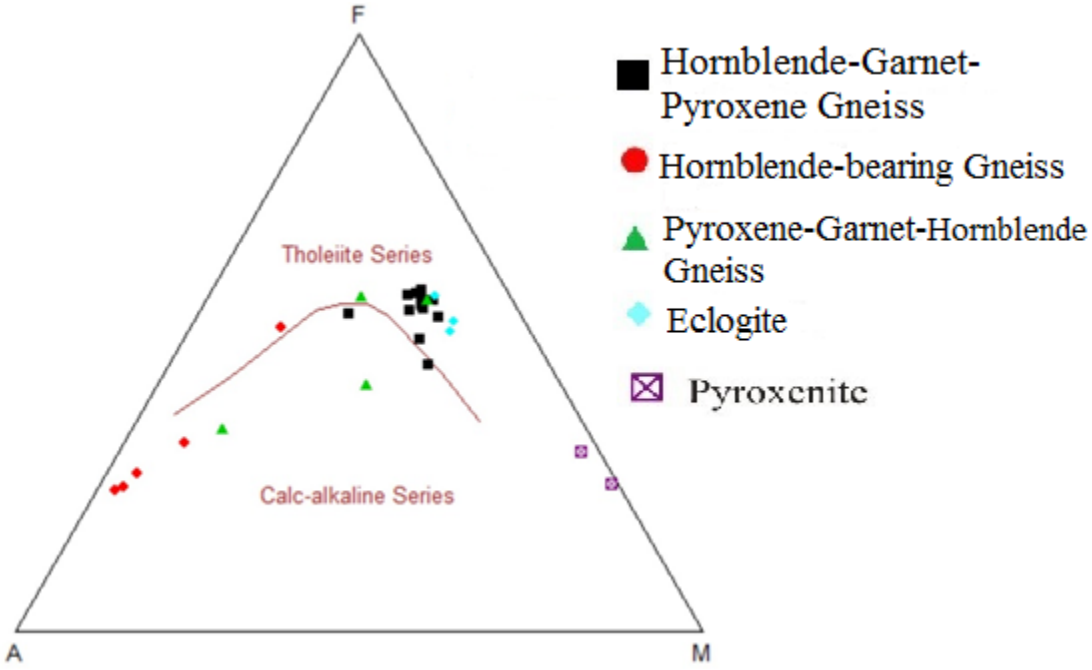

Fig. 5.6. AFM diagram showing samples from the different rocks in the study area. The pyroxenite plots closer to Mg, mafic gneisses and eclogite plot closer to FeOt whereas the felsic gneiss plots away from MgO and FeOt.

On this diagram, the samples of the mafic gneiss and eclogite plot closer to the FeOt end and away from the MgO end whereas the samples of the pyroxenite plot closer to the MgO. This gives an indication that the mafic gneisses and eclogite were not formed from primary magmas but rather from an evolved magma. This also suggests that the pyroxenite was formed from primary magma. The felsic gneiss has relatively low Mg# of 25, low Cr (10-30 ppm) and low Ni (<1.6 ppm) contents. They plot closer to the alkalis and away from the FeOt and MgO (Fig. 5.6). This may suggest that this rock is from a much evolved magma in which its primary magma has undergone different degrees of fractionation. The felsic gneiss evolved from the mafic granulites through metamorphic processes and partial melting.

5.5.2 Crustal influence during Subduction and Mantle Source

The ultramafic to felsic gneisses display negative Nb and Ta anomalies relative to LILE and LREE in the primitive mantle-normalized, trace element diagrams. Such anomalies could be produced by crustal contamination or involvement due to the enrichment of the elements in crustal materials (Zhao and Zhou, 2007). Weak positive Zr-Hf anomalies are displayed by the felsic gneiss (hornblende-bearing gneiss) whereas the ultramafic/mafic gneisses show almost flat and weak negative Zr-Hf anomalies. The felsic gneiss also displays a strong negative Ti anomaly. Upper crust rocks are typically enriched in U, Zr, and Hf elements, and depleted in Nb, Ta, and Ti. Therefore the weak positive Zr-Hf anomalies and strong Ti depletion exhibited by the felsic gneiss suggest crustal contamination or a role of the crust during the subduction and exhumation processes. The mafic/ultramafic rocks comparably show very little crustal contamination as these rocks show negative Th, moderate U and almost flat Zr-Hf anomalies. Also low Th/Yb and high Nb/Th ratios in the mafic/ultramafic rocks are inconsistent with crustal contamination (Fig. 5.7). However, comparably, the felsic gneiss has higher Th and Pb contents, higher Th/Yb and low Nb/Th ratios, suggesting some degree of crustal contamination during the evolution of these rocks at a subduction zone. From Fig. 5.7b and 5.7d it can be deduced that the lower crust played a major role during the subduction processes.

Very high Mg# and Ni content in the pyroxenites leave no doubts that their primary melts were derived from the mantle wedge. The pyroxenite show strong negative Nb anomaly and a visible positive Ta anomaly as well as moderate depletion in Zr and Hf. The negative Nb, Zr-Hf anomalies indicate the lack of an OIB component in the source region. Rather this pyroxenitic rock may have been derived from the lithospheric mantle source. Nb/Ta and Zr/Hf could be significantly fractionated and would be positively correlated during partial melting of the upper

mantle. Plank and White (1995) have proposed that mantle wedge-derived arc basalts may inherit such ratios, reflecting variable degrees of mantle depletion produced prior to episodes of melt generation. In this instance, very low HFSE contents and small Nb/Ta ratios in arc volcanic rocks are believed to reflect previous melt extraction from the mantle wedge (Woodhead et al., 1993). Woodhead et al. (1993) proposed that the process involved in melt extraction would also lead to positive correlation of sub-chondritic Nb/Ta ratios with La/Yb, Th/Yb, Zr/Yb, Zr/Ti, Ti/V and Y/Sc ratios, which would decrease with increasing depletion of the mantle wedge. Contrary, the pyroxenite does not exhibit such consistency in the elemental correlation (Fig 5.7). It appears that the mantle source region of the pyroxenite was a normal lithospheric mantle wedge, which had not been depleted by previous melt extractions.

Rare earth elements and HFSE are relatively immobile in aqueous fluids compared with LILE (Turner et al., 1997). Therefore the enrichment of REE and HFSE in a mantle wedge is attributed to inputs of slab melts than aqueous fluids (Turner et al., 1996, Elliott et al., 1997). Mantle sources modified by slab melt may have lower Th/Zr, Rb/Y (Kepezhinskas et al., 1997), Ba/ Nb and Ba/Th ratios (Hawkeswoth et al., 1997) than those modified by fluids. The chemical compositions of the pyroxenite suggest that its mantle source experienced largely fluid and some melt metasomatism above a subduction zone. The Th/U ratios of the pyroxenites vary from 1 to 2 and lesser than those of the OIB (3.5-3.8) and enriched mantle (EMI) which range from 4.5 to 4.9 (Weaver, 1991). The pyroxenite has high Ba/Nb (36-262), Ba/Zr (1.44-4.03), Ba/Th (144-524) and U/Th (0.5-1) relative to the primitive mantle. Such high elemental ratios in the pyroxenites, which is also higher than those of the average upper crust, suggest that they were likely derived from a mantle source strongly modified by hydrous fluids.

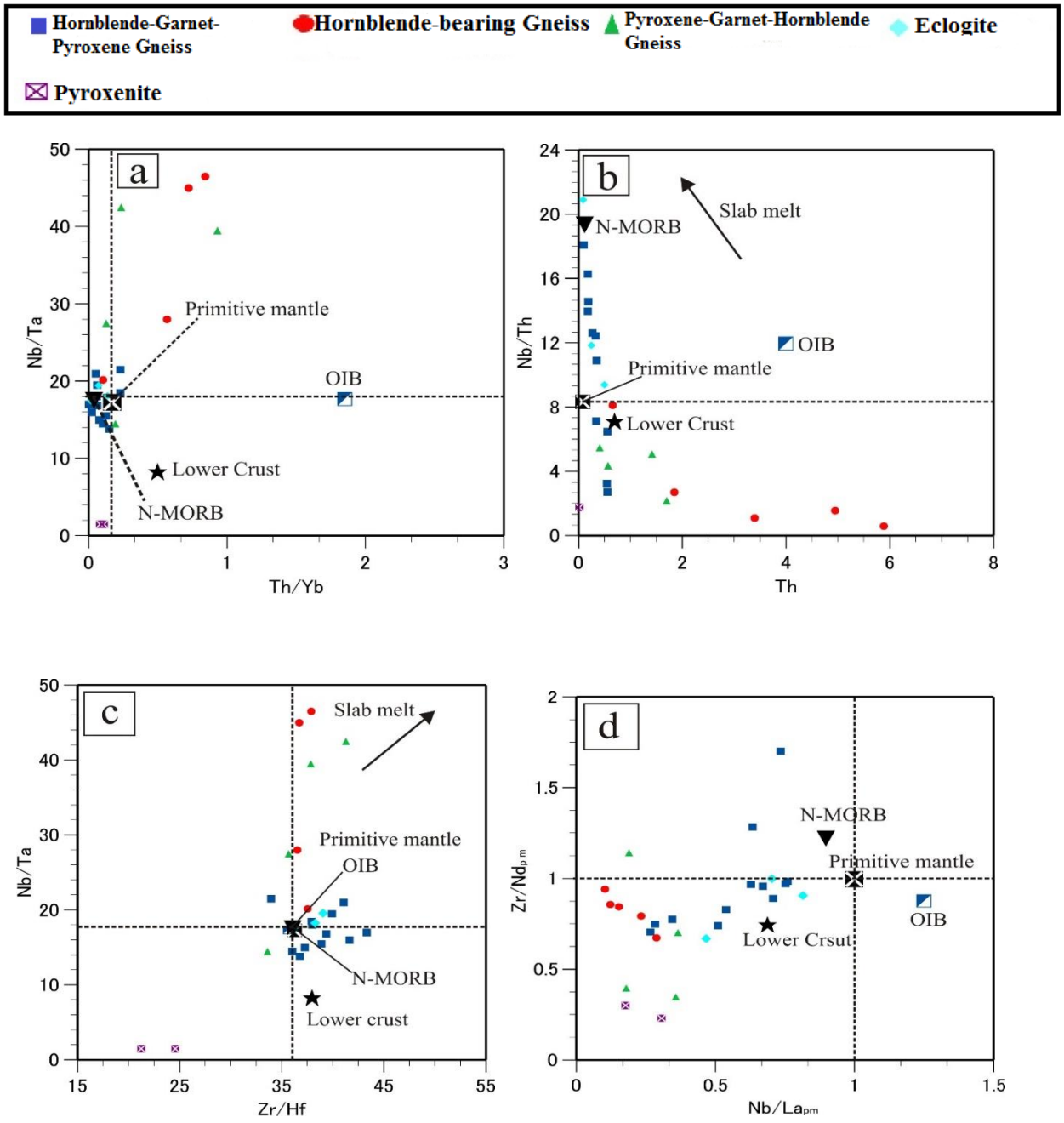

Figure 5.7. Plots of (a) Nb/Ta vs Th/Yb, (b) Nb/Th vs Th, (c) Nb/Ta vs Zr/Hf and (d) Zr/Nd_{pm} vs Nb/La_{pm} for the HP/UHP gneisses and pyroxenite rocks from the study area. Values of N-MORB, OIB and primitive mantle are from Sun and McDonough (1989). Values for the lower crust are from Rudnick and Fountain (1995).

5.6 Tectonic Setting

The new geochemical data presented in this report were used to deduce the geotectonic setting of these UHP/HP rocks. Both major and trace elements geochemical data were used to infer the tectonic setting of these rocks. Despite the variable amounts of major and trace element depletions associated with high pressure/ temperature metamorphism of the HP granulites, the data presented suggest that imprints of the trace element patterns of the magmatic protoliths in the rocks are preserved.

A plot of major elements TiO_2, P_2O_3 (x10) and MnO (x10) concentrations in the mafic and felsic gneisses (Fig. 5.8) show a tight cluster within the island-arc tholeiite (IAT) and MORB and few samples plot in the calc-alkaline basalt (CAB) field. This diagram shows major cluster of the eclogite and mafic gneiss samples within the MORB field. An estimation of lower crust by Rudnick and Fountain (1995) is shown on this diagram for comparison. Hence the Ti, P and Mn concentrations of the UHP/HP mafic gneisses are similar to that of the MORB and lower crust. Though this discriminant diagram was proposed for relatively unaltered basaltic rocks by Mullen (1983), it is used here to compare the concentrations of these elements in the eclogites, granulitic and felsic gneisses with those estimated for the mafic lower crust and with basaltic rocks formed in various tectonic environments.

A plot of La/10-Y/15-Nb/18 discrimination diagram proposed by Cabanis and Lecolle (1989) was used to discriminate between the volcanic-arc basalts, continental basalts and oceanic basalts (Fig. 5.9). Though this diagram has not been widely used, it offers another means of discriminating between different types of MORB. Rollinson (1993) stated that La is mobile under hydrothermal conditions; hence, highly altered and metamorphic rocks may therefore

show some distortions relative to the La apex. A plot of the geochemical data of the gneisses on this diagram shows major cluster of the mafic granulites mostly within the back-arc basin basalts and volcanic-arc tholeiites fields (Fig. 5.9). Some mafic samples plot within a field that overlaps between calc-alkali basalts and volcanic-arc tholeiites. The samples of the felsic gneiss plot within the calc-alkali basalts field.

Figure 5.10 shows a Cr vs Y plot of the HP eclogite and granulite samples with the felsic gneiss based on a diagram to distinguish basalts with N-MORB compositions from those with IAT affinities (Pearce et al., 1984). According to Rollinson (1993), concentration of Cr in volcanic-arc basalts is lower and Cr is compatible in minerals such as olivine, orthopyroxene, clinopyroxene, and the spinels in a basaltic melt. Yttrium (Y) on the other hand, is depleted in island-arc basalts relative to other basalt types for a given degree of fractionation (Rollinson, 1993). The Cr vs Y discriminant plot (Fig. 5.10) can therefore be used to effectively discriminate MORB and volcanic-arc basalts with only a small amount of overlap between them. The plot of rock samples define a broad sub-vertical trend depleted in Y with respect to MORB but with a wide range of Cr contents. They plot in the IAT and MORB fields, with the highest Cr contents in the granulite and eclogite.

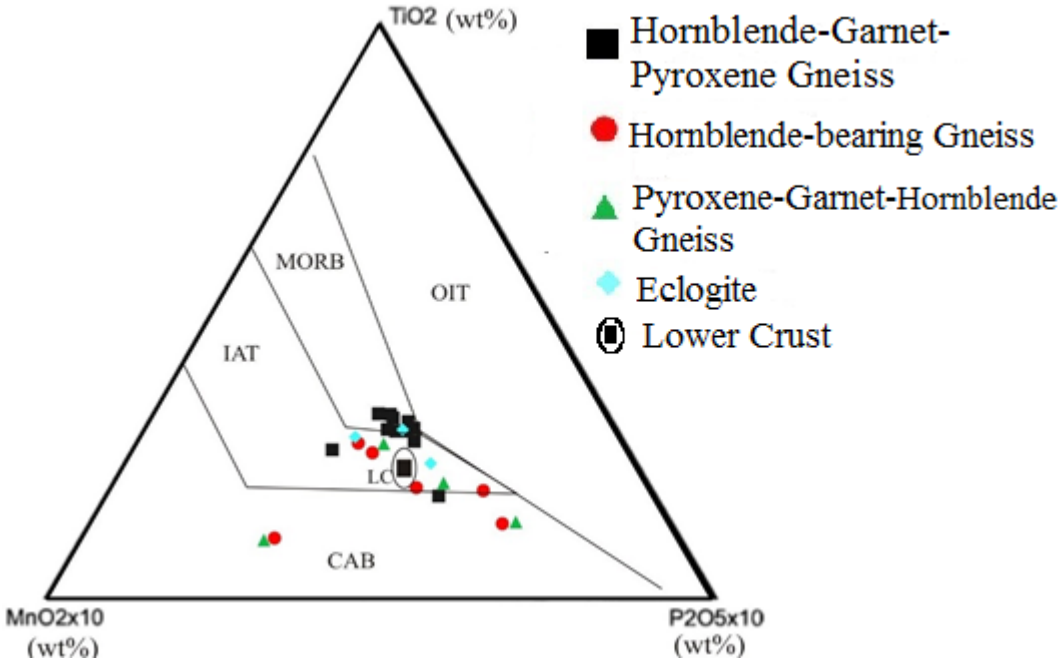

Fig. 5.8. TiO_2–MnO_2(x10)–P_2O_5(x10) plot of HP eclogite and granulite samples. Fields (after Mullen, 1983) are: IAT = island arc tholeiite, CAB = calc-alkaline basalt, MORB = mid-ocean ridge basalt, OIT = oceanic island basalt and LC = lower crust compositional range.

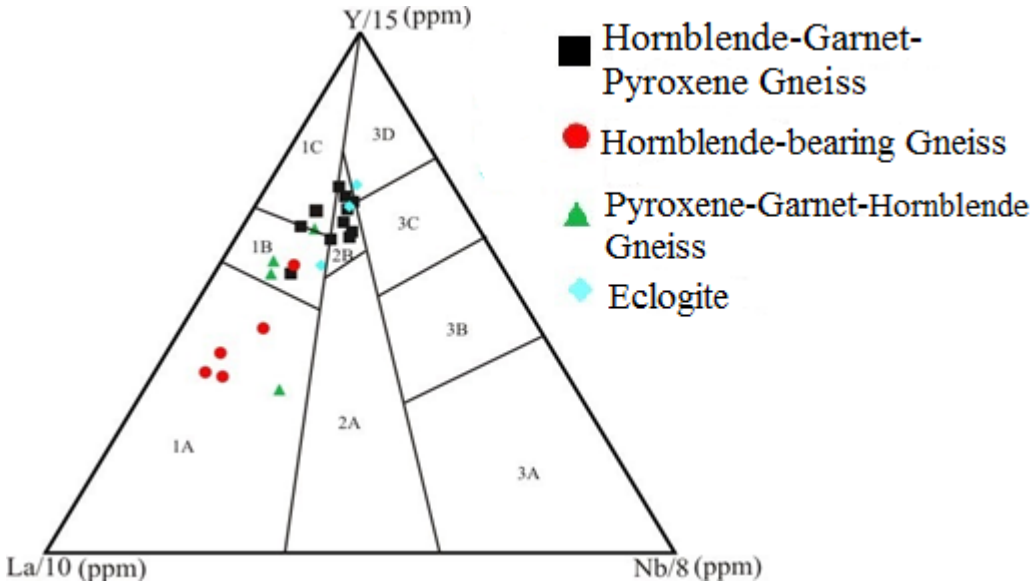

Fig. 5.9. La/10-Y/15-Nb/8 discrimination diagram (after Cabins and Lecolle, 1989). Field 1 contains volcanic-arc basalts, field 2 continental basalts and field 3 oceanic basalts. The subdivisions of the fields are: 1A, calc-alkali basalts; 1C, volcanic-arc tholeiites; 1B is an area that overlaps between 1A and IC; 2A, continental basalts; 2B, back-arc basin basalts; 3A, alkali basalts from intercontinental rift; 3B, 3C, E-type MORB and 3D, N-type MORB.

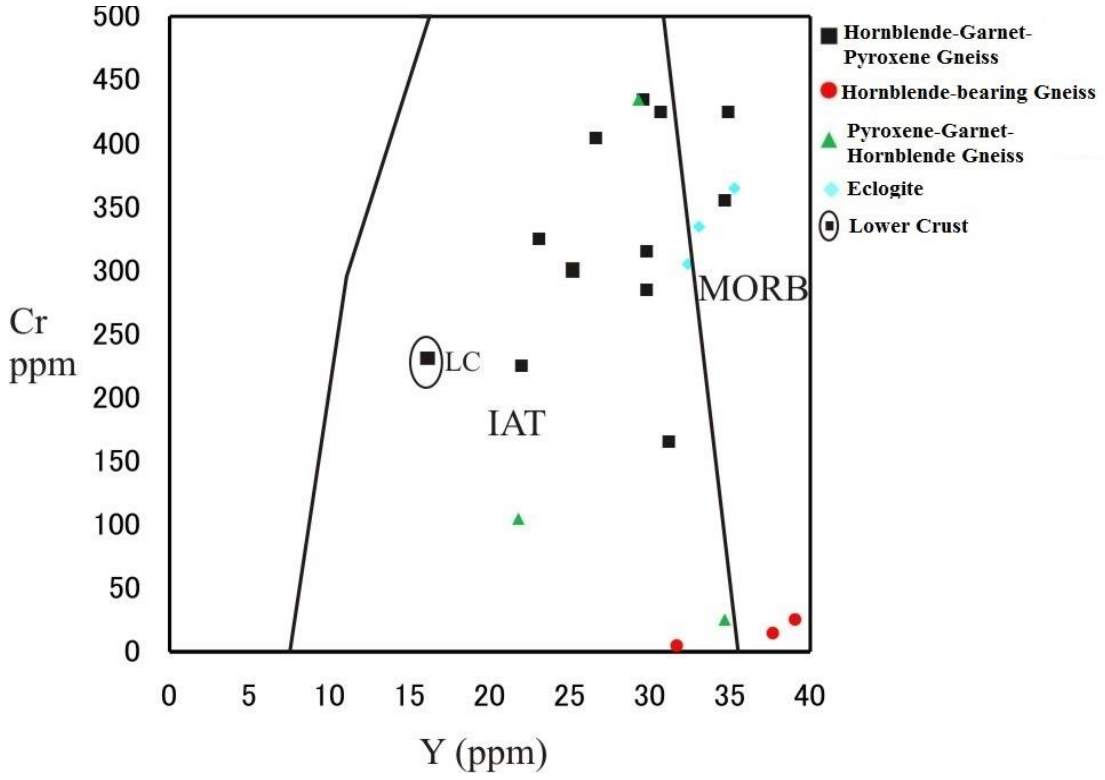

Fig. 5.10. Cr vs Y plot (fields for MORB and IAT after Pearce et al., 1984).

Figure 5.11 shows a plot of Zr/Y-Zr discrimination diagram (after Pearce and Norry, 1979). This diagram was used to discriminate between basalts from ocean-island arcs, MORB and within-plate basalts. This diagram was also used to subdivide island-arc basalts from oceanic arcs, and arcs developed at active continental margins. Majority of the samples plot within the continental arc field and very few in the oceanic arc (Fig. 5.11a). The samples plot in the MORB, island/volcanic-arc and within-plate basalts (Fig. 5.11b).

Ti-Zr-Y and Ti-Zr-Sr discrimination diagrams of Pearce and Cann (1973) were also used to subdivide the rocks into their different tectonic settings (Fig. 5.12). In these discrimination diagrams the samples of the rocks plotted exhibit typical arc setting characteristics. The plot

of samples are clustered in the fields of MORB, island-arc tholeiites and calc-alkaline basalts. The samples which plot in field B for the Ti-Zr-Y plot (Fig 12a) give an ambiguous result and hence were separated by plotting on a Ti-Zr-Sr diagram (Fig. 5.12b) though Ti-Zr-Sr diagram is most appropriately used for fresh samples because Sr is a relatively mobile element in hydrothermal fluids (Rollinson, 1993).

Figure 5.13 shows discrimination plot of Zr-Nb-Y (after Meschede, 1986) which also helped to deduce a tectonic setting for the rocks in the study area. According to Meschede (1986), the immobile trace element Nb can be used to separate the different types of ocean-floor basalt and hence has been useful in the recognition of two types of MORB (N-type MORB and E-type MORB). Samples plotted on the diagram (Fig. 5.13) plot in the N-MORB and volcanic-arc basalts and also within-plate tholeiite and volcanic-arc basalts which also confirms an arc setting for these rocks.

Th-Hf-Ta discrimination diagram for basalts (after Wood, 1980) was also used to deduce the tectonic setting of the rocks in the study area (Fig. 5.14) as this discrimination diagram is particularly good for identifying volcanic-arc basalts. Samples of rocks plotted on this diagram display a very wide range of distribution of plots in the N-MORB, IAT and CAB which also strongly confirms an arc setting environment for these UHP/HP mafic to felsic gneisses of the study area.

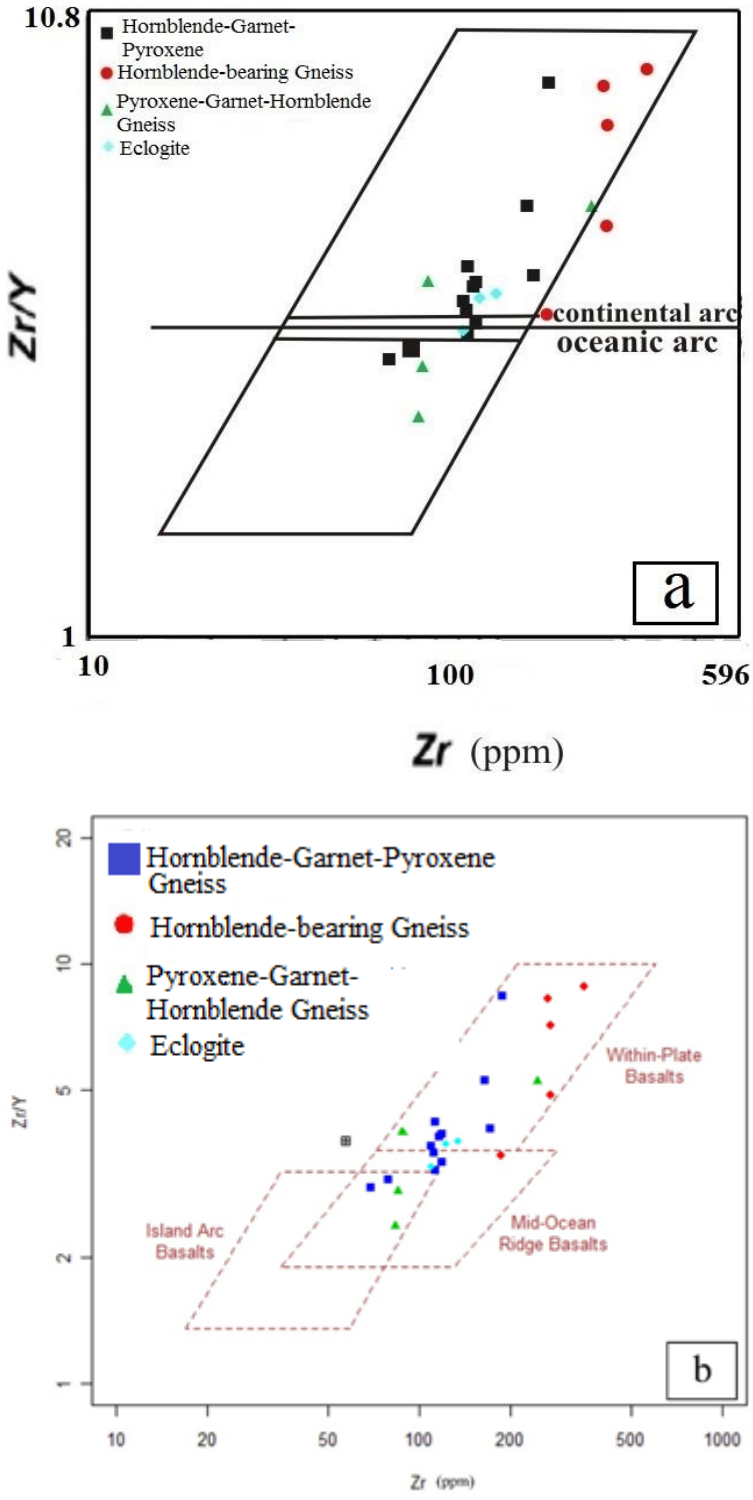

Fig. 5.11. Zr/Y-Zr discrimination diagram (after Pearce and Norry, 1979) used to effective discriminate (a) fields of continental and oceanic-arc basalts (b) fields of island-arc, MORB and within-plate basalts.

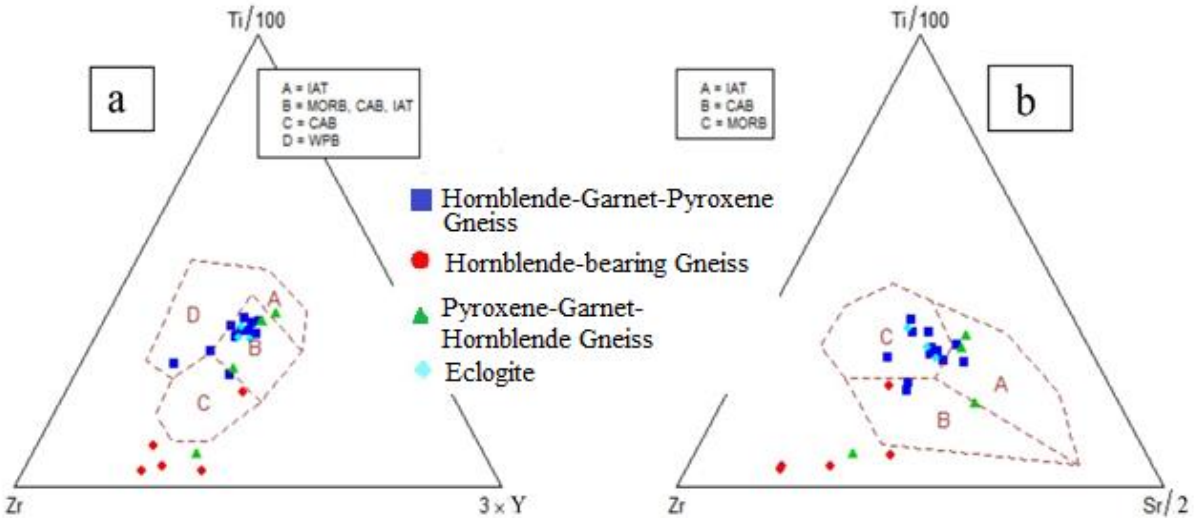

Fig. 5.12 Ti-Zr-Y and Ti-Zr-Sr discrimination plots (Pearce and Cann, 1973). (a) A is field of island-arc tholeiites, C the field of calc-alkali basalts, D is the field of within-plate basalts and B is the field of MORB, island-arc tholeiites and calc-alkali basalts; (b) Island-arc tholeiites plot in field A, calc-alkaline basalts plot in field B, and MORB plot in field C.

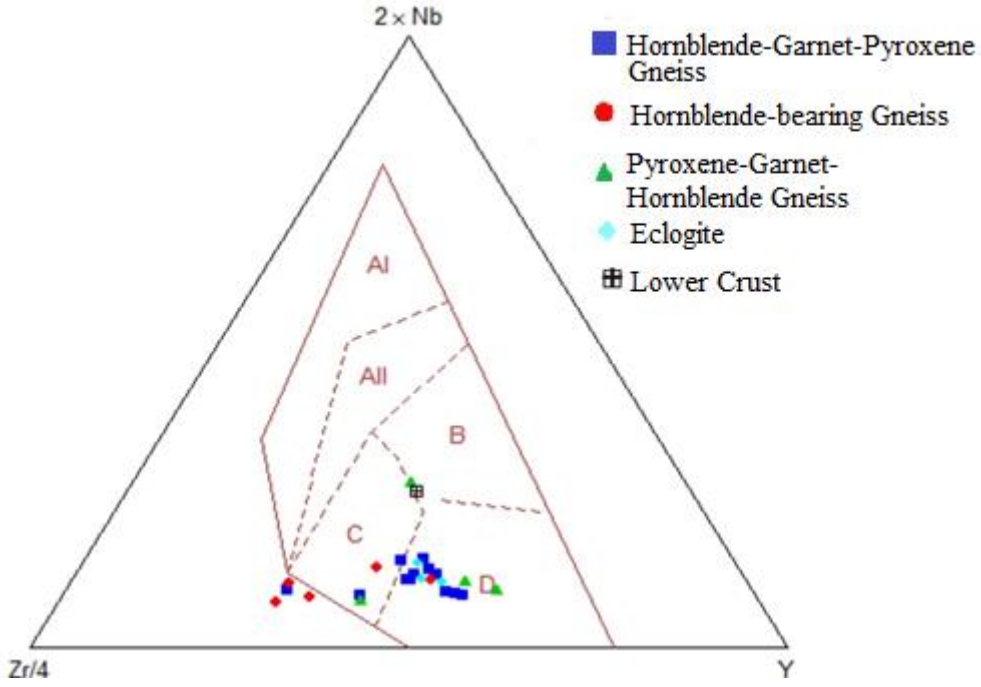

Fig. 5.13. Zr-Nb-Y discrimination diagram (after Meschede, 1986). The fields are defined as follows; AI, within-plate alkali basalts; AII, within-plate alkali basalts and within-plate tholeiites; B, E-MORB; C, within-plate tholeiites and volcanic-arc basalts; D, N-MORB and volcanic-arc basalts.

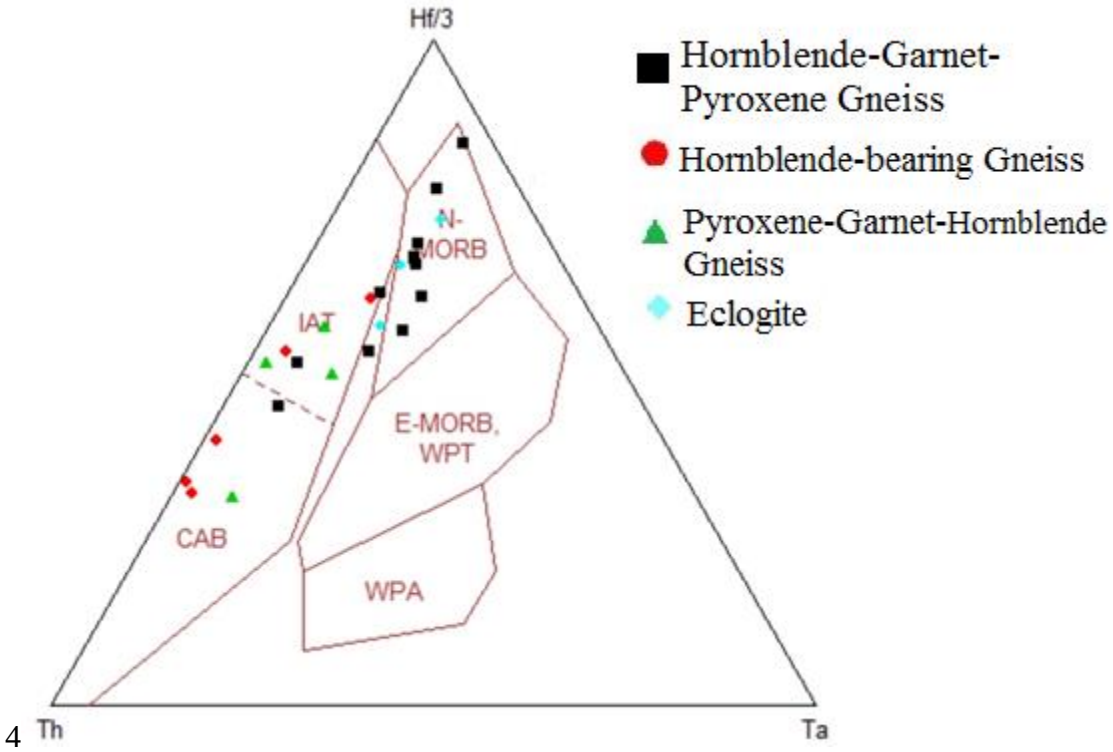

Fig. 5.14. Th-Hf-Ta discrimination diagram (after Wood, 1980) showing wide distribution of plots in the N-MORB, island-arc tholeiites and calc-alkaline basalts.

The samples were also plotted on the Hastie diagram (Fig. 5.15) which was proposed by Hastie (2007) to replace previous plot of Peccerillo and Taylor (1976) by using less mobile elements such as Co and Th. This diagram was proposed particularly for altered arc rocks. The samples plotted on this diagram are clustered mainly in the island-arc tholeiite (IAT) and cal-alkaline (CA) portions (Fig. 5.15). On this diagram, the samples of the mafic granulites and eclogite mainly show basaltic composition and very few plot in the basaltic-andesite region. The samples of the felsic gneiss plot in the dacites-rhyolite portion. None of them plots in the high-K portion of the diagram. The extensively low K tholeiitic and subordinate calc-alkaline character of the samples plotted suggests that the magma genesis of these rocks occurred in a subduction related magmatic arc environment.

Depletion of incompatible trace elements like Nb and Ta in the samples plotted on the spider diagram reflects a source characteristic confirming an arc environment for the mafic rock genesis in area.

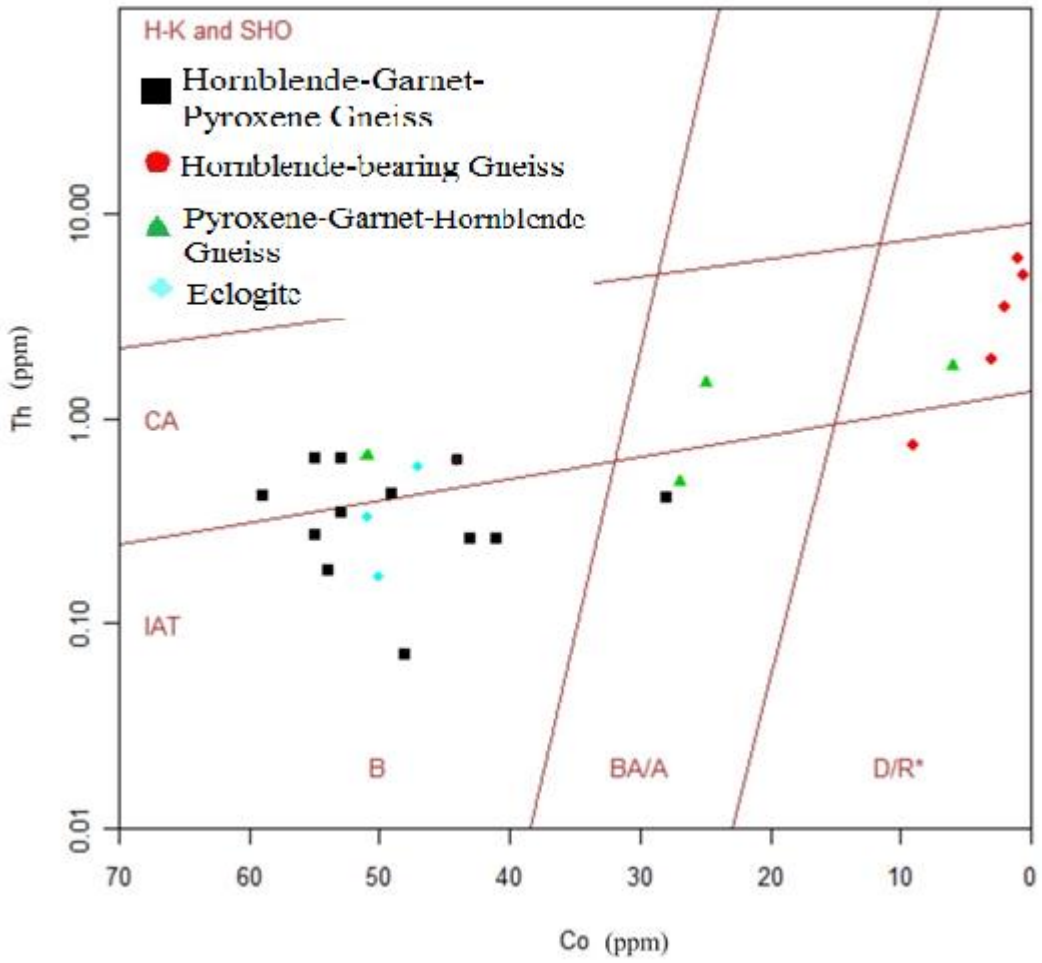

Fig. 5.15. Co-Th diagram (after Hastie, 2007) showing clustered plots of the samples in the island-arc tholeiite (IAT) and cal-alkaline (CA) portions.

From the different plots of major and trace element compositions it can be inferred that the suture zone rocks in the study area consist largely of rocks with IAT affinities and also include suites of rocks with N-MORB (oceanic crust) and calc-alkaline geochemical signatures. Pearce

et al. (1984) proposed that the association of rock suites with IAT and N-MORB imprints could suggest the existence of a subduction zone complex where oceanic crust might have formed in either a back-arc basin or intra-arc basin environment. The rock suites in the area therefore reflects subduction of passive margin of the WAC to result in the formation of UHP/HP granulitic and eclogitic gneisses. Attoh (1998) deduced that the processes involved in the formation of lower continental crust from the roots of a Pan-African volcanic arc included subduction to great depths to produce eclogite facies rocks followed by thermal re-equilibration to produce HP granulite facies metamorphism which was accompanied by partial melting. Exhumation of these UHP/HP rocks might have resulted in retrograding to amphibolite and greenschist facies metamorphism.

Ratios of some critical incompatible element concentrations in the rocks (Table 5.1) can be very useful in the deduction of the geodynamic evolution/setting of these rocks. Th/U ratio in the lower crust is of interest in models of heat production in the earth. Th/U ratio calculated for lower crust by Rudnick and Fountain (1995) is approximately 6. Th/U ratio for the HP granulites and eclogites are variable. Th/U ratio range from 1.4-4.6 in the HP granulites, 2.96-16.8 in the felsic gneiss, 3.25-5 in the pyroxene-garnet-hornblende gneiss and 1.3-2.75 in the eclogite. Only one sample of the granulite has relatively higher Th/U ratio of 10.7. Nonetheless the Th/U ratio of the granulite and eclogite are lower than Rudnick and Fountain's (1995) estimate for lower crust and hence suggests a mantle source of origin for these rocks. That of the pyroxene-garnet-hornblende gneiss is in somehow within the range and hence this rock may represent a lower crustal material which was subducted to mantle depth and later exhumed to the surface. Th/U ratio for the pyroxenite is relatively low (Th/U~1.5 in average).

The K/Rb ratios (Table 5.1) of the gneisses are extremely variable and high (434.83-2324.40 for hornblende-garnet-pyroxene gneiss, 482.47 - 2943.19 for the hornblende-bearing gneiss, 402.32 - 2213.68 for the pyroxene-garnet-hornblende gneiss, 583.30 - 2121.44 for the eclogite and 415.07 for the pyroxenite). The high K/Rb values reflect low Rb content of the protolith. High K/Rb values are inversely correlated with K concentrations as observed for the intermediate composition granulites (Attoh and Morgan, 2004 and references therein) suggesting that high K/Rb may reflect low Rb content of the protolith. Hence these HP gneisses might have suffered severe Rb loss and hence are enriched in highly incompatible elements.

Table 5.1. Ranges of some trace elements ratios used.

Ratios	Samples				
	Hornblende-Garnet-Pyroxene Gneiss	Hornblende-bearing Gneiss	Pyroxene-Garnet-Hornblende Gneiss	Eclogite	Pyroxenite
Th/U	1.40 - 10.70	2.96 - 16.76	3.25 - 5	1.31 - 2.75	1 to 2
K/Rb	434.83 - 2324.4	482.47 - 2943.19	402.32 - 2213.68	583.33 - 2121.44	415.07
Eu/Eu*	0.82-1.01	0.48 - 1.11	0.68 - 0.93	0.85 - 0.93	0.79 - 0.94
Nb/Ta	15 - 22	20.7 - 50	15 - 43	18 - 20	2
Th/Yb	0.03 - 0.26	0.14 - 1.52	0.16 - 0.96	0.05 - 0.17	0.11 - 0.14
Zr/Nd_{pm}	0.73 - 1.72	0.69 - 0.96	0.37 - 1.16	0.69 - 1.02	0.25 - 0.32
Nb/La_{pm}	0.29 - 0.77	0.12 - 0.30	0.19 - 0.38	0.48 - 0.83	0.19 - 0.32
Nb/Th	2.97 - 50	0.83 - 8.38	2.42 - 5.71	9.66 - 21.78	2 to 4
Zr/Hf	34.35 - 43.72	36.94 - 41.69	36.09 - 41.69	36.67 - 39.35	21.67 - 25
Zr/Nb	22.92 - 53.71	11 - 57.21	11 - 57.21	24.11 - 30.56	25 - 65
Ba/Nb	3.14 - 52.05	32.37 - 112.79	32.37 - 112.79	6.81 - 20.18	36 - 262
Ba/Zr	0.09 - 1.45	1.14 - 8.73	1.14 - 8.73	0.22 - 0.84	1.44 - 4.03
Ba/Th	44.62 - 1892.86	149.38 - 512	149.38 - 512	144.12 - 203.64	144 - 524
U/Th	0.09 - 0.71	0.36 - 0.76	0.2 - 0.31	0.36 - 0.76	0.5 - 1

5.7 GEODYNAMIC EVOLUTION MODEL

From field observations, microscopic work (including compositional and textural analyses) and geochemical data, it is confirmed that rocks in the study area are eclogite, the mafic granulites, HP felsic gneisses and pyroxenite. Based on petrographical, geochemical and field data an attempt is made to provide a litho-tectonic model for the geodynamic evolution of the suture zone rocks of at Adaklu. From the field relations observed, the HP diopside-rich granulite gneiss (hornblende-garnet-pyroxene gneiss) will be put at the bottom of the stratigraphic sequence of the study area (Fig. 5.16). On top of the HP granulite are the hornblende-bearing felsic gneiss and hornblende-rich granulite, followed by the eclogite which lies on top of the felsic gneiss. Lithologic contact between the HP diopside-rich granulitic gneiss and the felsic gneiss was observed at SW of Abuadi where the felsic gneiss lies on top of the granulitic gneiss (Fig. 4.4). At Torko, the UHP eclogitic rock lies on top of the felsic gneiss (Fig. 4.5) though enclaves and boudinage of this ultramafic rock are embedded in the felsic gneiss (Fig. 4.53). This means the felsic gneiss which exhibits flow texture and lies beneath the eclogite was derived from the eclogite through partial melting or metamorphic processes and hence possibly younger than the ultramafic rock body. Thrusting of these suture zone rocks can result in the exhumation of the older materials on top of the younger ones. The pyroxenite is the youngest among the rocks as it is weakly deformed and metamorphosed. Hence this ultramafic igneous plutonic body was not affected by the three main deformational events which affected the area.

The study area is part of the suture zone of the Dahomeyide which marks the collision between the WAC and the Sahara Metacraton (SMC). Field observations and geochemical data presented in this research confirms the area to be a continental arc environment where

cessation of subduction of an oceanic slab of the WAC beneath the Benino-Nigerian shield resulted in the collision of the two continental land masses and later exhumation of deep seated rocks to the surface (Fig.5.17). Considerably the dominantly westward verging of the structures along the Dahomeyide suture zone (Attoh, 1998; Agbossoumondé et al., 2004; Agbossoumondé et al., 2013; this study) and the occurrence of eclogitic bodies with WAC affinity, it has been proposed that the initial subduction plane was dipping eastward, beneath the Benino-Nigerian shield (Attoh, 1998; Agbossoumondé et al., 2004; this study).

The presence of UHP rocks indicates subduction of the suture zone rocks to mantle depth during the Pan-African orogeny. Association of granulitic and eclogitic mafic bodies along this area reflects a tectonic mélange of different high grade rocks coming from both plates (the WAC and SMC) acting during subduction (Duclaux et al., 2006). Thermobarometric calculations by Attoh (1998) indicated that the rocks of the suture zone preserve a record of prograde garnet crystallization during eclogite facies metamorphism at high temperature and ultrahigh pressures, followed by HP granulite facies metamorphism with relative high temperature and high pressure and then later followed by decompression along a retrograded path at low temperatures and pressures. Exhumation of these rocks to the surface led to the retrograding of the rocks to amphibolite and greenschist facies metamorphism.

Kinematic indicators observed on the field and microstructures in the suture-zone nappes indicate an early NW-thrusting followed by southerly nappe transport in the southern Dahomeyides (Attoh, 1990; Castaing et al., 1993; this study). These displacements produced the dominant NE-SW folding and superposed folds with ESE axial surfaces observed on the field.

The Lower Crust is believed to be characterized by positive Eu anomalies and depleted in LILE like Rb and Cs (Rudnick, 1992). However the author also stated that most granulites from surface outcrops do not have positive Eu anomalies as exhibited by those reported in this study. The new geochemical data on the mafic granulites and eclogites of lower crustal compositions (this study) show slight negative Eu anomalies in the chondrite-normalized trace element patterns with strong depletions in Cs and Rb. However the felsic gneiss which might be products of the mafic granulites (by anatexis, differentiation or metamorphic processes) show strong negative Eu anomaly. It is therefore possible that small melts of this felsic components remained in the residue to form leucocratic veins in the granulites and hence responsible for the slightly negative Eu anomaly exhibited by the mafic granulites (Attoh, 1998; Rudnick, 1992). Nude et al. (2012) also proposed a slight positive Eu anomaly in mantle-normalized trace element patterns in metasomatic granulitic rocks along the Dahomeyide suture zone in southeastern Ghana supporting the fact that these mafic granulite may be of lower crustal affinity.

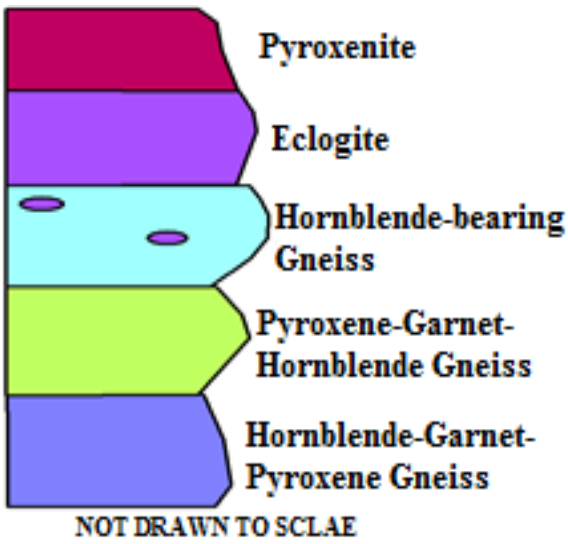

Fig. 5.16. Stratigraphic sequence of rocks in the study area.

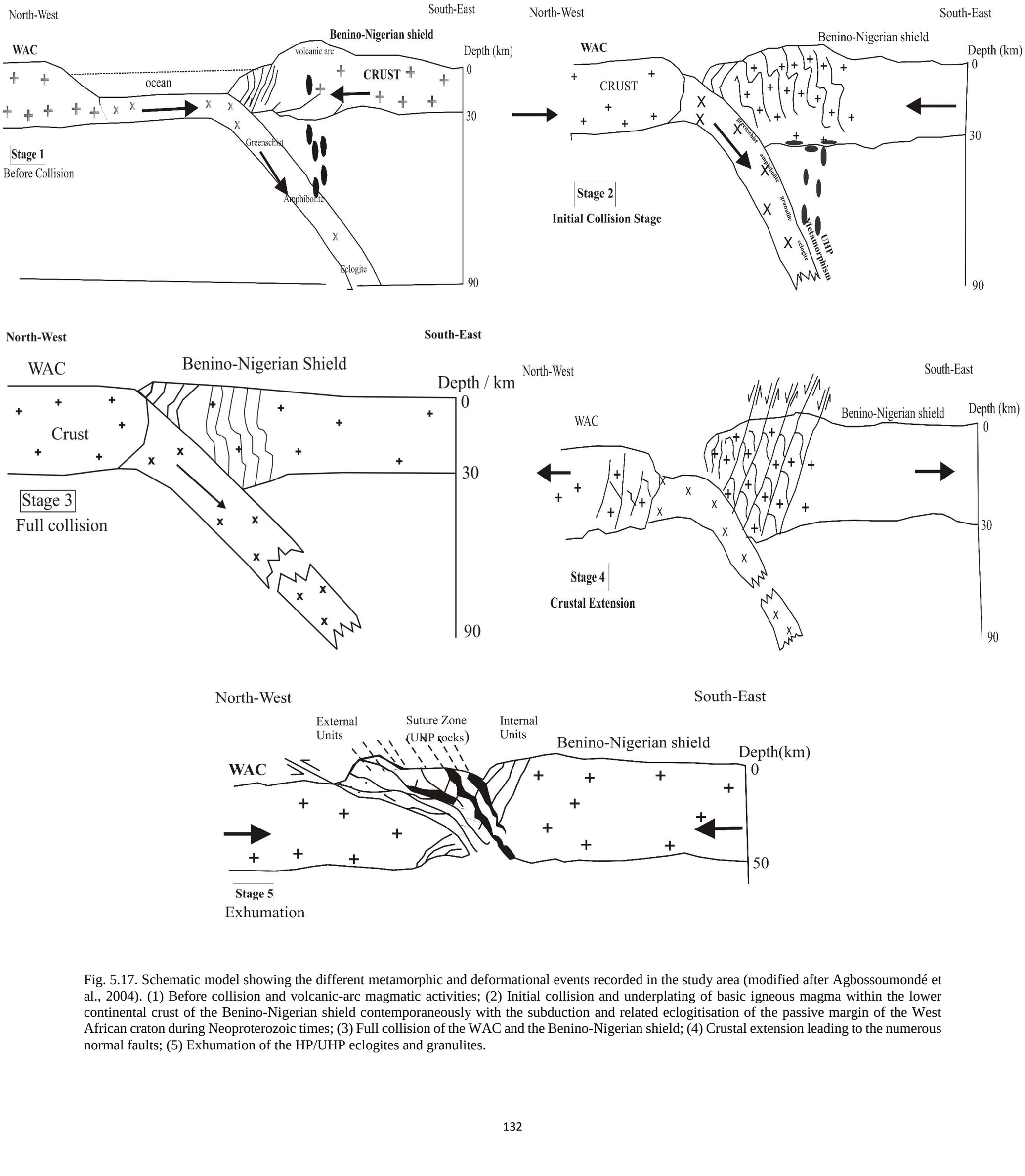

Fig. 5.17. Schematic model showing the different metamorphic and deformational events recorded in the study area (modified after Agbossoumondé et al., 2004). (1) Before collision and volcanic-arc magmatic activities; (2) Initial collision and underplating of basic igneous magma within the lower continental crust of the Benino-Nigerian shield contemporaneously with the subduction and related eclogitisation of the passive margin of the West African craton during Neoproterozoic times; (3) Full collision of the WAC and the Benino-Nigerian shield; (4) Crustal extension leading to the numerous normal faults; (5) Exhumation of the HP/UHP eclogites and granulites.

CHAPTER SIX

CONCLUSION AND RECOMMENDATION

6.1 CONCLUSION

The HP/UHP granulite, eclogite and HP felsic gneisses as well as the associated ultramafic plutonic rock of the Dahomeyide suture zone at Adaklu (SE Ghana) have been studied based on petrography, structures, textures, mineralogical and chemical compositions of the rocks and on new petrological and geochemical data of the rocks presented. With the new petrological and geochemical data, the petrogenesis and sources of the UHP rocks as well as the tectonic evolution and setting have been provided. Listed below are the main conclusions made for this research:

1. The area is made of HP/UHP eclogitic and granulitic gneisses with associated garnet and hornblende-bearing felsic gneiss and an ultramafic plutonic rock (pyroxenite).
2. The presence of small rods of rutile exsolution which have filled cracks and fractures within the garnet porphyroblasts of the mafic granulites can be attributed to UHP metamorphism. Gradual stages of prograde basalt/gabbro-to-eclogite and retrograde transformations are preserved by the disequilibrium textures (corona textures) of incomplete reactions observed within the granulites and eclogites.
3. The presence of UHP rocks indicates subduction of the suture zone rocks to mantle depth during the Pan-African orogeny.
4. The HP mafic granulites are subalkaline and have basaltic/gabbroic composition. Hence, these rocks could have basaltic/gabbroic protoliths (Al_2O_3 concentrations <

18% and Na_2O concentrations around 2-5% for all the gneisses in the area are consistent with normal igneous mafic rocks/protoliths).

5. The HP mafic granulite and UHP eclogite show N-MORB-like characteristics whereas the HP felsic gneiss shows lower crust characteristics. There is also some degree of crustal contamination in the mafic rocks and hence the crust (lower crust) played an active role during the evolution of these rocks. The lower crust from the roots of a Pan-African volcanic arc was part of subduction to greater mantle depths to produce eclogite facies rocks followed by thermal re-equilibration to produce HP granulite facies metamorphism which was accompanied by partial melting to produce the felsic gneisses.
6. From the structural analysis and geochemical data plotted on the discrimination diagrams it can be deduced that these rocks were formed at a passive margin continental arc setting. The rocks exhibit IAT, N-MORB, volcanic-arc tholeiites and calc-alkaline signatures. The IAT and N-MORB signatures exhibited by the rocks suggest the existence of a subduction zone complex where oceanic crust may have formed in either a back-arc basin or intra-arc basin environment.
7. Formation of these rock suites can therefore be attributed to basic magma emplaced and cooled at an active continental setting and subduction of passive margin of the WAC beneath the Benino-Nigerian shield. Agbossoumondé et al. (2004), proposed same mechanism for the Agou massif of the Dahomeyide suture zone in southern Togo.
8. On the basis of the geochemical data represented on the pyroxenites (this study), it can be concluded that the primary melts of these ultramafic plutonic rocks in the area were

derived from the normal lithospheric mantle wedge which had not been depleted by previous melt extractions and strongly modified by hydrous fluids.

6.2 RECOMMENDATION

It is recommended that mineral chemistry, geothermobarometric calculations (PT-t curves), isotopic studies and dating must be carried out on these rocks of the suture zone at Adaklu to strongly come out with a vivid geodynamic evolution of these rocks.

This study is the only extensive localized work on the NE extension of the Dahomeyide suture zone rocks at Adaklu in SE Ghana. It is therefore recommended that further work, including detailed structural interpretations and petrogenesis must be carried out for these rocks at Adaklu.

Detailed petrographic and geochemical studies of the pyroxenite must be done to understand the geodynamic evolution of the suture zone ultramafic plutonic igneous rocks of the Dahomeyide.

REFERENCES

Abati, J., Abdel, M. A., Gerdes, A., Ennih, N. (2012). Insights on the crustal evolution of the West African Craton from Hf isotopes in detrital zircons from the Anti-Atlas belt. Precambrian Research 212–213 (2012) 263–274.

Agbossoumondé, Y. (1998). Les complexes ultrabasiquesbaslques de la chaine panafricaine au Togo (axe Agou-Atakpamé, Sud-Togo). Etudes pétrographlque, minéralogique et. géochimique. Thése de I'Université de Saint-Etienne (UJM), Saint-Etienne, France, 306p.

Agbossoumondé, Y., Ménot, R.P., Guillot, S. (2001). Metamorphic evolution of Neoproterozoic eclogites from south Togo West Africa. Journal of African Earth Sciences 332, 227 - 244.

Agbossoumondé, Y., Guillotb, S., Ménot, R. P. (2004). Pan-African subduction–collision event evidenced by high-P coronas in metanorites from the Agou massif (southern Togo). Precambrian Research 135, 1–21.

Agbossoumondé, Y., Ménot, R.-P., Nude, P. M. (2013). Geochemistry and Sm–Nd isotopic composition of the Agou Igneous Complex (AIC) from the Pan-African orogen in southern Togo, West Africa: Geotectonic implications. Journal of African Earth Sciences 82, 88–99.

Abouchami, W., Boher, M., Michard, A., Albarede, F. (1990). A major 2.1 Ga event of mafic magmatism in West Africa: an early stage of crustal accretion. Journal of Geophysical Research 95, 17605–17629.

Affaton, P., Sougy, J., Trompette, R. (1980). The tectono-stratigraphic relationships between the Upper Precambrian and Lower Paleozoic Volta basin and the Pan African Dahomeyide orogenic belt (West Africa). American Journal of Science 280, 224–248.

Affaton, P., Rahaman, M.A., Trompette, R., Sougy, J. (1991). The Dahomeyide orogen: tectonothermal evolution and relationship with Volta basin. In: Dallmeyer, R.D., Lecorche, J.-P. (Eds.), The West African Orogens and Circum-Atlantic Correlatives. Springer-Verlag, New York, pp. 95–111.

Affaton, P., Aguirre, L., Ménot, R.-P. (1997). Thermal and geodynamic setting of the Buem volcanic rocks near Tiélé, Northwest Benin, West Africa. Precambrian Research 82, 191–209.

Affaton, P., Kröner, A., Seddoh, K.F. (2000). Pan-African granulite formation in the Kabye Massif of northern Togo (West Africa): Pb–Pb zircon ages. International Journal of Earth Sciences 88, 778–790.

Asiedu, D. K., Dampare, S. B., Shibata, T., Banoeng – Yakubo, B. and Osae, S. (2006). The chemical composition and significance of chromian spinels in the Neoproterozoic Anum serpentinites obtained from Anum and Dake – Peki in south eastern Ghana. Journal of Ghana Science Association. 10: 1: 36 – 43.

Attoh, K. (1990). Dahomeyides of southeastern Ghana - evidence for oceanic closure and crustal imbrication in a Pan-African orogen. 15th Colloquium on African Geology, Nancy, France. CIFEG Publ. 22, 159 164.

Attoh, K., Hawkins, D., Bowring, S. (1991). U-Pb zircon ages of gneisses from the Pan African Dahomeyide orogen, West Africa. EOS Trans. American Geophysical Union 72, S299.

Attoh, K., Dallmeyer, R. D., Affaton, P. (1997). Chronology of nappe assembly in the Pan African Dahomeyide orogeny, West Africa: evidence from $^{40}Ar/^{39}Ar$ mineral ages. Precambrian Research 82, 153 – 171.

Attoh, K. (1998). High-pressure granulite facies metamorphism in the Pan-African Dahomeyide orogen, West Africa. Journal of Geology 106 (2), 236–246.

Attoh, K., and Morgan, J. (2004). Geochemistry of high-pressure granulites from the Pan African Dahomeyide orogen, West Africa: constraints on the origin and composition of the lower crust. Journal of African Earth Sciences 39, 201-208.

Attoh, K., Corfu, F., and Nude, P. M. (2007). U-Pb zircon age of deformed carbonatite and alkaline rocks in the Pan-African Dahomeyide suture zone, West Africa. Precambrian Research 155, 251-260.

Attoh, K., and Nude, P. M. (2008). Tectonic significance of carbonatite and ultrahigh-pressure rocks in the Pan-African Dahomeyide suture zone, southeastern Ghana. Geological Society, London, Special Publications 297, 217-231; doi: 10.1144/sp297-10.

Attoh, K., Samson, S., Agbossoumondé, Y., Nude, P. M., Morgan, J. (2013). Geochemical characteristics and U–Pb zircon LA-ICPMS ages of granitoids from the Pan-African Dahomeyide orogen, West Africa. Journal of African Earth Sciences 79, 1–9.

Auvray, B., Peucat, J.-J., Potrel, A., Burg, J.-P., Caruba, C., Dars, R., Lo, K. (1992). Donnees geochronologiques nouvelles sur l'Archeen de l'Amsaga (Dorsale Reguibat Mauritanie). Comptes Rendus de l'Academie des Sciences 315 (1), 63–70.

Bernard-Grifiths, J., Peucat, J.J., Menot, R.P. (1991). Isotopic (Rb–Sr, U–Pb, and Sm–Nd) and trace element geochemistry of eclogites from the Pan-African belt: a case study of REE fractionation during high grade metamorphism. Lithos 27, 43–57.

Blay, P. K. (1991). Applying subduction tectonics to the evolution of the Pan-African Dahomeyide deformed belt of Ghana, West Africa: Proceedings of the first Local Conference on Mineral Exploration and Development and their Impact on the Economy of Ghana, Accra, 7th December 1990, Minerals Commission Publication. P. 52-75.

Bonhomme, M. (1962). Contribution a l'etude geochronologique de la platforme de l'ouest africaine. Annales Faculte Science Universite.

Bozhko, N.A., Kazakov, G.A., Trofimov, D.M., Knorre, K.G., Gatinsky, Y.U.A. (1971). New absolute dating of West Africa glauconites. Acad. Nauk. SSSR, Doklady, Earth Science Section 198, 138–139 (AGI translations).

Boynton, W.V. (1984). Cosmochemistry of the rare earth elements; meteorite studies. In: Rare earth element geochemistry. Henderson, P. (Editors), Elsevier Science Publishing Company, Amsterdam. 63-114.

Brunsmann, A., Franz, G., Erzinger, J. (2001). REE mobilization during small-scale high pressure fluid–rock interaction and zoisite/ fluid partitioning of La to Eu, Geochimica et Cosmochimica Acta 65 (2001) 559– 570.

Burke, K.C., Dewey, J. F. (1973). An outline of Precambrian plate development. In: Tarling, D.M., Runcorm, S.K. (Eds.), Implication of Continental Drift to the Earth Sciences, vol. 2. Academic Press, London, pp. 1035–1045.

Cabanis, B., Lecolle M. (1989). Le diagramme La/10-Y/15-Nb/8: un outil pour la discrimination Des series volcaniques et la mise en evidence des processus de mélange et/ou de contamination crustale. Comptes Rendus de l'Académie des Sciences II, 309, 2023-2029.

Castaing, C., Triboulet, C., Feybesse, J.-L., Chevrement, P. (1993). Tectonometamorphic evolution of Ghana, Togo and Benin in the light of the Pan-African Brasiliano orogeny. Tectonophysics 28, 423~432.

Clifford, T.N. (1972). The evolution of the crust of Africa. Service Ge´ol. Maroc., Notes Me´m. No. 236, pp. 29–39. Cox, K.G., Bell, J.D., Pankhurst, R.J. (1979).The Interpretation of Igneous Rocks. George Allen and Unwin (Publishers), London. 450pp.

Cox, K.G., Bell, J.D., Pankhurst, R.J. (1979).The Interpretation of Igneous Rocks. George Allen and Unwin (Publishers), London. 450pp.

Crook, J. P. (1963). The geology of the field sheets 142, 144 and 147. Ho, S. E. and N. E and Honuta N. W. Unpublished report of Ghana Geological Survey.

Crook, J. P. (1970). Some preliminary notes on the classification of rocks of Eastern Ghana in Geological Survey Bulletin no. 38 – Symposium Fiftieth Anniversary – Ghana Geological Survey 1913 – 1963. pp. 27 – 32.

Dalziel, I.W.D., Mosher, S., Gahagan, L.M. (2000). Laurentia-Kalahari Collision and the assembly of Rodinia. Journal Geology 108, 499–513.

Dampare, S. B. (2008). Geochemistry of Paleoproterozoic metavolcanic rocks from the southern Ashanti volcanic belt, Ghana: Petrogenetic and tectonic setting implications. Precambrian Research, vol. 162, pp. 403–423.

Dickson, K. B., & Benneh G. (1998). A new geography of Ghana – Longman Group Ltd., London.

Duclaux, G., Ménot, R. P, Guillot, S., Agbossoumondé, Y., Hilairet, N. (2006). The mafic layered complex of the Kabyé massif (north Togo and north Benin): Evidence of a Pan-African granulitic continental arc root. Precambrian Research. 151, 101–118.

Eisenlohr, B.N. (1992). Conflicting evidence on the timing of mesothermal and paleoplacer gold mineralization in early Proterozoic rocks from southwest Ghana, West Africa. Mineral. Deposita. 27, 23–29.

Elliott, T., Plank, T., Zindler, A., White, W., and Bourdon, B. (1997), Element transport from slab to volcanic front at the Mariana arc: Journal of Geophysical Research, v. 102, p. 14,991–15,019, doi: 10.1029/97JB00788.

Fitches, W.R. (1970), "Pan African Orogeny" in the coastal region of Ghana: Nature, 226, 744-746.

Floyd, P.A. Winchester, J.A. (1975). Magma type and tectonic setting discrimination using immobile elements. Earth Planet Science, Letters, 27, 211–218.

Grant, N.K. (1969). The late Precambrian to early Paleozoic Pan-African orogeny in Ghana, Togo, Dahomey and Nigeria. Geological Society of America Bulletin 80, 45–55.

Griffis, J. R., Barning, K., Agezo, L. F., and Akosah, K. F. (2002). Gold deposits of Ghana. Copyright (2002) by Minerals Commission, Accra, Ghana. 7 – 8.

Griffiths, J. B., Cornichet, J. (1985). Origin of eclogites from South Brittany, France; a Sm Nd isotopic REE study, Chemical Geology 52, 185–201.

Hastie, A. R., Kerr, A. C., Pearce, J. A. & Mitchell, S. F. (2007). Classification of altered volcanic island arc rocks using immobile trace elements: development of the Co-Th discrimination diagram. Journal of Petrology 48, 2341–2357.

Hawkesworth C., Turner S., Peate D., McDermott F., and Van Calsteren P. (1997a) Elemental U and Th variations in island arc rocks: Implications for U-series isotopes. Chemical Geology 139, 207–221.

Hefferan, K.P., Admou, H., Karson, J.A., Saquaque, A. (2000). Anti-Atlas (Morocco) role in Neoproterozoic Western Gondwana reconstruction. Precambrian Research 103, 89–96.

Henry, O. (2000). Soil classification in Ghana. Centre for Policy Analysis No. 35 Josif Broz Tito Avenue Switchback Road Accra. Selected Economic Issues, No.3.

Hirdes, W., Davis, D.W., Eisenlohr, B.N. (1992). Reassesment of Proterozoic granitoid ages in Ghana on the basis of U-Pb zircon and monazite dating. Precambrian Research 56, 89-96.

Hirdes, W., and Davis W. D. (2002). U-Pb zircon and rutile metamorphic ages of Dahomeyan garnet-hornblende gneiss in southeastern Ghana, West Africa. Journal of African Earth Sciences 35, 445-449.

Hoffman, P.F. (1991). Did the breakout of Laurentia turn Gondwana inside-out? Science 252, 1409–1412.

Hoffman, P. (1999). The break-up of Rodinia, birth of Gondwana, true polar wander and the snowball Earth. Journal of African Earth Sciences, 28, 17-33.

Holm, R.F. (1974), Petrology of alkalic gneiss in the Dahomeyan of Ghana: Geological Society of America Bulletin, 85, 1441-1448.

Holm, P.E. (1985). The geochemical fingerprints of different tectonic magmatic environments using hydromatophile element abundances of tholeiitic basalts and basaltic andesites. Chemical Geology 51, 303–323.

Humphris, S.E., Thompson, G. (1978). Hydrothermal alteration of oceanic basalts by seawater. Geochimica et Cosmochimica Acta 42, 107–125.

John, T., Schenk, V., Haase, K., Scherer, E., Tembo, F. (2003). Evidence for a Neoproterozoic ocean in south central Africa from midoceanic- ridge-type geochemical signatures and pressure temperature estimates of Zambian eclogites, Geology 31, 243–246.

Jones, W.B. (1990). The Buem volcanic and associated sedimentary rocks, Ghana: a field and geochemical investigation. Journal African Earth Sciences 11, 373–383.

Junner, N.R. (1940). Geology of the Gold Coast and Western Togoland. Gold Coast Geological Survey Bulletin 11.

Junner, N. R. and Hirst, T. (1946). The geology and hydrology of the Voltaian basin. Gold Coast Geological Survey Memoir. Vol. 8, pp. 51.

Kennedy, W. Q. (1964). The structural differentiation of African in the Pan-African (+ 500 m.y.) tectonic episode. Annual Report - Research Institute of African Geology, University of Leeds, England, p. 48 49.

Kepezhinskas, P., McDermott, F., Defant, M.J., Hochstaedter, A., Drummond, M.S., Hawkesworth, C.J., Koloskov, A., Maury, R.C., and Bellon, H. (1997). Trace element and Sr-Nd Pb isotopic constraints on a threecomponent model of Kamchatka Arc petrogenesis: Geochimica et Cosmochimica Acta, 61, 577–600.

Kesse, G.O. (1985). Rock and Mineral Resources of Ghana. A.A. Balkema, Boston, p. 610.

Key, R.M., Loughlin, S.C., Gillespie, M., Del Rio, M., Horstwood, M.S.A., Crowley, Q.G., Darbyshire, D.P.F., Pitfield, P.E.J., Henney, P.J. (2008). Two mesoarchaean terranes in the Reguibat shield of NW Mauritania. Geological Society, London, Special Publications 297 (1), 33–52.

Kitson, A.E. (1928). Provisional geological map of the Gold Coast and Western Togoland, with brief descriptive notes thereon. Gold Coast Geological Survey Bulletin 2. Accra, Ghana.

Knorring, O. von, Kennedy, W.Q. (1958). The mineral paragenesis and metamorphic status of garnet-hornblende-pyroxene-scapolite gneiss from Ghana. Mineralogical Magazine 31, 846–859.

Koert, W. (1910). "Begleit worte zur geologischer kante von Togo" in Hans Mayer's Das Deutsche kolonia – ireich, Leipzig and Vienna, vol. 2.

Kroner, A. (1984). Late Precambrian plate tectonics and orogeny: A need to redefine the term Pan-African. In: African Geology, J. Klerkx and J. Michot (Eds). Musee Royal de l'Afrique Centale, Tervuren, 23-28.

Kroner, A., Ekwueme, B.N., Pidgeon, R.T. (2001). The oldest rocks in West Africa: SHRIMP zircon age for early archean migmatitic orthogneiss at Kaduna, Northern Nigeria. The Journal of Geology 109 (3), 399–406.

Kröner, A. and Stern, R.J. (2005). Pan- African orogeny, North Africa phanerozoic rift valley. Encyclopedia of Geology, Elsevier, Amsterdam. Vol. 1, pp.

Liegeois, J.P., Claessens, W., Camara, D., Klerkx, J. (1991). Short-lived Eburnian orogeny in southern Mali. Geology, tectonics, U-Pb and Rb-Sr geochronology. Precambrian Research 50 (1–2), 111–136.

Mani, R. (1978). The geology of the Dahomeyan of Ghana; Geology of Ghana Project. Accra: Ghana Geological Survey Department.

Meschede, M. (1986). A method of discriminating between different types of mid-ocean ridge basalts and continental tholeiites with the Nb-Zr-Y diagram. Chemical Geology 56, 207-218.

Milesi, J.-P., Feybesse, J.L., Ledru, P., Dommanget, A., Ouedraogo, M.F., Marcoux, E., Prost, A., Vinchon, C., Sylvain, J.P., Johan, V., Tegyey, M., Clavez, J.Y., Lagny, Ph. (1989). Mineralisations aurif˜eres de l'Afrique de l'ouest, leurs relations avec l'´evolution litho structurale au Paleoproterozo¨ıque inf˜erieur. Chronology Research. Min. 497, 3–98.

Milligan, P. R., Gunn, P.J. (1997). Enhancing and Presentation of airborne geophysical data. AGSO Journal of Australian Geology and Geophysics, 17(2) 63-75.

Möller, A., Appel, P., Mezger, K., Schenk, V. (1995). Evidence for a 2Ga subduction zone; eclogites in the Usagaran Belt of Tanzania, Geology 23, 1067–1070.

Mullen, E.D. (1983). $MnO–TiO_2–P_2O_5$ a major element discriminant diagram for basaltic rocks of the oceanic environments and its applications for petrogenesis. Earth and Planetary Science Letters 62, 53–62.

Nude, P.M., Shervais, J.W., Attoh, K., Vetter, S.K., Corey Barton, C. (2009). Petrology and geochemistry of nepheline syenite and related carbonate-rich rocks in the Pan-African Dahomeyide orogen, southeastern Ghana, West Africa. Journal of African Earth Sciences 55(3-4), 147 157.

Nude, P. M., Shervais, J. W., Attoh, K., and Foli, G. (2012). Petrological and geochemical characteristics of mafic granulites associated with alkaline rocks in the Pan-African Dahomeyide suture zone, southeastern Ghana. In Ali Ismail Al-Juboury (ed.) Petrology - New Perspectives and Applications. ISBN978-953-307-424-5, 21-38.

Osae, O., Asiedu, D. K., Bruce, B., Koeberl, C., Dampare S. B. (2006). Provenance and tectonic setting of Late Proterozoic Buem sandstones of southeastern Ghana: Evidence from geochemistry and detrital modes. Journal of African Earth Sciences 44, 85–96.

Pearce, J.A., Cann, J.R. (1973). Tectonic setting of basic volcanic rocks determined using trace element analyses. Earth and Planetary Science Letters 19, 290–300.

Pearce, J.A. (1975). Basalts geochemistry used to investigate past tectonic environments on Cypus. Tectonophysics, 25, 41-67.

Pearce, J. A., Norry, M. J. (1979). Petrogenetic implications of Ti-Zr-Y amd Nb variations in volcanic rocks. Contributions to Mineralogy and Petrology, 69, 33-47.

Pearce, J.A., Lippard, S.J., Roberts, S. (1984). Characteristics and tectonic significance of supra-subduction zone ophiolites. In: Kokelaar, B.P., Howells, M.F. (Eds.), Marginal basin geology; volcanic and associated sedimentary and tectonic processes in modern and ancient marginal basins. Geological Society Special Paper, pp. 74–94.

Pearce, J. A. (1996). A user's guide to basalt discrimination diagrams. In: Wyman, D. A. (ed.) Trace Element Geochemistry of Volcanic Rocks: Applications for Massive Sulphide Exploration. Geological Association of Canada, Short Course Notes 12, 79–113.

Pearce, J. A. (2014). Immobile Element Fingerprinting of Ophiolites, Elements, 10, 101–108.

Peccerillo, A. & Taylor, S. R. (1976). Geochemistry of Eocene calc-alkaline volcanic rocks from the Kastamonu area, Northern Turkey. Contributions to Mineralogy and Petrology 58, 63 81.

Plank, T., and White, W. M. (1995). Nb and Ta in arc and mid-ocean ridge basalts: Eos (Transactions, American Geophysical Union), 76, 655.

Potrel, A., Peucat, J.J., Fanning, C.M., Auvray, B., Burg, J.P., Caruba, C. (1996). 3.5 Ga old terranes in the West African Craton, Mauritania. Journal of the Geological Society 153 (4), 507–510.

Potrel, A., Peucat, J.J., Fanning, C.M. (1998). Archean crustal evolution of the West African Craton: example of the Amsaga Area (Reguibat Rise) U-Pb and Sm-Nd evidence for crustal growth and recycling. Precambrian Research 90, 107–117.

Robertson, T. (1925). The sedimentary and volcanic rocks of western Togoland. Geological Magazine. 62: 1: 1 – 21.

Rollinson, H. R. (1993). Using geochemical data: evaluation, presentation, interpretation. Longman Group UK Limited, 352 pp.

Roques, M. (1948). Le Precambrien de lAfrique occidentale francaise. Bulletin Societe Geologique Francaise 18 (7–8), 589–628.

Rudnick, R. L. (1992). Restites, Eu anomalies, and the lower continental crust, Geochimica et Cosmochimica Acta, 56, 963-970

Rudnick, R.L., Fountain, D.M. (1995). Nature and composition of the continental crust: a lower crustal perspective. Reviews of Geophysics 33, 267–309.

Samson, S.D., Inglis, J.D., D'Lemos, R.S., Admou, H., Blichert-Toft, J., Hefferan, K. (2004). Geochronological, geochemical, and Nd-Hf isotopic constraints on the origin of Neoproterozoic plagiogranites in the Tasriwine ophiolite, Anti-Atlas orogeny, Morocco. Precambrian Research 135 (1–2), 133–147.

Saquaque, A., Admou, H., Karson, J., Hefferan, K., Reuber, I. (1989). Precambrian accretionary tectonics in the Bou Azzer-El Graara region, Anti-Atlas, Morocco. Geology 17 (12), 1107–1110.

Schiano, P., Allegre C., Lewin, E. and Joron, J. L. (1993). Variability of trace elements in Basaltic suites. Earth Planetary Science Letters, vol. 119, pp 37-91.

Schofield, D.I., Horstwood, M.S.A., Pitfield, P.E.J., Crowley, Q.G., Wilkinson, A.F., Sidaty, H.C.O. (2006). Timing and kinematics of Eburnean tectonics in the central Reguibat shield, Mauritania. Journal of the Geological Society 163 (3), 549–560.

Shirey, S. B., Hanson, G. N. (1984). Mantle-derived Archaean monzodiorites and trachyandesites. Nature, V. 310, no. 5974, p. 222-224.

Sibson, R. H. (1977). Fault rocks and fault mechanisms: Journal of Geological Society of London, v.133, p.190-213.

Sibson, R. H. (1983). Continental fault structure and the shallow earthquake source: Journal of Geological Society of London, 140, 741-767.

Stern, R., Hanson, G. N., Shirey, S. B. (1989). Petrogenesis of Mantle derived LILE-enriched Archaean Monzodiorite, Trachyandesites (Sanukitoids) in southern Superior Province. Canadian Journal of Earth Sciences, 26, 1688-1712.

Sun S. S. (1980). Lead isotopic study of young volcanic rocks from mid-ocean ridges, ocean Islands and island arcs. Phil Trans R. Soc., A297, 409-445.

Sun, S., McDonough, W. (1989). Chemical and isotopic systematics of oceanic basalts: implications for mantle composition and processes. Geological Society London Special Publications 42, pp. 313–345.

Taylor, P. N., Moorbath, S., Leube, A., Hirdes, W. (1988). Geochronology and crustal evolution of Early Proterozoic granite-greenstone terrains in Ghana/ West Africa. Abstr., International conference on the Geology of Ghana with emphasis on Gold Comm. 75th Anniversary of the Geological Survey Department, Accra, pp 43-45.

Thieblemont, D., Goujou, J.C., Egal, E., Cocherie, A., Delor, C., Lafon, J.M., Fanning, C.M. (2004). Archean evolution of the Leo Rise and its Eburnean reworking. Journal of African Earth Sciences 39 (3–5), 97–104.

Thomas, R.J., Chevallier, L.P., Gresse, P.G., Harmer, R.E., Eglington, B.M., Armstrong, R.A., de Beer, C.H., Martini, J.E.J., de Kock, G.S., Macey, P.H., Ingram, B.A. (2002). Precambrian evolution of the Sirwa Window, Anti-Atlas Orogen, Morocco. Precambrian Research 118 (1–2), 1–57.

Trompette, R. (1994). Geology of Western Gondwana (2000–500 Ma) Panafrican-Brasiliano Aggregation of South America and Africa. Balkema, Rotterdam, p. 366.

Trompette, R. (2000). Gondwana evolution; its assembly at around 600Ma. C. R. Academie Sci. 330, 305–315.

Tullis, J. A., Snoke, A. W., and Todd, V. R. (1982). Penrose Conference report: Significance and petrogenesis of mylonitic rocks: Geology, v.10, p.227-230.

Turner, S. T., Hawkesworth, C., van Calsteren, P., Heath, E., Macdonald, R. & Black, S. (1996). U-series isotopes and destructive margin magma genesis in the Lesser Antilles. Earth and Planetary Science Letters 142, 191–207.

Turner, S., Hawkesworth, C. J., Rogers, N., Bartlett, J., Worthington, T., Hergt, J., Pearce, J. & Smith, I. (1997). U-238– Th-230 disequilibria, magma petrogenesis, and flux rates beneath the depleted Tonga–Kermadec island arc. Geochimica et Cosmochimica Acta 61, 4855 4884.

Vidal, M., Delor, C., Pouclet, A., Siméon, Y., Alric, G. (1996). Evolution géodynamique de l'Afrique de l'Ouest entre 2,2 Ga et 2 Ga: le style ―archéen‖ des ceintures vertes etdes ensembles sédimentaires birimiens du nord-est de la Côte-d'Ivoire. Bulletin. Geological Society France 167 (3), 307–319.

Weaver B. L., and Tarney J. (1984). Empirical approach to estimating the composition of the continental crust. Nature, 310, 575-57.

Weaver B. L. (1991). The origin of ocean island basalt end-member composition: trace element and isotopic constraints. Earth and Planetary Science Letters, 104, 3810-397.

Whitford, D.J., Korsch, M.J., Porritt, P.M., Craven, S.J. (1988). Rare-earth mobility around the volcanogenic polymetallic massive sulfide deposit at Que River, Tasmania, Australia. Chem. Geol. 68, 105–119.

Wickham M. S., Janardhan A.S., & Stern R. J. (1994). Regional Carbonate Alteration of the Crust by Mantle-Derived Magmatic Fluids. The Journal of Geology, 4, 379-398.

Winter, D. J. (2001). An Introduction to Igneous and Metamorphic Petrology. (P. Lynch, Ed.) Upper Saddle River, New Jersey 07458, USA: Prentice Hall, pp 424-471.

Wright, J., Hastings, D., Jones, W., & Williams, H. (1985). Geology and Mineral Resources of West Africa. London: George Allen and Unwin publishers Ltd.

Wood, D. A. (1980). The application of a Th-Hf-Ta diagram to problems of tectonomagmatic classification and to establishing the nature of the crust contamination of basaltic lavas of the British Tertiary volcanic province. Earth and Planetary Science Letters, 50, 11 30.

Woodhead, J., Eggins, S. & Gamble, J. (1993). High field strength and transition elementsy stematics in island arc and back-arc basin basalts: evidence for multi-phase melt extraction and a depleted mantle wedge. Earth and Planetary Science Letters 114, 491 504.

Zhao, J. H., & Zhou M. F. (2007). Neoproterozoic Adakitic Plutons and Arc magmatism along the Western margin of the Yangtse Block, South China. The Journal of Geology. 115, 675-689.

APPENDIX

Appendix 1. Table showing the some sample locations of outcrops in the study area.

Location Samples	Longitudes / E (degree)	Latitudes / N (degree)	Outcrop Description
IKE1	0.5207	6.4978	Hornblende-garnet-pyroxene gneiss
IKE1B	0.5207	6.4978	Hornblende-garnet-pyroxene gneiss
IKE2B	0.5161	6.4936	Hornblende-garnet-pyroxene gneiss
IKE2C	0.5146	6.4926	Hornblende-garnet-pyroxene gneiss
IKE5	0.5018	6.4902	Hornblende-garnet-pyroxene gneiss
IKE6	0.5006	6.4905	Hornblende-garnet-pyroxene gneiss
IKE9	0.5061	6.4886	Hornblende-garnet-pyroxene gneiss
IKE11	0.4912	6.4914	Hornblende-garnet-pyroxene gneiss
IKE12	0.4912	6.4921	Hornblende-garnet-pyroxene gneiss
IKE14	0.5226	6.4999	Hornblende-garnet-pyroxene gneiss
IKE14B	0.5226	6.4996	Hornblende-garnet-pyroxene gneiss
IKE18	0.5109	6.4958	Hornblende-garnet-pyroxene gneiss
IKE29	0.5027	6.4947	Hornblende-garnet-pyroxene gneiss
IKE33	0.5208	6.49597	Hornblende-garnet-pyroxene gneiss
IKE33C	0.5208	6.4969	Hornblende-garnet-pyroxene gneiss
IKE37	0.5003	6.4989	Hornblende-garnet-pyroxene gneiss
IKE2	0.5161	6.4936	Hornblende-bearing gneiss
IKE4	0.5090	6.490	Hornblende-bearing gneiss
IKE7	0.4990	6.490	Hornblende-bearing gneiss
IKE15	0.5114	6.4964	Hornblende-bearing gneiss
IKE16	0.5107	6.4966	Hornblende-bearing gneiss
IKE17	0.5105	6.4959	Hornblende-bearing gneiss
IKE19	0.5112	6.4956	Hornblende-bearing gneiss
IKE20	0.5101	6.5011	Hornblende-bearing gneiss
IKE21	0.5096	6.4997	Hornblende-bearing gneiss
IKE22	0.5094	6.4996	Hornblende-bearing gneiss
IKE23	0.5029	6.5024	Hornblende-bearing gneiss
IKE24	0.5035	6.5022	Hornblende-bearing gneiss
IKE25	0.5033	6.5017	Hornblende-bearing gneiss
IKE25B	0.5033	6.5017	Hornblende-bearing gneiss
IKE26	0.5103	6.4918	Hornblende-bearing gneiss
IKE30	0.5011	6.4921	Pyroxene-garnet-hornblende gneiss
IKE31	0.5004	6.4922	Pyroxene-garnet-hornblende gneiss
IKE31B	0.5004	6.4922	Pyroxene-garnet-hornblende gneiss
IKE32	0.4994	6.4947	Pyroxene-garnet-hornblende gneiss
IKE34	0.4984	6.5023	Pyroxene-garnet-hornblende gneiss
IKE35	0.5004	6.5002	Pyroxene-garnet-hornblende gneiss
IKE36	0.5008	6.500	Pyroxene-garnet-hornblende gneiss
IKE41	0.4988	6.4946	Pyroxene-garnet-hornblende gneiss
IKE3	0.5114	6.490	Eclogite
IKE3B	0.5114	6.490	Eclogite
IKE8	0.5119	6.4903	Eclogite
IKE28	0.5095	6.4892	Eclogite
IKE38	0.4950	6.4956	Eclogite
IKE10	0.4939	6.484	Pyroxenite
IKE13	0.4617	6.4746	Pyroxenite